CHEMICAL AND MECHANICAL CHARACTERIZATION OF PYROLYSIS IN WOOD

by

LAURA E. HASBURGH

A dissertation submitted in partial fulfillment

of the requirements for the degree of

DOCTOR OF PHILOSOPHY

(MATERIALS SCIENCE)

at the

UNIVERSITY OF WISCONSIN – MADISON

2020

Date of final oral examination: April 27, 2020

The dissertation is approved by the following members of the Final Oral Committee:

Donald S. Stone, Professor, Materials Science and Engineering

Dane D. Morgan, Professor, Materials Science and Engineering

Gregory F. Nellis, Professor, Mechanical Engineering

Alex C. Wiedenhoeft, Research Botanist, Forest Products Laboratory

Samuel L. Zelinka, Supervisory Materials Research Engineer, Forest Products Laboratory

To my loving and amazing family,

Abstract

Pyrolysis of wood is a series of chemical and physical changes that occur simultaneously. Previous investigations of pyrolysis have often simplified the process. For wood building materials, the pyrolysis process is typically simplified to the formation of "char" at 300°C. Pyrolysis models are often simplified by using the thermal degradation of isolates reference polymers in an inert atmosphere. This approach assumes that the structure of bulk wood performs similarly to that of the isolated polymers being used and ignores reactions with oxygen. This dissertation explores the molecular-scale changes in wood and lignocellulosic polymers using innovative techniques to obtain a deeper understanding of the materials as they undergo pyrolysis.

Thermogravimetric analysis (TGA) was used on isolated lignocellulosic polymers and solid Douglas-fir latewood to obtain a baseline of the thermal degradation of the specific materials that can be used to compare against the current literature. It was found that the thermal degradation of the Douglas-fir latewood was not completely represented by a weighted average of the individual polymers as the in situ interactions between the polymers are not considered and, instead, a rate-limiting model is necessary.

X-ray photoelectron spectroscopy (XPS) was used to evaluate the chemical changes as a function of temperature in lignocellulosic polymers and Douglas-fir latewood. The chemical changes that occur through charred Douglas-fir latewood using XPS showed the thermal degradation of the holocellulose in the Douglas-fir occurred at lower temperature ranges than those observed in the isolated cellulose and is likely due to the in situ hemicellulose. Additionally, the bond scission observed using XPS on the charred Douglas-fir correlated well with the mass loss results obtained using TGA.

Nanoindentation was used to study the effect of polymer degradation on the mechanical response of wood cell wall. Ultimately, under dry conditions, the mechanical changes observed occur in a narrow, 2 mm / 100°C region.

The experiments conducted and the findings presented in this dissertation on the charred Douglas-fir latewood provide the first chemical and mechanical changes caused by pyrolysis in thermally thick wood, increasing the understanding of pyrolysis for model verification and creating new avenues for research directions.

Acknowledgements

I admittedly entered graduate school somewhat blindly and in a postpartum haze and fully realize I would not have survived the rollercoaster without the unbelievable support and guidance from my advisors, collaborators, technical staff, friends and family.

First, I would like to thank my PhD thesis advisor, Don Stone, for the opportunity to work in his research group, the encouragement to learn new techniques, and the patience on days when sick kids took precedence over science. I am also grateful to my co-advisor, Samuel Zelinka at the Forest Products Laboratory (FPL) for his guidance and support during this scientific journey and inspiring me to become a better researcher.

My experiments would not have been successful without the assistance of my colleagues at FPL. I'm particularly grateful to Nayomi Plaza Rodriguez and Joseph Jakes, whose guidance and critique undoubtedly strengthened this work. I also want to recognize Nayomi's artful coding skills helped fit the fastidious XPS peaks and thank her for her endless encouragement. Without Joseph's finesse in making tiny pyramids and help with the nanoindentation experiments, the mechanical properties would not have been obtained. I owe my gratitude to CR Boardman for his help in calibrating the dynamic scanning calorimeter and assistance with thermogravimetric analysis. I thank Fred Matt for conducting the carbohydrate analysis on the specimens. I want to acknowledge Joe Balczewski in the FPL carpenter shop for his help cutting charred wood – sorry your tools get dirty because of my specimens. I am also eternally grateful for the friendship and support from my other colleagues, Kara Yedinak and Keith Bourne, who took on extra work so I could focus on this research and were always available to cheer me on and talk fire.

I wish to thank my parents for their unlimited support, proof-reading, and babysitting. To my friends and family for their support and distractions: thank you for the much-needed work-life balance, inspirational gifs and laughs. Thank you to my kids for your unconditional love and patience.

And last, but not least, thank you to my incredible husband, Colin. Thank you for embarking on this crazy journey with me, providing steadfast support needed to accomplish this goal, and for not asking me how much longer it was going to take me to finish. You are amazing.

Laura Hasburgh

Financial support for my thesis is acknowledged from the USDA Forest Service Pathways program. The use of the x-ray photoelectron spectroscopy facilities and instrumentation was supported by NSF through the University of Wisconsin Materials Research Science and Engineering Center (DMR-1720415).

Nomenclature

In order of appearance.

MF	Mass fraction
MF'	Change in mass fraction (derivative)
x_i	Fraction of total yeild for each species, i
MF_{WA}	Mass fraction calculated as the weighted average
MF_i	Mass fraction of each component i
α	Degree of conversion
m_o	Initial specimen mass
m_∞	Specimen mass at the end of pyrolysis
t	Time
T	Temperature
k(T)	Reaction rate as a function of temperature
n	Reaction order
A	Pre-exponential factor for each reaction
E	Activation energy
R	Universal gas constant
β	Heating rate

h	Plank's constant
ν	Frequency of incident radiation
A_P	Area under the peak (via trapeziod function)
A_N	Normalized peak area
TXFN	Transmission fuction
SF	Sensitivity factor
ECF	Energy correction factor
H	Hardness
P_0	Maximum load
A_0	Contact area
E_{eff}	Effective modulus
S	Contact stiffness
E_s^{NI}	Nanoindentation elastic modulus
E_d	Young's modulus of diamond
ν_d	Poisson's ratio of diamond
ν_s	Poisson's ratio assumed for S2 cell wall layer
β	Nanoindentation numerical factor

Abbreviations

In alphabetical order.

AFM	Atomic force microscopy
Al K_α	K-alpha x-rays of aluminum
BE	Binding energy
C_C	Carbon atom bound to only carbon or hydrogen atoms
CL	Cellulose
CML	Compound middle lamella
C_O	Carbon atom bound to oxygen atoms
DF	Douglas-fir
DSC	Differential scanning calorimeter
DTG	Differential thermogravimetric curve
ESCA	Electron spectroscopy for chemical analysis
FDS	Fire Dynamics Simulator
FTIR	Fourier-transform infrared spectroscopy
GC-MS	Gas chromatography–mass spectrometry
HC	Hemicellulose
HPLC-PAD	High-performance liquid chromatography with pulsed amperometric detector

KE	Kinetic Energy
LG	Lignin
Mg K_α	K-alpha x-rays of magnesium
ML	Middle lamella
MOE	Modulus of elasticity
NERL	National Renewable Research Laboratory
NI	Nanoindentation
RH	Relative humidity
SCWL	S2 cell wall lamina
TEM	Transmission electron microscopy
TGA	Thermogravimetric analysis
XPS	X-ray photoelectron spectroscopy

List of Figures

List of Tables

Table of Contents

Chapter 1. Introduction

Wood is a historically common building material that has recently expanded into marketplaces where it was previously not permitted to be used before, such as high-rise structures. This expansion is due to new innovations in wood construction and the development of mass timber products (such as cross laminated timber) allowing architects, engineers, designers and developers to build a wide range of projects [1, 2]. However, the combustibility of wood limits its use as a building material via building code restrictions. Most of the existing research related to the fire performance of wood products focuses on determining effective charring rates with limited understanding of the chemical changes occurring in wood below the charred surface. As a result, current engineering practice utilizes a semi-empirical prescribed nominal char rate with an additional 20% safety factor to account for reductions in mechanical properties of the heated wood below the char layer. Char is the solid material that remains after the wood has been exposed to high temperatures and, for engineering analyses, the wood is considered to be converted to char at a temperature of 288°C or 300°C [3, 4]. The length scale of this work, while generally adequate for engineering calculation, does not allow for an understanding of the effect of thermal degradation on the wood cell structure.

Fire models have become a popular, modern approach to determine the effects of fire [5, 6]. Most of these models include a sub-model for pyrolysis, which is the thermal decomposition of a material at elevated temperatures. While these models provide valuable insight into the consequences of fire, users must be careful and understand the limitations when interpreting the results. For instance, many models are only applicable for 1) specific heat flux levels and oxygen concentrations, 2) homogeneous materials with simple decomposition kinetics, and 3) materials that don’t change volume [7]. For wood, the pyrolysis of the solid (condensed phase) involves

many complex chemical and physical changes that modify material properties (e.g., density, thermal conductivity, and emissivity). Additionally, measuring the material properties and chemical changes while a specimen is on fire is difficult so limits the input data available for pyrolysis models. Because of the complex nature and limited input data, modeling the condensed phase pyrolysis for wood is often simplified. However, the simplifications used for bulk wood pyrolysis may lead to inaccurate models. One method of simplification often employed is to use the known thermal degradation of isolated reference polymers in an inert atmosphere. This approach assumes that the separation process to obtain the isolated polymers does not affect the structure or thermal degradation of the polymers. This also assumes that the structure of bulk wood performs similarly to that of the isolated polymers being used. Ultimately, there is limited scientific understanding of the behavior of the polymers and chemical changes that occur in bulk wood during pyrolysis. What is known is derived from small, thermally thin specimens or individual polymers. The current body of work needs to be validated, but in order to do so, a deeper understanding of the chemical changes that occur in bulk wood must be gained.

The aim of this work is to develop a deeper understanding of the molecular-scale changes in bulk wood as it undergoes pyrolysis. Thermal degradation of the wood polymers in the pyrolysis zone are examined. Specifically, this dissertation describes the following:

- An examination of the effect of oxygen in the atmosphere on pyrolysis of wood polymers;
- An assessment of whether pyrolysis of isolated wood polymers can be used to estimate pyrolysis of wood;
- An X-ray photo-spectroscopy (XPS) study of the chemical changes in bulk wood exposed to flaming combustion and;

- Nanoindentation evaluation of the effect of pyrolysis on wood cell wall mechanical properties.

1.1 Wood structure and chemical composition

A general discussion of the composition and structure of wood is necessary for understanding wood pyrolysis. The following discussion is limited to softwoods (gymnosperms, conifers), which were examined in this thesis.

Structure of wood

At the macroscale, wood is both anisotropic and porous. The principal direction from root to crown is known as the longitudinal direction; the radial direction goes from the center of the trunk to the outermost layers, and the tangential direction follows the circumference of the trunk perpendicular to both longitudinal and radial directions. Anisotropy is usually referenced with respect to three different planes: the tangential-longitudinal, radial-longitudinal, and transverse, illustrated in Figure 1.1(a). The tangential-longitudinal plane is parallel with longitudinal direction and forms a tangent with the concentric growth rings. The radial-longitudinal plane is also parallel with the longitudinal direction but is cut perpendicular to the concentric growth rings. The transverse plane, also referred to as the end grain, is perpendicular to the longitudinal direction.

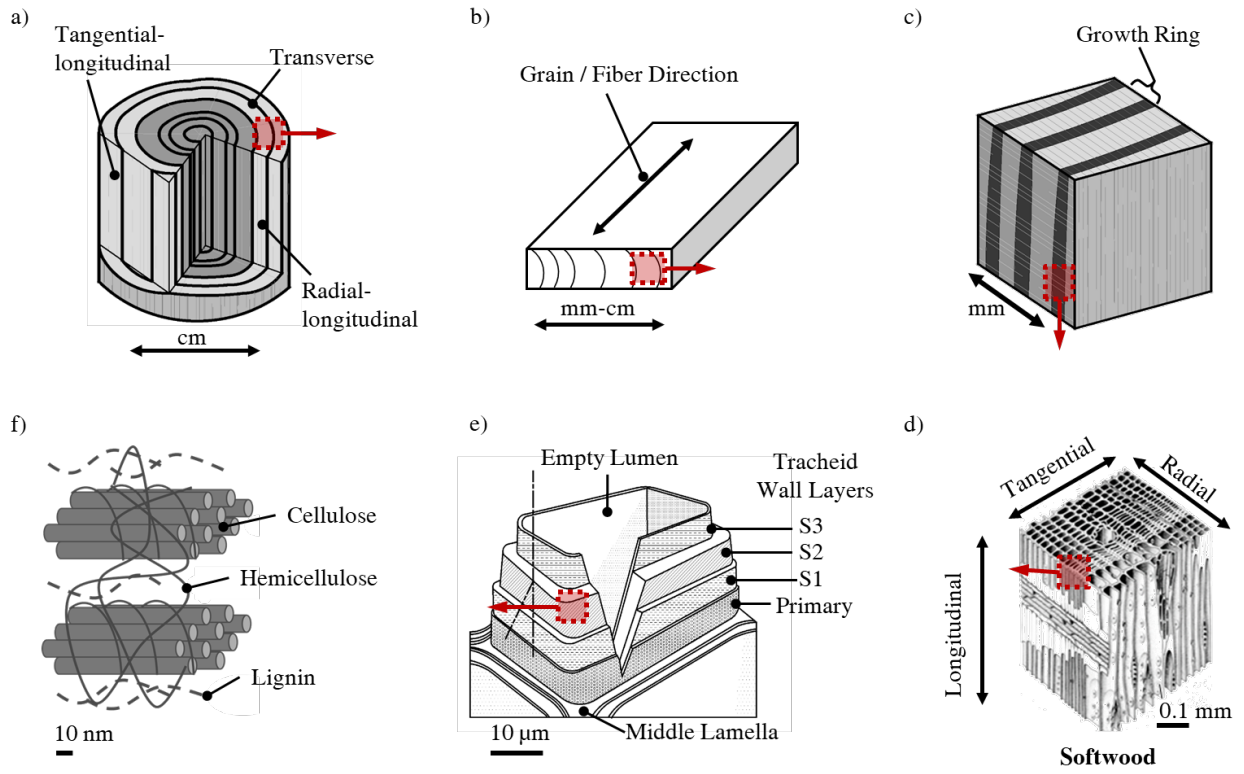

Figure 1.1 Graphical illustration of the hierarchical structure of softwood from the a) bulk to the b) board of lumber to the c) growth rings to the d) cellular to the e) cell wall to the f) lignocellulose matrix Adapted from [8, 9]. d) is from an unknown Forest Products Laboratory artist.

Wood building products are typically from wood cut parallel with the longitudinal direction to maximize strength properties [10]. When examining the end grain of a board of lumber, the growth rings are distinct and consist of earlywood and latewood. The strength of the wood is largely derived from the latewood cells with thicker walls and narrower lumen that results in a denser cell structure when compared to earlywood [11]. Earlywood is characterized by wider lumen and thinner cell walls. The ratio of cell wall thickness between earlywood and latewood cells is approximately 1:2 with earlywood measuring approximately 2.1 µm and latewood measuring approximately 4.3 µm [12]. Since the transverse surface of the latewood cell wall provided a larger area for analysis, the experiments conducted herein were carried out only on latewood. Additionally, the variation in density at this scale between the wood types will affect the burning

rate of wood as the denser material has a lower burning rate due to decreased mass transport [13, 14]. This was important to consider when developing charred wood specimens and the radial plane was chosen such that heat conducted through the types of wood without interruption. The development of the charred wood specimen is discussed further in Chapter 3.

Wood cell types and structure

The cellular structure of a softwood is schematically shown in Figure 1.1(d). In a softwood, such as Douglas-fir, the most common cell type is the tracheid, which accounts for over 90% of the softwood volume [11]. Tracheid cells run longitudinally and have a length to diameter ratio of approximately 100 to 1. The main function of the tracheid cells is to transport water between the roots and the leaves or needles. The secondary function is to provide structural strength.

Both early and latewood cell walls are broken down into three main regions with varying amounts of the main polymeric constituents. Figure 1.1(e) illustrates the three main cell wall regions: the middle lamella, the primary wall and the secondary wall. The middle lamella is the outermost region and provides adhesion between two or more cells and consists of mostly lignin. For wood, the primary wall is thin and, when using light microscopy or transmission electron microscopy, is not distinguishable from the middle lamella [11]. The inner most region of the cell wall is the secondary cell wall which consists of three layers with S2 being the thickest wall layer. Since the S2 cell wall is the thickest, it is the cell wall layer used for nanoindentation experiments conducted in Chapter 4.

Chemical constituents of softwood

Wood cell walls are made up of three main polymeric components: cellulose, hemicellulose and lignin. Materials made of these polymers are often referred to at lignocellulosic. The dry weight

of softwoods is made up of approximately 40% cellulose, 30% hemicellulose, and 30% lignin with the breakdown for each layer in the secondary cell wall provided in Table 1.1.

Table 1.1. Chemical composition of each secondary cell wall layer. Percentages correspond to tracheid cells in southern yellow pine latewood. Data from [15].

Secondary cell wall layer	Cellulose	Hemicellulose	Lignin
S1	30.0%	18.3%	51.7%
S2	54.3%	30.6%	15.1%
S3	13.0%	87.0%	~0%

A brief background on the chemistry of each wood polymer is discussed below with detailed reviews available elsewhere [12, 15].

Cellulose is the main constituent in the wood cell walls and comprises approximately 40% of the dry mass of softwoods. Cellulose has a high degree of polymerization (the number of monomer units in a macromolecule) that ranges between 8000 and 10000. In wood, cellulose exists in both crystalline (highly ordered) or amorphous (less ordered) phases [16]. While the degree of crystallinity varies across wood species and even within a wood cell wall, nominally 40% of the cellulose in softwoods are crystalline [17]. With a chemical formula of $(C_6H_{10}O_5)_n$, cellulose is a linear polysaccharide whose primary unit is the cellobiose (see Figure 1.2, drawn with ChemDraw Direct [18]). Each cellobiose unit is comprised of two glucose units linked by a $\beta(1\rightarrow4)$ glycosidic (covalent C-O-C) bond [8, 15, 19]. Additionally, each cellobiose unit has six hydroxyl (OH) groups that can build hydrogen bonds. For amorphous cellulose, these hydroxyl units bond to water molecules and for crystalline cellulose, they form intermolecular bonding [12]. Chains of cellulose are packed into partially crystalline fibers called microfibrils. In a microfibril, the chains are arranged in sheets with hydrogen bonding between cellulose chains and between monomers in each chain [20].

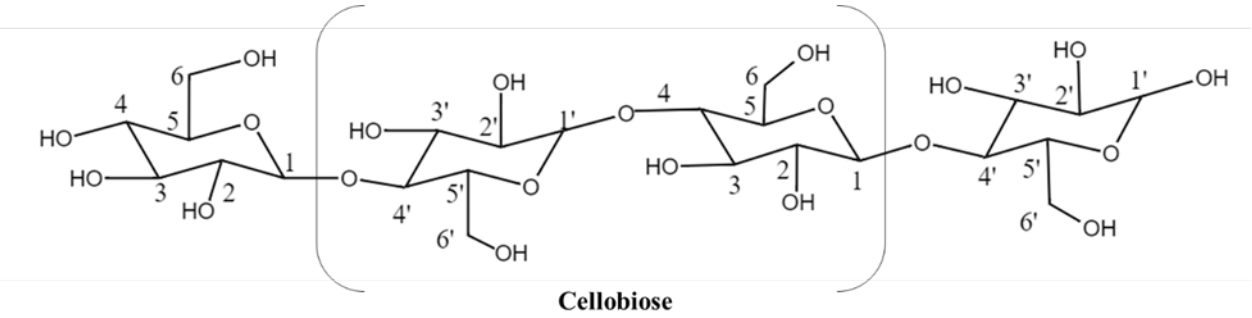

Figure 1.2: Molecular structure of cellulose showing the cellobiose unit, indicated by brackets.

Hemicelluloses (Figure 1.3) are polysaccharides that consist branched molecules that form hydrogen bonds with the cellulose [21, 22]. Compared to cellulose, hemicelluloses have a significantly lower degree of polymerization, typically around 200, and consist of several different monomers such as mannose, arabinose, xylose, galactose, glucose, galacturonic acid and glucuronic acid [15, 19]. These monomers are combined to make up hemicelluloses and the composition varies across the cell wall. Common hemicellulose components found in the secondary cell wall are shown in Figure 1.3, which was redrawn from [15] using ChemDraw Direct [18]. Both hemicelluloses and cellulose are saturated with single carbon-oxygen bonds. They also contain a carbonyl bond, oxygen double bonded to carbon, which is not present in lignin. The presence of these types of bonds are important when evaluating the chemical changes caused by thermal degradation and are discussed further in Chapter 3.

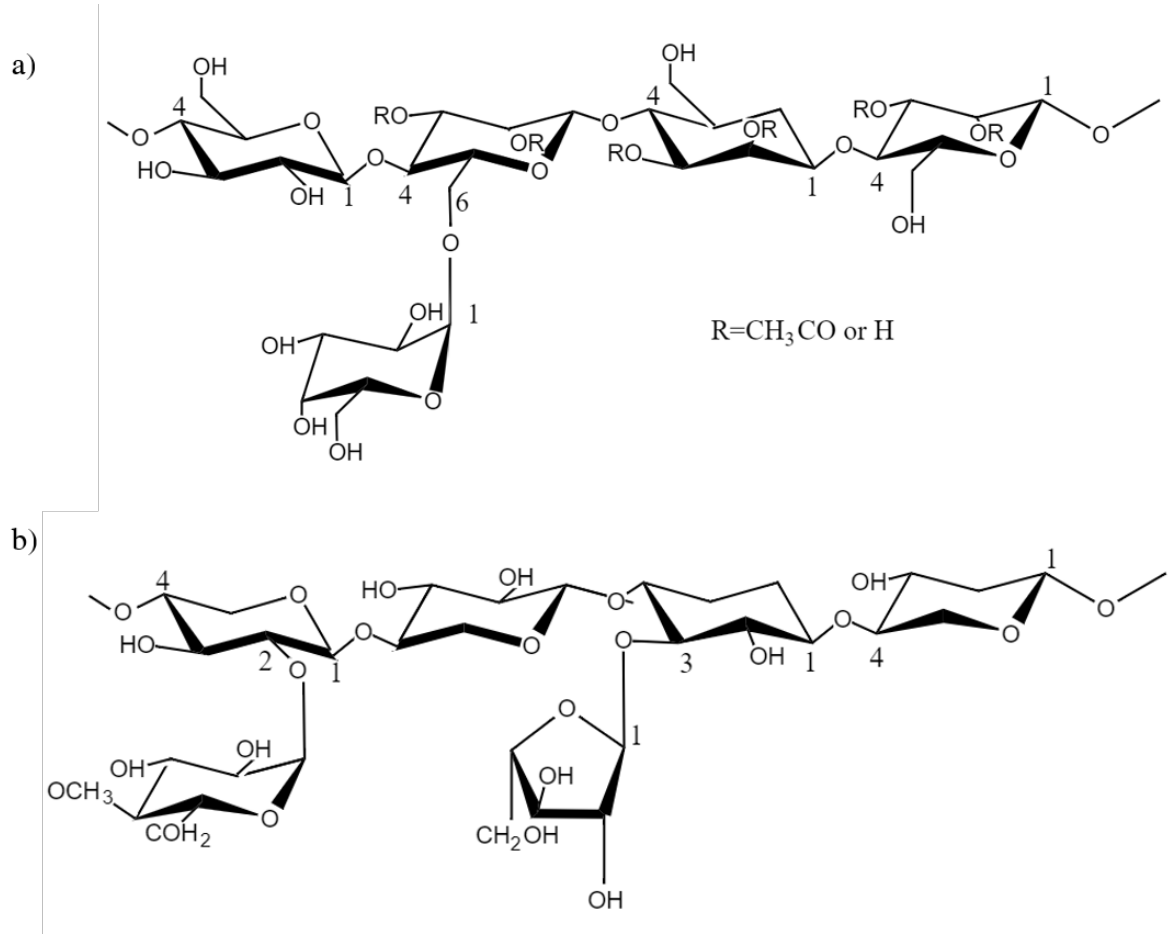

Figure 1.3: Structure of common hemicelluloses found in softwood: (a) glucomannan and (b) xylan.

Lignin consists of cross-linked phenol polymers that help bond cellulose and hemicelluloses within cell walls [22]. Due to the heterogeneity of lignin, the degree of polymerization is difficult to measure but has been recorded between 50 and 500. Lignin also forms the brittle matrix material of the middle lamella (ML) between the cells. The structure of lignin is complex, consisting of a three-dimensional aromatic polymer network. It is particularly important to point out the carbon double bonds that exist in the aromatic ring of lignin as this bond does not exist in hemicellulose or cellulose. It is composed of phenylpropane units, including coniferyl alcohol, sinapyl alcohol and p-coumaryl alcohol, that are linked by ether and carbon-carbon bonds [23]. These basic units

as well as a schematic of the softwood lignin structure are shown in Figure 1.4, redrawn from [23] and [24] using ChemDraw [18].

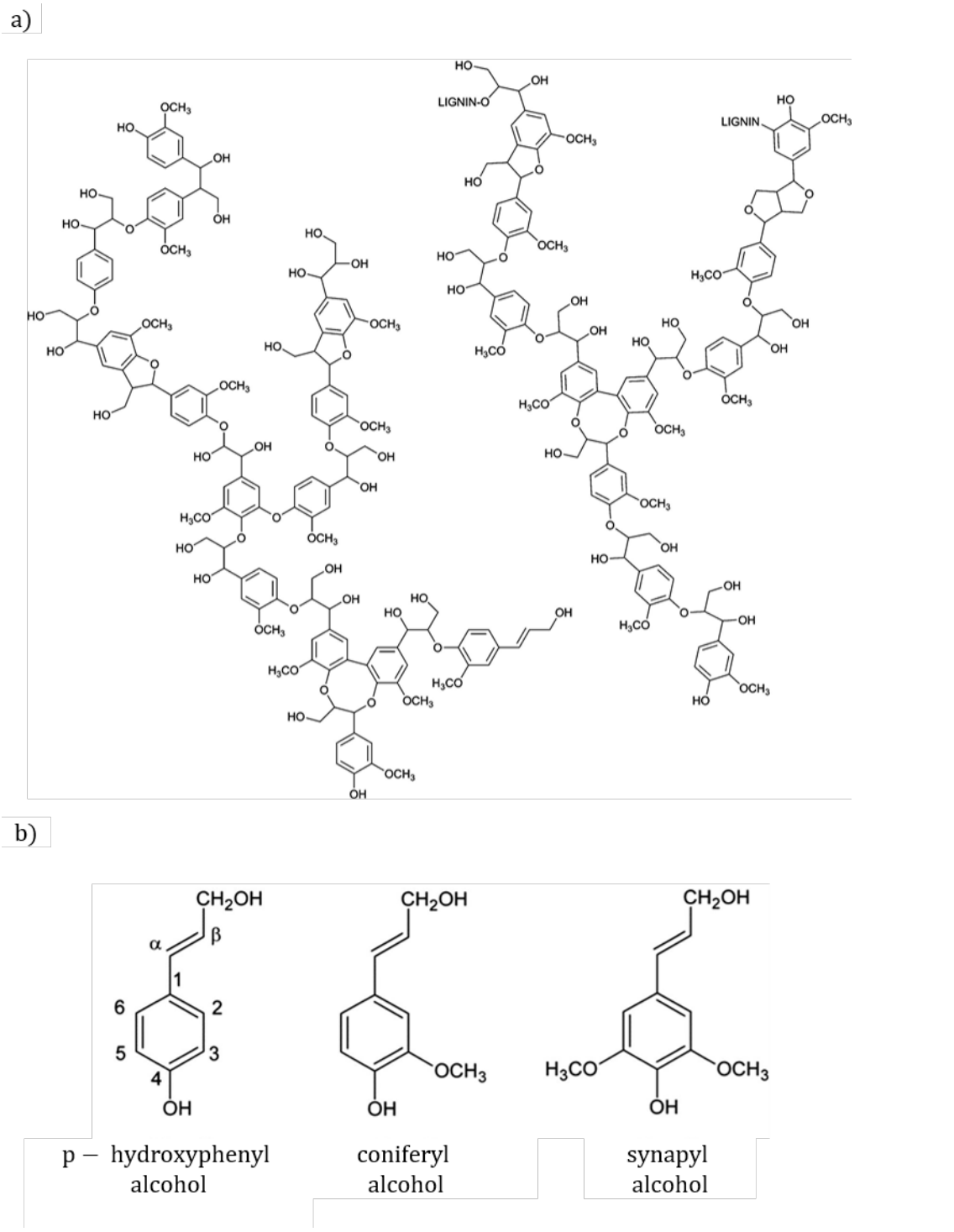

Figure 1.4: a) Structure model of lignin in softwood and b) monolignols, the primary precursors of lignin.

Extractives account for the remaining part of the constituents. Although the amount of extractives is quite small (roughly 1.4% of the dry mass of softwoods), they markedly influence the appearance and microbial characteristics of wood [12]. Extractives are attributed to properties such as color, odor and decay resistance and are a mixture of aromatic compounds, terpenes, and aliphatic acids and alcohols. It has been found that extractives decompose in the same temperature range as the three main polymers [25]. Additionally, removing the extracts results in a decrease in the fixed carbon content and char yield [26]. The overall effect of extractives on the thermal degradation of wood depends on species, however, for all species studied to date, the removal of extractives resulted in improved thermal stability [26-28]. Since extractives have been shown to influence the thermal degradation of wood and they would still be present in most wood building products, they were not removed prior to exposing specimens to high temperatures herein.

1.2 Thermal degradation of wood

These chemical reactions and the subsequent degradation of a material exposed to high temperatures is known as pyrolysis. Within the literature, it is generally agreed that pyrolysis for wood occurs in stages delineated by temperature ranges [14, 19, 29-31]. For wood construction products of appreciable thickness, a gradient within the wood will occur with the phases of pyrolysis simultaneously present. This gradient is illustrated in Figure 1.5.

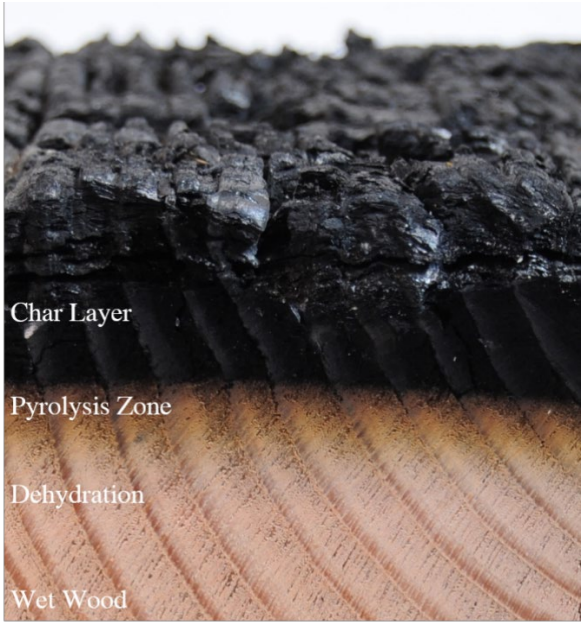

Figure 1.5: Cross-section of a Douglas-fir exposed to fire, showing evidence of the gradient caused by pyrolysis.

Prior to being exposed to high temperatures, wood has both free and bound water [32]. As temperatures increase between 100°C and 200°C, dehydration occurs marking the beginning of pyrolysis in wood with the evaporation of both types of water found in wood. As the water begins to evaporate, water vapor as well as other noncombustible gases and liquids including carbon dioxide, carbon monoxide, and formic acid are generated [33]. Some water vapor will migrate to the heat-exposed surface and some will move deeper into the wood and recondense, increasing the local moisture content in the wet wood zone [34]. The boundary between the dehydration zone and the wet zone are not visible in Figure 1.5. However, as the local moisture content increases, the wet zone may appear darker.

With temperatures increasing above 200°C, a gradient in the color is more noticeable as the formation of tar and char begins in what is referred to as the pyrolysis zone. The thermal degradation of the polymeric components that leads to the release of volatiles (flammable gases) gives rise to this zone. While the pyrolysis zone is typically assumed to be between 200°C and

300°C, the temperature ranges vary throughout the literature and are influenced by heating rates, species, and experimental methods. However, there is agreement in the order in which the individual polymeric components thermally degrade. Hemicelluloses pyrolyze at lower temperatures with cellulose and lignin at higher temperatures [33]. Cellulose has been shown to degrade via two processes including 1) breaking of a link in the carbon ring and cross-linking to produce char or 2) depolymerization and the production of levoglucosan (tar) which breaks down further into combustible gases or repolymerizes into char [19, 21]. Lignin has a more complex structure resulting in thermal degradation occurring over a wider temperature range (200-500°C) [29, 35, 36]. A more complete discussion related to the thermal degradation of each component is provided in Chapter 2.

Current engineering practice uses an isotherm at 288°C or 300°C as the delineation between the pyrolysis zone and the char layer [3, 4]. Using this isotherm has led to the development of a standard char formation rate which then allows engineers to calculate the residual strength of wood building products [37-40]. From Figure 1.5, there are two domains to the char layer. The domain closer to the pyrolysis zone has a temperature range between 300°C and 450°C and the structure of the wood still intact with visible distinctions between the earlywood and latewood. At 300°C the production of flammable pyrolyzates, products of pyrolysis, increases significantly. Between 300°C to 350°C, significant depolymerization of hemicellulose and cellulose occurs via the breaking of carbon-carbon bonds and leads to the formation of char, tar, and pyrolyzates [41]. Additionally, the aliphatic side chains in lignin begin splitting off from the aromatic rings [42]. At approximately 400°C, the carbon–carbon double bonds in the aromatic rings of lignin begin to split. As heat is conducted through the material, the phases will propagate into the wood and more wood will be converted to char. The char layer acts as an insulating layer and slows down the

pyrolysis kinetics, impeding further degradation of the wood [37]. At temperatures greater than 450°C, the second char layer domain is more degraded, and the structure is lost. This residue is a non-volatizing char, which undergoes further degradation referred to as glowing combustion. Glowing combustion, also called smoldering or afterglow, results from solid-phase oxidation of the remaining char [41]. Glowing combustion is the last phase and, when it goes to completion, the solid left behind is ash. Wood ash consists of all the minerals found in wood such as calcium, in the form of calcium carbonate or calcium oxide, and potassium in the form of potassium oxide or potassium carbonate [43].

There is a large body of literature on the pyrolysis of wood at various magnitudes from bulk wood to the individual polymeric components. Detailed studies and reviews exist for the char formation and the effects on strength in bulk wood [13, 37, 39, 40, 44-49], pyrolysis of wood and its components [4, 19, 21, 41, 50-57], and related models [7, 21, 51, 58-67]. Overall, there is agreement in the literature regarding pyrolysis of wood. The stages of pyrolysis, the order in which the polymeric components degrade along with their char yields, and the onset of rapid pyrolysis and char formation occurring at approximately 300°C are all commonly accepted. However, depending on the experimental methods, heating rates, and material tested, there is a wide scatter in the literature regarding the polymeric components' degradation temperatures [4]. Additionally, the degradation of the polymeric components is assumed to apply to bulk material but the chemical changes through the gradient caused by pyrolysis in bulk wood is still unknow. The studies that focused on the reduced strength of the fire exposed to wood [40, 49, 68-70] occurred at a length scale too large (>mm) to evaluate the microscopic effects of wood polymer degradation during pyrolysis. Evaluating the mechanical properties of the wood cell wall will provide necessary insight into the effect of the chemical changes during pyrolysis.

1.3 Outline of Work

This thesis work was divided along three different experimental lines. Each was focused at addressing specific gaps within current knowledge of wood degradation in fire and exploring new ways of probing how wood polymers thermally degrade in-situ.

The second chapter of this dissertation expands the current body of work on thermal degradation of wood to include a systematic comparison of the effect of atmosphere on thermal degradation of Douglas-fir latewood and the three main polymeric components using thermogravimetric analysis (TGA). Here, the pyrolysis reactions in nitrogen, which are historically used, are compared to the reactions in air up to 550°C. In addition to the effect of air, this study aims to address the critical question of whether pyrolysis of wood can be represented as the simple addition of its components, or if the components interact chemically or physically in a way that causes wood to have its own unique thermal degradation, that cannot be explained by the sum of its isolated components. Ultimately, the results provide a thermal degradation baseline that is used for comparison between thermal degradation based on mass loss versus thermal degradation based on bond scission investigated using a new technique in Chapter 3 of this work.

The third chapter describes experiments using x-ray photoelectron spectroscopy (XPS) to evaluate changes in chemical composition caused by thermal degradation of the wood polymers in bulk wood. While XPS has increased as a material characterization technique over the past 30 years [71], XPS has not been extensively used to study wood with a few exceptions [72-86]. To ensure proper measurements and instrumentation settings, a study of the use of XPS on wood was conducted. After this, the chemical bonds in isolated wood polymers exposed to high temperatures were evaluated. Finally, the chemical changes caused by pyrolysis were analyzed in charred

Douglas-fir latewood. This information provides, for the first time, an understanding of the chemical changes of thermally thick wood caused by pyrolysis in situ.

The fourth chapter describes characterization of the changes in mechanical properties at the cellular level. The chemical structure of wood and presence of the various wood polymers play an important role in the mechanical properties. Nanoindentation was used to evaluate mechanical changes in the S2 wood cell wall layer caused by pyrolysis. Evaluating the local effect on mechanical properties with regard to the chemical changes that occur during pyrolysis provides new insight into the sensitivity of the cell wall mechanics.

1.4 References

[1] L. M. Guss, "Engineered wood products: the future is bright," *Forest Products Journal,* vol. 45, p. 17, 1995.

[2] (March 1). Available: https://www.thinkwood.com/opportunities-for-wood/marketplace

[3] E. L. Schaffer, *Review of information related to the charring rate of wood* vol. 145: Forest Products Laboratory, 1966.

[4] A. I. Bartlett, R. M. Hadden, and L. A. Bisby, "A Review of Factors Affecting the Burning Behaviour of Wood for Application to Tall Timber Construction," *Fire Technology,* vol. 55, pp. 1-49, 2019/01// 2019.

[5] K. McGrattan, S. Hostikka, R. McDermott, J. Floyd, C. Weinschenk, and K. Overholt, "Fire dynamics simulator user's guide," *NIST special publication,* vol. 1019, 2013.

[6] K. B. McGrattan, H. R. Baum, R. G. Rehm, A. Hamins, G. P. Forney, J. Floyd*, et al.*, *Fire dynamics simulator--Technical reference guide*: National Institute of Standards and Technology, Building and Fire Research Laboratory, 2000.

[7] C. Lautenberger, "A Generalized Pyrolysis Model for Combustible Solids (PhD. thesis) University of California," ed: Berkeley, 2007.

[8] R. J. Moon, A. Martini, J. Nairn, J. Simonsen, and J. Youngblood, "Cellulose nanomaterials review: structure, properties and nanocomposites," *Chemical Society Reviews,* vol. 40, pp. 3941-3994, 2011.

[9] J. E. Jakes, C. G. Hunt, S. L. Zelinka, P. N. Ciesielski, and N. Z. Plaza, "Effects of Moisture on Diffusion in Unmodified Wood Cell Walls: A Phenomenological Polymer Science Approach," *Forests,* vol. 10, p. 1084, 2019.

[10] D. Green, J. Winandy, and D. Kretschmann, "Mechanical properties of wood-wood as an engineering material," *General Technical Report FPL-TR,* vol. 113, 1999.

[11] A. C. Wiedenhoeft and R. B. Miller, "Structure and function of wood," *Handbook of wood chemistry and wood composites,* pp. 9-33, 2005.

[12] D. Fengel and G. Wegener, *Wood: chemistry, ultrastructure, reactions*: Walter de Gruyter, 2011.

[13] E. Mikkola, "Charring of wood," *Tutkimuksia-Valtion Teknillinen Tutkimuskeskus,* 1990.
[14] A. Atreya, "Pyrolysis, ignition and fire spread on horizontal surfaces of wood," Harvard University, 1983.
[15] R. M. Rowell, *Handbook of wood chemistry and wood composites*: CRC press, 2012.
[16] S. Park, J. O. Baker, M. E. Himmel, P. A. Parilla, and D. K. Johnson, "Cellulose crystallinity index: measurement techniques and their impact on interpreting cellulase performance," *Biotechnology for biofuels,* vol. 3, p. 10, 2010.
[17] N. Plaza, "Neutron scattering studies of nano-scale wood-water interactions," *Madison, Wisconsin, University,* 2017.
[18] PerkinElmer. (2001). *ChemDraw*. Available: https://chemdrawdirect.perkinelmer.cloud/js/sample/index.html#
[19] F. Shafizadeh, "The Chemistry of Pyrolysis and Combustion," in *The Chemistry of Solid Wood*. vol. 207, R. M. Rowell, Ed., ed Washington, DC: American Chemical Society, 1984.
[20] A. N. Fernandes, L. H. Thomas, C. M. Altaner, P. Callow, V. T. Forsyth, D. C. Apperley, *et al.*, "Nanostructure of cellulose microfibrils in spruce wood," *Proceedings of the National Academy of Sciences,* vol. 108, pp. E1195-E1203, 2011.
[21] S. Sinha, A. Jhalani, M. Ravi, and A. Ray, "Modelling of pyrolysis in wood: A review," *SESI Journal,* vol. 10, pp. 41-62, 2000.
[22] H. Chen, *Biotechnology of lignocellulose*: Springer, 2005.
[23] A. Duval and M. Lawoko, "A review on lignin-based polymeric, micro-and nano-structured materials," *Reactive and Functional Polymers,* vol. 85, pp. 78-96, 2014.
[24] C. Crestini, M. Crucianelli, M. Orlandi, and R. Saladino, "Oxidative strategies in lignin chemistry: A new environmental friendly approach for the functionalisation of lignin and lignocellulosic fibers," *Catalysis today,* vol. 156, pp. 8-22, 2010.
[25] E. Mészáros, E. Jakab, and G. Várhegyi, "TG/MS, Py-GC/MS and THM-GC/MS study of the composition and thermal behavior of extractive components of Robinia pseudoacacia," *Journal of Analytical and Applied Pyrolysis,* vol. 79, pp. 61-70, 2007.
[26] G. Várhegyi, M. G. Grønli, and C. Di Blasi, "Effects of sample origin, extraction, and hot-water washing on the devolatilization kinetics of chestnut wood," *Industrial & engineering chemistry research,* vol. 43, pp. 2356-2367, 2004.
[27] M. G. Grønli, G. Várhegyi, and C. Di Blasi, "Thermogravimetric analysis and devolatilization kinetics of wood," *Industrial & Engineering Chemistry Research,* vol. 41, pp. 4201-4208, 2002.
[28] A. Shebani, A. Van Reenen, and M. Meincken, "The effect of wood extractives on the thermal stability of different wood species," *Thermochimica Acta,* vol. 471, pp. 43-50, 2008.
[29] F. Beall, "Thermogravimetric analysis of wood lignin and hemicelluloses," *Wood and Fiber Science,* vol. 1, pp. 215-226, 1969.
[30] F. L. Browne, *Theories of the combustion of wood and its control*: Madison, Wis.: US Dept. of Agriculture, Forest Service, Forest Products Laboratory, 1958.
[31] F. Shafizadeh and P. P. Chin, "Thermal deterioration of wood," *Wood technology: chemical aspects,* vol. 43, pp. 57-81, 1977.
[32] E. T. Engelund, L. G. Thygesen, S. Svensson, and C. A. Hill, "A critical discussion of the physics of wood–water interactions," *Wood science and technology,* vol. 47, pp. 141-161, 2013.

[33] M. Dietenberger and L. Hasburgh, "Wood Products Thermal Degradation and Fire," *Reference Module in Materials Science and Materials Engineering,* pp. 1-8, 2016.
[34] R. H. White and E. L. Schaffer, "Transient moisture gradient in fire-exposed wood slab," *Wood and Fiber Science,* vol. 13, pp. 17-38, 2007.
[35] H. Kawamoto, "Lignin pyrolysis reactions," *Journal of Wood Science,* vol. 63, pp. 117-132, 2017.
[36] M. Brebu and C. Vasile, "Thermal degradation of lignin—a review," *Cellulose Chemistry & Technology,* vol. 44, p. 353, 2010.
[37] R. H. White, *Charring rates of different wood species*: University of Wisconsin--Madison, 1988.
[38] R. H. White and E. V. Nordheim, "Charring rate of wood for ASTM E 119 exposure," *Fire Technology,* vol. 28, pp. 5-30, 1992.
[39] R. H. White and H. C. Tran, "Charring rate of wood exposed to a constant heat flux," 1996.
[40] J. Schmid, A. Just, M. Klippel, and M. Fragiacomo, "The reduced cross-section method for evaluation of the fire resistance of timber members: discussion and determination of the zero-strength layer," *Fire Technology,* vol. 51, pp. 1285-1309, 2015.
[41] F. Shafizadeh, "Introduction to pyrolysis of biomass," *Journal of Analytical and Applied Pyrolysis,* vol. 3, pp. 283-305, 1982.
[42] J. G. Speight, *The biofuels handbook*: Royal Society of Chemistry, 2011.
[43] T. R. Naik and R. N. Kraus, "Wood ash: a new source of pozzolanic material," *Submitted to Concrete International,* 2001.
[44] E. L. Schaffer, "CHARRING RATE OF SELECTED WOODS--TRANSVERSE TO GRAIN," DTIC Document1967.
[45] V. Babrauskas, "Charring rate of wood as a tool for fire investigations," *Fire Safety Journal,* vol. 40, pp. 528-554, 2005.
[46] K. L. Friquin, "Charring rates of heavy timber structures for Fire Safety Design: A study of the charring rates under various fire exposures andthe influencing factors," 2010.
[47] J. König, *One-dimensional charring of timber exposed to standard and parametric fires in initially unprotected and postprotection situations*, 1999.
[48] T. T. Lie, "A method for assessing the fire resistance of laminated timber beams and columns," *Canadian Journal of Civil Engineering,* vol. 4, pp. 161-169, 1977.
[49] J.-i. Suzuki, T. Mizukami, T. Naruse, and Y. Araki, "Fire Resistance of Timber Panel Structures Under Standard Fire Exposure," *Fire Technology,* vol. 52, pp. 1015-1034, 2016/07/07/2016- -12 2016.
[50] A. A. A. Abuelnuor, M. A. Wahid, S. E. Hosseini, A. Saat, K. M. Saqr, H. H. Sait*, et al.*, "Characteristics of biomass in flameless combustion: A review," *Renewable & Sustainable Energy Reviews,* vol. 33, pp. 363-370, 2014/05// 2014.
[51] C. Di Blasi, "Modeling chemical and physical processes of wood and biomass pyrolysis," *Progress in Energy and Combustion Science,* vol. 34, pp. 47-90, 2008.
[52] T. R. Rao and A. Sharma, "Pyrolysis rates of biomass materials," *Energy,* vol. 23, pp. 973-978, 1998.
[53] K. Raveendran, A. Ganesh, and K. C. Khilar, "Pyrolysis characteristics of biomass and biomass components," *Fuel,* vol. 75, pp. 987-998, 1996.
[54] F. Shafizadeh, "Pyrolysis and combustion of cellulosic materials," in *Advances in carbohydrate chemistry*. vol. 23, ed: Elsevier, 1968, pp. 419-474.

[55] K. Slopiecka, P. Bartocci, and F. Fantozzi, "Thermogravimetric analysis and kinetic study of poplar wood pyrolysis," *Applied Energy,* vol. 97, pp. 491-497, 2012.
[56] H. Yang, R. Yan, H. Chen, D. H. Lee, and C. Zheng, "Characteristics of hemicellulose, cellulose and lignin pyrolysis," *Fuel,* vol. 86, pp. 1781-1788, 2007.
[57] A. C. Y. Yuen, T. B. Y. Chen, G. H. Yeoh, W. Yang, S. C. P. Cheung, M. Cook*, et al.*, "Establishing pyrolysis kinetics for the modelling of the flammability and burning characteristics of solid combustible materials," *Journal of Fire Sciences,* vol. 36, pp. 494-517, 2018/11// 2018.
[58] K. M. Bryden and M. J. Hagge, "Modeling the combined impact of moisture and char shrinkage on the pyrolysis of a biomass particle☆," *Fuel,* vol. 82, pp. 1633-1644, 2003.
[59] K. M. Bryden, K. W. Ragland, and C. J. Rutland, "Modeling thermally thick pyrolysis of wood," *Biomass and Bioenergy,* vol. 22, pp. 41-53, 2002.
[60] Y. M. Ding, R. Zhou, C. J. Wang, K. H. Lu, and S. X. Lu, "Modeling and analysis of bench-scale pyrolysis of lignocellulosic biomass based on merge thickness," *Bioresource technology,* vol. 268, pp. 77-80, 2018/11// 2018.
[61] T. Fateh, T. Rogaume, J. Luche, F. Richard, and F. Jabouille, "Modeling of the thermal decomposition of a treated plywood from thermo-gravimetry and Fourier-transformed infrared spectroscopy experimental analysis," *Journal of analytical and applied pyrolysis,* vol. 101, pp. 35-44, 2013.
[62] A. Galgano, C. Di Blasi, S. Ritondale, and A. Todisco, "Numerical simulation of the glowing combustion of moist wood by means of a front-based model," *Fire and Materials,* vol. 38, pp. 639-658, 2014/10// 2014.
[63] A. M. Grishin and A. S. Yakimov, "Mathematical modeling of the wood ignition process," *Thermophysics and Aeromechanics,* vol. 20, pp. 463-475, 2013/12// 2013.
[64] M. Janssens, "Thermo-physical properties for wood pyrolysis models," in *Pacific Timber Engineering Conference, Gold Coast, Australia*, 1994, pp. 607-618.
[65] H.-C. Kung, "A mathematical model of wood pyrolysis," *Combustion and flame,* vol. 18, pp. 185-195, 1972.
[66] K. Y. Li, D. S. W. Pau, J. H. Wang, and J. Ji, "Modelling pyrolysis of charring materials: determining flame heat flux using bench-scale experiments of medium density fibreboard (MDF)," *Chemical Engineering Science,* vol. 123, pp. 39-48, 2015/02// 2015.
[67] N. Liu, W. Fan, R. Dobashi, and L. Huang, "Kinetic modeling of thermal decomposition of natural cellulosic materials in air atmosphere," *Journal of Analytical and Applied Pyrolysis,* vol. 63, pp. 303-325, 2002.
[68] P. Moss, A. Buchanan, M. Fragiacomo, and C. Austruy, "Experimental Testing and Analytical Prediction of the Behaviour of Timber Bolted Connections Subjected to Fire," *Fire Technology,* vol. 46, pp. 129-148, 2010/01/07/2014- -19 2010.
[69] D. Bender, F. Woeste, E. Schaffer, and C. Marx, "Reliability Formulation for the Strength and Fire Endurance of Glued-Laminated Beams," ed. Madison, WI: USDA Forest Products Laboratory, 1985.
[70] Z. P. Ni and P. F. Qiu, "Experimental Study on Fire Resistance Performance of Glulam Beams," *Applied Mechanics and Materials,* vol. 193-194, p. 539, 2012/08/10/2018- -06 2012.
[71] G. Greczynski and L. Hultman, "X-ray photoelectron spectroscopy: Towards reliable binding energy referencing," *Progress in Materials Science,* p. 100591, 2019.

[72] X. Hua, S. Kaliaguine, B. Kokta, and A. Adnot, "Surface analysis of explosion pulps by ESCA Part 1. Carbon (1s) spectra and oxygen-to-carbon ratios," *Wood Science and Technology,* vol. 27, pp. 449-459, 1993.

[73] X. Hua, S. Kaliaguine, B. Kokta, and A. Adnot, "Surface analysis of explosion pulps by ESCA Part 2. Oxygen (1s) and sulfur (2p) spectra," *Wood Science and Technology,* vol. 28, 1993.

[74] D. Kamdem, B. Riedl, A. Adnot, and S. Kaliaguine, "ESCA spectroscopy of poly (methyl methacrylate) grafted onto wood fibers," *Journal of applied polymer science,* vol. 43, pp. 1901-1912, 1991.

[75] K. Koljonen, M. Österberg, L.-S. Johansson, and P. Stenius, "Surface chemistry and morphology of different mechanical pulps determined by ESCA and AFM," *Colloids and Surfaces A: Physicochemical and Engineering Aspects,* vol. 228, pp. 143-158, 2003.

[76] J. Bañuls-Ciscar, M.-L. Abel, and J. F. Watts, "Characterisation of cellulose and hardwood organosolv lignin reference materials by XPS," *Surface Science Spectra,* vol. 23, pp. 1-8, 2016.

[77] J. Bañuls-Ciscar, D. Pratelli, M. L. Abel, and J. F. Watts, "Surface characterisation of pine wood by XPS," *Surface and Interface Analysis,* vol. 48, pp. 589-592, 2016.

[78] G. N. Inari, M. Pétrissans, S. Dumarcay, J. Lambert, J. Ehrhardt, M. Šernek*, et al.*, "Limitation of XPS for analysis of wood species containing high amounts of lipophilic extractives," *Wood Science and Technology,* vol. 45, pp. 369-382, 2011.

[79] G. N. Inari, M. Petrissans, J. Lambert, J. Ehrhardt, and P. Gérardin, "XPS characterization of wood chemical composition after heat-treatment," *Surface and interface analysis,* vol. 38, pp. 1336-1342, 2006.

[80] L.-S. Johansson, J. Campbell, P. Fardim, A. H. Hultén, J.-P. Boisvert, and M. Ernstsson, "An XPS round robin investigation on analysis of wood pulp fibres and filter paper," *Surface science,* vol. 584, pp. 126-132, 2005.

[81] L.-S. Johansson, J. Campbell, K. Koljonen, and P. Stenius, "Evaluation of surface lignin on cellulose fibers with XPS," *Applied surface science,* vol. 144, pp. 92-95, 1999.

[82] D. Kocaefe, X. Huang, Y. Kocaefe, and Y. Boluk, "Quantitative characterization of chemical degradation of heat-treated wood surfaces during artificial weathering using XPS," *Surface and interface analysis,* vol. 45, pp. 639-649, 2013.

[83] C.-M. Popescu, C.-M. Tibirna, and C. Vasile, "XPS characterization of naturally aged wood," *Applied Surface Science,* vol. 256, pp. 1355-1360, 2009.

[84] Q. Shen, P. Mikkola, and J. B. Rosenholm, "Quantitative characterization of the subsurface acid–base properties of wood by XPS and Fowkes theory," *Colloids and Surfaces A: Physicochemical and Engineering Aspects,* vol. 145, pp. 235-241, 1998.

[85] G. Sinn, A. Reiterer, and S. Stanzl-Tschegg, "Surface analysis of different wood species using X-ray photoelectron spectroscopy (XPS)," *Journal of materials science,* vol. 36, pp. 4673-4680, 2001.

[86] N. M. Stark and L. M. Matuana, "Surface chemistry changes of weathered HDPE/wood-flour composites studied by XPS and FTIR spectroscopy," *Polymer Degradation and Stability,* vol. 86, pp. 1-9, 2004.

Chapter 2. Thermal degradation of wood and its constituents

2.1 Introduction

The thermal degradation of wood consists of a series of complex chemical reactions and physical transformations. There is a large body of literature on this subject with variables ranging from the physical and chemical heterogeneity of wood, different wood species and representative lignocellulosic materials studied, and differences in experimental methods (e.g. preparation of the material, heating rate, atmosphere) [1]. Frequently, since cellulose is the main cell wall component of wood and its pyrolysis is simpler to model than wood itself, the thermal degradation of cellulose is often used as a surrogate for thermal degradation of wood [2]. Despite being the largest cell wall component of wood, it represents only approximately 40% of the dry weight of wood, leaving the other components that together form the majority of the wood cell wall ignored. Wood has also been represented as a combination of its polymeric components[3]. These oversimplifications may lead to inaccuracies when predicting the thermal degradation of solid wood. Only recently was the exact chemical composition of olive trees determined and the thermal degradation of the components compared to the biomass as a whole [4]. Additionally, a bulk of the literature focuses on the conversion of biomass to bioenergy and, as such, carries out the experiments in inert environments typical of the conditions used during biomass gasification process. However, during a structure fire, wood building products will be exposed to varying levels of oxygen, which has been shown to affect the pyrolysis kinetics [5]. A systematic study comparing thermal degradation of both wood and its constituents in air and nitrogen is necessary for two reasons. The first is to determine the effect of atmosphere on the initial thermal degradation of wood exposed to fire

before a char layer is formed. The second is to learn if using the individual cell wall components to model wood pyrolysis is valid for any given atmosphere.

Here, I describe experiments using thermogravimetric analysis (TGA) in both inert and oxidizing atmospheres to examine the thermal degradation of the three main polymeric components of wood as well as intact Douglas-fir latewood. I compare Douglas-fir with the behavior of a composite ("rule-of-mixtures") system composed of the three polymers proportioned for Douglas-fir.

2.2 Background on Thermogravimetric Analysis

TGA measures changes in sample mass either as temperature varies (dynamic) or for a period of time at one temperature (isothermal) in a controlled atmosphere which may include nitrogen, argon, carbon dioxide, air, oxygen or other gases. Change in mass is commonly used to detect physical phenomena such as phase transitions, sorption in hygroscopic materials, thermal decomposition, and solid-gas reactions like oxidation or reduction [6].

Thermogravimetric Analysis and Wood

Numerous TGA studies have been conducted on wood and its polymeric components. Most of the previous TGA literature on lignocellulosic materials was motivated by the need to understand pyrolysis kinetics for use of these materials as biofuel feedstock. Due to this, many of the experiments related to the pyrolysis of lignocellulosic materials have been conducted in nitrogen-rich atmospheres and focused on non-woody biomass such as corn [7] and cotton [8]. Studies on the isolated wood polymers, hemicellulose, cellulose, and lignin, have also been carried out showing hemicellulose as the least thermally stable component and lignin being the most thermally stable component [1, 9]. Furthermore, these studies have shown that the thermal decomposition proceeds in three stages regardless of what material is being pyrolyzed: water evaporation, active

pyrolysis (main decomposition phase), and passive pyrolysis (small mass loss above 500°C). However, these conclusions drawn from previous TGA measurements on wood [10, 11] and its components [12, 13] have used inert (non-oxidizing) environments.

Experimental and theoretical studies evaluating the effect of oxygen concentration on the pyrolysis of wood and its constituents have been conducted, but there exists no comparison of wood with its components [5, 9, 14, 15], which would be helpful for understanding the physical processes behind pyrolysis. In nitrogen, the thermal degradation of wood and its polymeric components occurs in two main stages denoted as active and passive pyrolysis [7]. As defined by Kumar [3], the active pyrolysis stage is characterized by rapid weight loss. Passive pyrolysis is when the residue continues to lose mass, but at a much slower rate. The passive pyrolysis stage observed in nitrogen becomes a second active pyrolysis stage known as the residual pyrolysis stage in air [7]. After the residual pyrolysis stage, the remaining, negligible mass is composed of not readily combustible components such as minerals and is known as ash. Ohlemiller et al. evaluated white pine (*Pinus strobus*) and red oak (*Quercus rubra*) using a radiant heating apparatus under oxygen concentrations of 0%, 10.5% and 21% and found that the maximum mass loss rate increased with increasing oxygen concentration. In a fire, the surface of wood will increase in temperature rapidly, pyrolyze and then release volatiles. In the presence of oxygen and heat, the volatiles may ignite and undergo a rapid, exothermic combustion reaction [16]. Ignition is the onset of combustion, whether flaming or smoldering. After ignition, most of the available oxygen from air at the wood's surface will be consumed by the flame and greatly limiting the air that is able to diffuse into the wood. Flames provide a heat flux into the wood in addition to that provided by an external heat source, continuing the production of pyrolysis products in an energy feedback process [17]. The oxygen levels throughout a compartment available to sustain flaming will vary along with the

phases of the fire [5]. Fang et al. investigated the effects of oxygen concentration from 0% to 100% on the pyrolysis of merbau wood (*Intsia* spp.) and found similar mass loss rates in different atmospheres below temperatures of 250°C with maximum mass loss rates shifting to lower temperatures with increased oxygen concentrations. The presence of oxygen has also been shown to promote thermal degradation at lower temperatures, promote the combustion of the char residue [18], and cause pyrolysis and combustion to coexist [14]. As a result, pyrolysis in air is more complex than most of the literature data collected in inert atmospheres and a deeper understanding of pyrolysis applicable to wood building products in varying levels of oxygen is needed.

It has also been suggested that the pyrolysis of wood can be considered as an aggregate of its three main components, namely, cellulose, hemicelluloses and lignin [1, 19-21]. Some have found this method is not appropriate [22-24], but their experiments were carried out in inert environments and rapid pyrolysis conditions and the applicability of their findings to the pyrolysis of wood building products is unknown. Garcia-Maraver et al. evaluated the chemical composition of biomass (leaves, pruning residues, and wood) from olive trees and found the concentration of hemicellulose, cellulose and lignin directly affected the thermal behavior in air [4]. However, the findings are applicable to olive tree residues as a source of thermal energy and not to the thermal degradation behavior of wood building products.

2.3 Materials and Methods

Materials

Three Douglas-fir (*Pseudotsuga menziesii*) specimens for the TGA experiments were obtained from the latewood of a single growth ring with approximate dimensions of 1.5 mm by 1.5 mm by 0.5 mm (longitudinal by tangential by radial). Douglas-fir was chosen as it accounts for over 45%

of the softwood lumber produced annually in the United States. It is also a common construction material due to its high strength-to-weight ratio [25, 26].

Three typical lignocellulosic materials were obtained from Sigma Aldrich: α–cellulose (CAS Registry #: 9004-34-6), arabinogalactan from larch wood (CAS Registry #: 9036-66-2), and Kraft lignin (CAS Registry #: 8068-05-1). The α–cellulose, referred to here as cellulose, was made by generating wood pulp and soaking it in a solution of sodium hydroxide resulting in a white, homogeneous powder [27]. The arabinogalactan, hereafter referred to here as hemicellulose, from larch (*Larix decidua*) is a highly branched polysaccharide consisting of a galactan backbone with side-chains of galactose and arabinose sugars and comes in the form of a white powder. The Kraft lignin, referred to here as lignin, was a brown powder with low sulfonate content. Each experiment was run in triplicate.

Methods

Two total carbohydrate analyses were conducted on wood from the same board of Douglas-fir that the TGA specimens were obtained from to determine the composition. Fred Matt, a chemist at the Forest Products Laboratory, conducted the carbohydrate analysis of the Douglas-fir. The method used was that published by the National Renewable Research Laboratory (NERL) [28] combined with the high-performance liquid chromatography with pulsed amperometric detector (HPLC-PAD) method from Davis [29].

For the purposes of setting lower and upper bounds of the atmosphere found for wood building products, two atmospheres were tested: nitrogen and air (breathing quality, grade D). The oxygen content of the air was between 19.5 and 23.5%. The thermal stability of the wood and the polymer materials were measured using a TGA (Pyris 1 TGA, PerkinElmer Inc., Waltham, MA) with a

reported precision for the balance is reported to be 0.001% and temperature precision of ±2°C. The samples (3-15 mg initial weight) were held at 105°C for 10 minutes to remove all moisture. After this initial period, the samples were heated from 105°C to 550°C at a heating rate of 10°C/min with 20 mL/min of either nitrogen or air in the 2.5 mL furnace chamber. Mass was recorded at a frequency of 1 Hz. Each material (Douglas-fir latewood, hemicellulose, cellulose, and lignin) was run in triplicate.

2.4 Results

Composition of the Wood

The results of the analyses are presented in Table 2.1. The glucan (cellulose) for these specimens are on the lower end of values typically observed for Douglas-fir, which has been reported between 35-48% of the total composition [30-32].

Table 2.1: Lignin and carbohydrate composition of Douglas-fir

	Hemicelluloses				Cellulose	Lignin	Total Carbohydrate	Total Yield
Sample	Arabinan	Galactan	Xylan	Mannan	Glucan	K. Lignin		
1	0.65%	4.75%	5.42%	10.87%	36.72%	30.9%	58.43%	89.4%
2	0.69%	4.31%	5.16%	10.82%	35.64%	30.9%	56.61%	87.5%

Comparison between pyrolysis under inert and oxidizing environments

The dehydration stage reported by others [7, 33] was not observed here because all samples were dried at 105°C for 10 minutes prior to increasing the temperature. In nitrogen, the thermal degradation of all four materials occurred in active and passive pyrolysis. Thermal analysis of the four materials heated dynamically at a heating rate of 10°C/min reveals distinct differences between inert and reactive environments. Figure 2.1 shows the mass fraction (MF), normalized to the initial mass, for each material. Figure 2.1 presents the averages for each material since the

individual curves in the triplicate are almost undistinguishable. From these TGA curves, the thermal degradation for hemicellulose in nitrogen begins slowly at 193°C active pyrolysis from approximately 250°C to 350°C. Above 350°C, the passive pyrolysis stage occurs. In air, the active pyrolysis stage occurs between 250°C to 330°C with the residual stage occurring between 330°C and 450°C. The cellulose behaves similarly to hemicellulose in both the nitrogen and air environments, but at higher temperatures. The thermal degradation for cellulose in nitrogen begins slowly at 230°C active pyrolysis between 320°C and 390°C, and a leveling out in the passive pyrolysis stage at 400°C. In air, the active pyrolysis stage for cellulose begins at 246°C with a rapid decrease in a smaller temperature range of 320°C to 350°C. The residual pyrolysis stage for cellulose in air occurs between 350°C and 490°C. The lignin is the most thermally stable with a slow, consistent mass loss in nitrogen and similar mass loss in air until 350°C where the degradation increases until 500°C. Based on the TGA curve features, Douglas-fir latewood responds in the same way to the dynamic heating as cellulose with the onset of degradation beginning at 218°C in nitrogen and 233°C in air. The Douglas-fir latewood active pyrolysis in both nitrogen and air occurred between 250°C and 375°C with residual pyrolysis stage in air between 350°C and 480°C.

a)

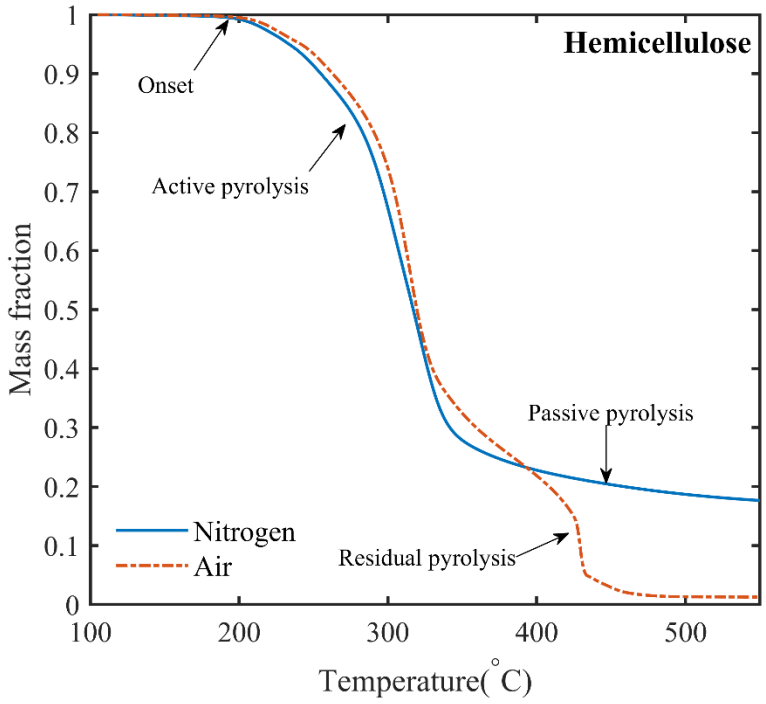
Hemicellulose
Onset
Active pyrolysis
Passive pyrolysis
Residual pyrolysis
Nitrogen
Air
Mass fraction
Temperature(°C)
0
0.1
0.2
0.3
0.4
0.5
0.6
0.7
0.8
0.9
1
100
200
300
400
500

b)

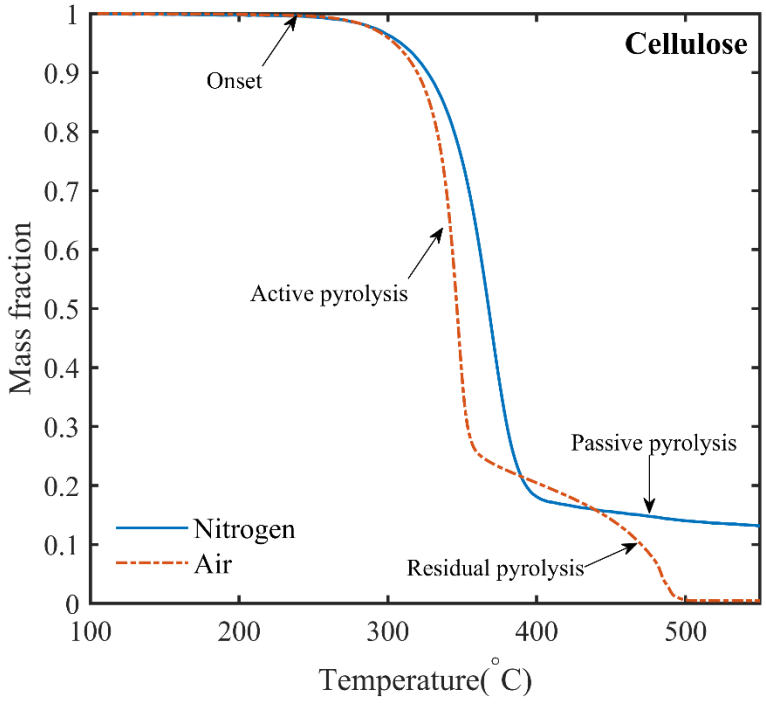
Cellulose
Onset
Active pyrolysis
Passive pyrolysis
Residual pyrolysis
Nitrogen
Air
Mass fraction
Temperature(°C)
0
0.1
0.2
0.3
0.4
0.5
0.6
0.7
0.8
0.9
1
100
200
300
400
500

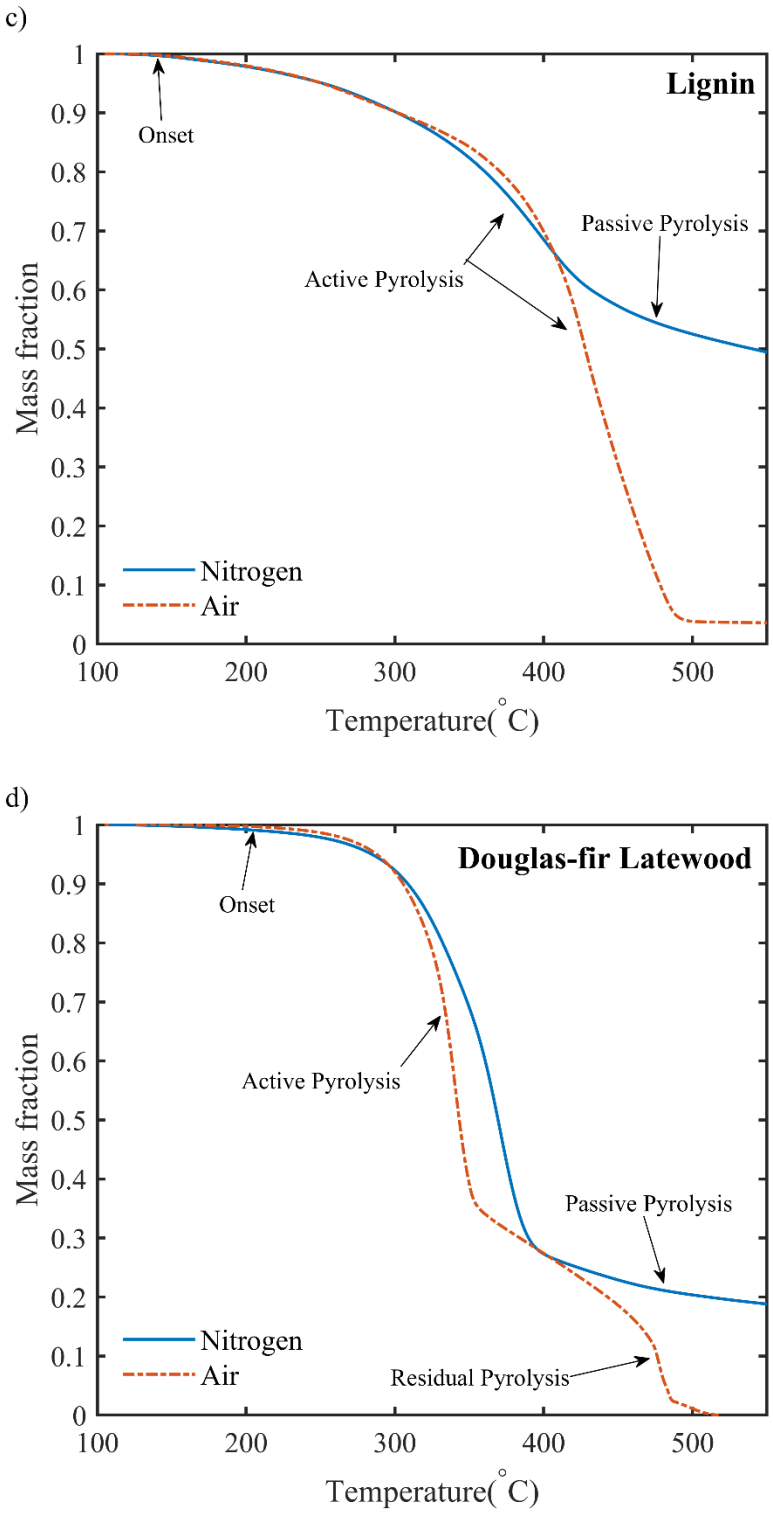

Figure 2.1: Dynamic TGA curves of a) Hemicellulose, b) Cellulose, c) Lignin and d) Douglas-fir latewood. Averages of triplicates are presented for the materials conducted in both air and nitrogen.

At high temperatures in air, the mass appears to suddenly move backwards along the abscissa and then continues to move forward, particularly for cellulose and Douglas-fir latewood materials (Figure 2.1b and 2.1d, respectively). As pointed out by Freiman et al., this behavior is more easily explained as ignition events when the temperature is plotted versus the time as shown in Figure 2.2 [34]. The sharp peaks in Figure 2.2 represent the ignition points with a sharp increase in temperature. The hemicellulose material self-ignites at 430°C while the cellulose and Douglas-fir latewood self-ignite at higher temperatures of 490°C and 480°C, respectively. Interestingly, lignin does not have the same sharp peak but still exhibits an increase in temperature between 400°C and 493°C, indicating an exothermic reaction taking place. This exothermic reaction is part of the residual pyrolysis phase in lignin and is akin to combustion.

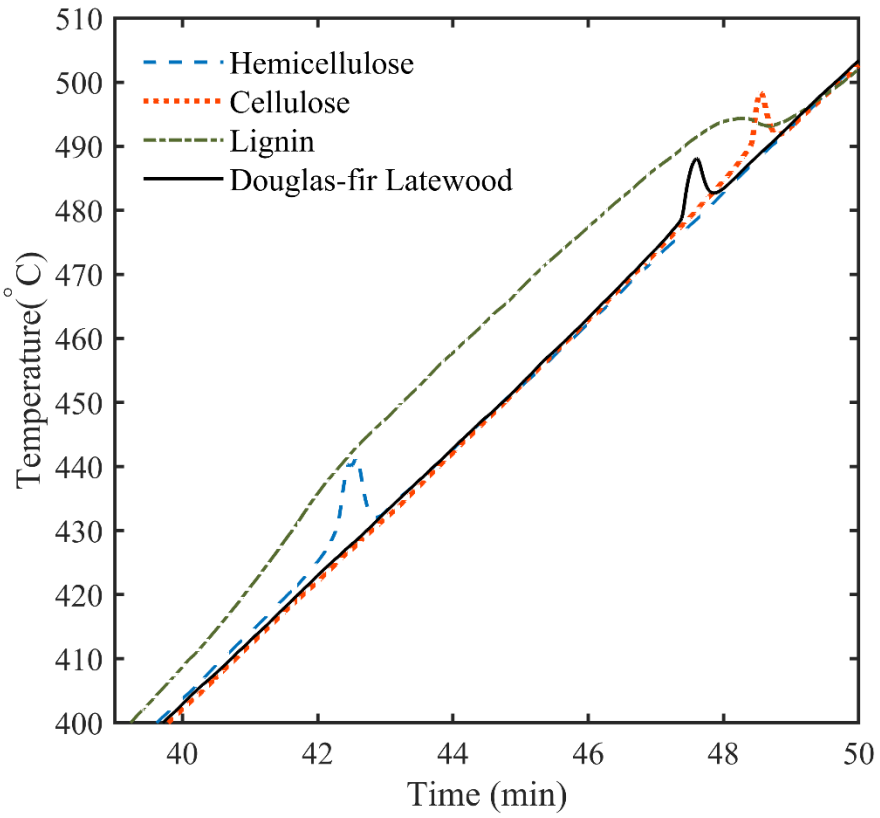

Figure 2.2: Plot of average sample temperature in air vs. time for each material. This plot is focused on the higher temperature range (380°C to 520°C) to highlight specific features in the data.

The differential thermogravimetric curve (DTG) is often used to evaluate features that are not readily discernable in the thermogravimetric curve. For instance, any change in rate of weight loss may be seen more clearly as a trough and the height of that trough above $\frac{dMF}{dt} = 0$ provides a measurement of the stability of the intermediate material and the amount two consecutive reactions (peaks) overlap. Figure 2.3 includes the DTG curves for the four materials tested with the change in mass fraction (MF′) with respect to time versus temperature.

a)

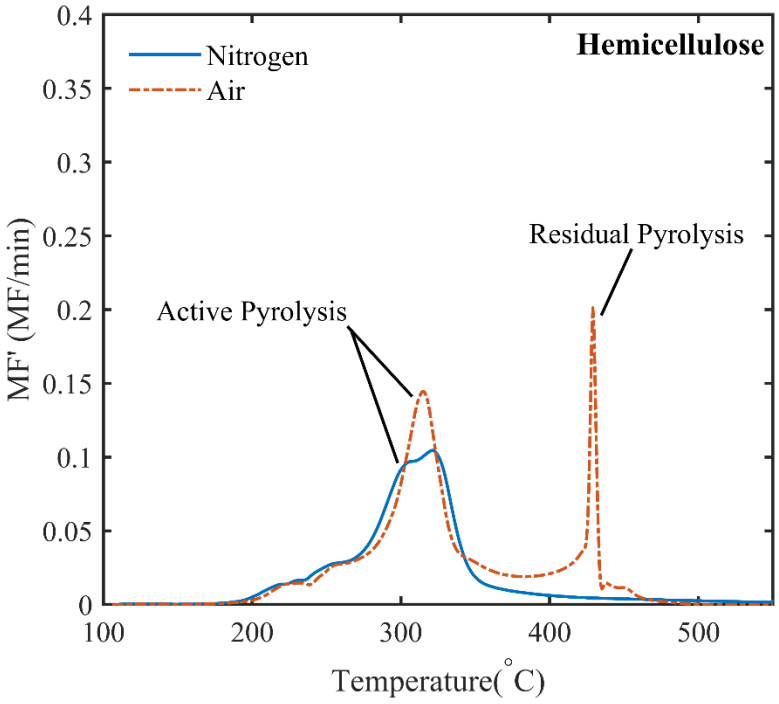
Hemicellulose
Nitrogen
Air
Residual Pyrolysis
Active Pyrolysis
MF' (MF/min)
0.4
0.35
0.3
0.25
0.2
0.15
0.1
0.05
0
100
200
300
400
500
Temperature(°C)

b)

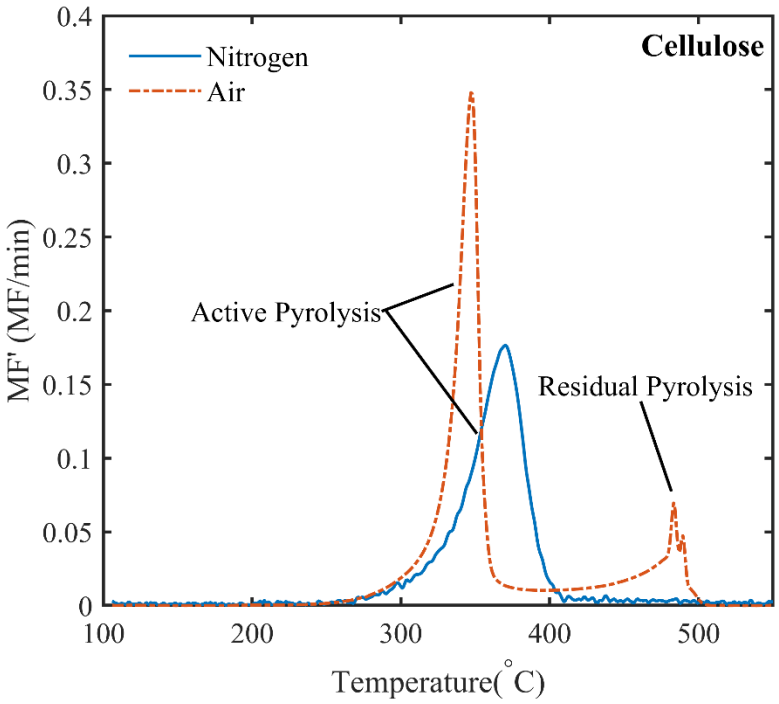
Cellulose
Nitrogen
Air
Active Pyrolysis
Residual Pyrolysis
MF' (MF/min)
0.4
0.35
0.3
0.25
0.2
0.15
0.1
0.05
0
100
200
300
400
500
Temperature(°C)

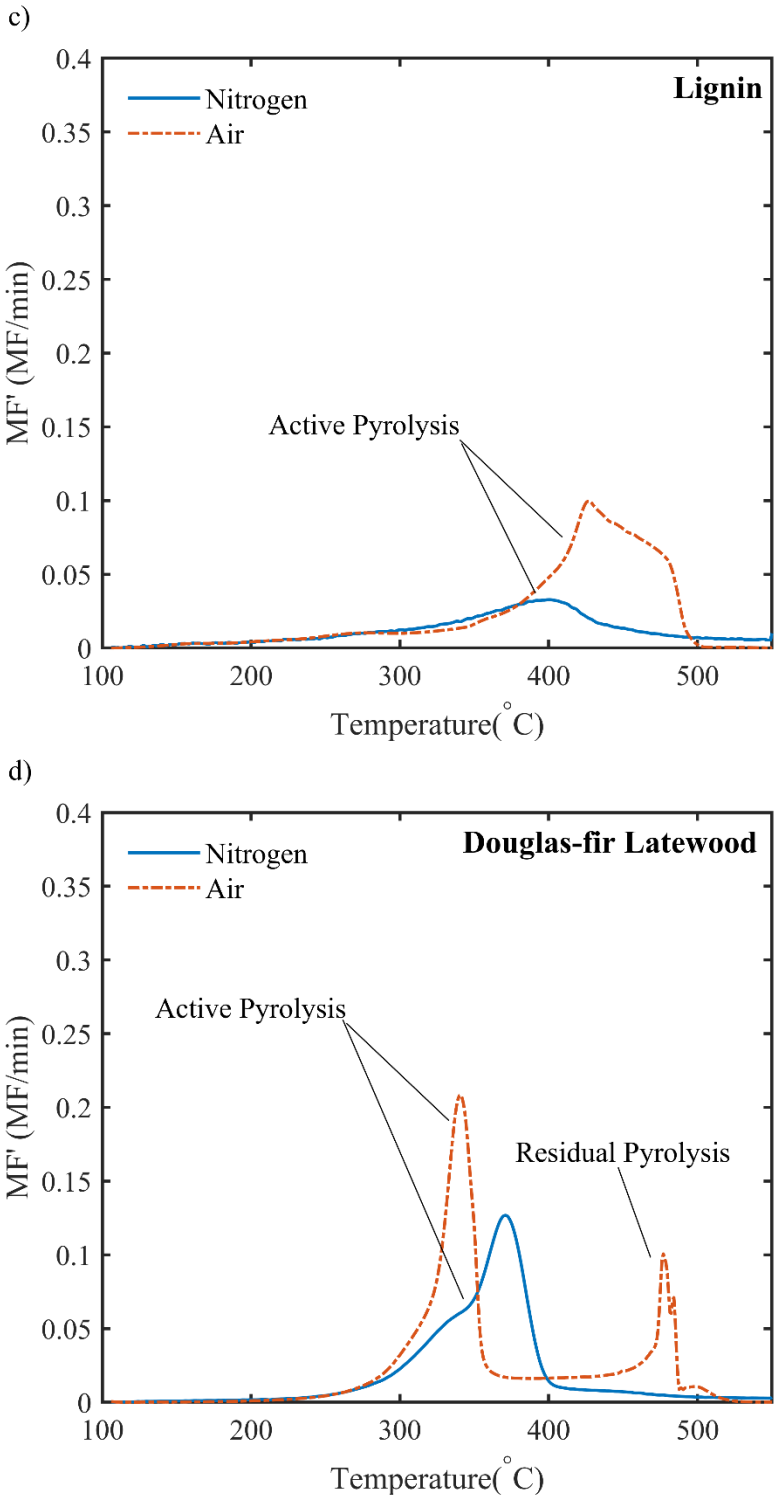

Figure 2.3: DTG curves of a) Hemicellulose, b) Cellulose, c) Lignin and d) Douglas-fir latewood. Averages of triplicates for each material are presented.

For the hemicellulose in both nitrogen and air, active pyrolysis begins with slowly between the temperatures of 190°C to 230°C. At 230°C there is a trough before increasing again to a shoulder before the peak mass loss rate. In air, the trough between temperatures of 340°C and 420°C is above the line $\frac{dMF}{dt} = 0$, indicating that the intermediate material is not stable at high temperatures in air and is still losing mass before ignition occurs where there is a second peak mass loss rate at 428°C. The cellulose in nitrogen has lower mass loss rates during active pyrolysis. Also, the peak mass loss rate for the cellulose in nitrogen occurs at a higher temperature compared to samples in air. Similar to the hemicellulose, the cellulose residue is not stable and continues to lose mass until ignition occurs. In nitrogen, the initial mass loss rate for the lignin is the same as in air but continues to increase steadily to a small but detectable peak, indicating slow pyrolysis. In air, the differential TGA curve for lignin reveal shoulders both before and after the largest peak during active pyrolysis, indicating overlapping reactions. Again, the Douglas-fir latewood reacted like the hemicellulose and cellulose with slightly slower rates during active pyrolysis in nitrogen compared to samples in air and higher temperatures required to start pyrolysis. Additionally, the trough between peaks in air indicates a slightly less stable material left after the initial active pyrolysis.

Table 2.2 summarizes the temperatures at the onset of volatilization and at the first peak of active pyrolysis, as well as the percent volatilization at given temperatures. The values in the table are averages for each material. The onset temperature is based on when a deflection is first observed from the established baseline prior to the thermal event [35]. For each material, the percent mass volatized in nitrogen versus air are similar until temperatures are above 300°C. A substantial difference in the percent of material volatized occurred at 350°C in both the cellulose and Douglas-fir latewood. At this temperature, the volatized percent of the cellulose and Douglas-fir latewood in air is more than twice that in nitrogen. Before the cellulose and Douglas-fir latewood reach

400°C in either environment, they reach similar amounts of material volatilized and diverge again above 500°C. The presence of oxygen has also been shown to promote thermal degradation at lower temperatures. However, here, lignin had a peak mass loss rate at a higher temperature in air than nitrogen while the other three materials had a peak mass loss rate at lower temperatures in air indicating they were less stable in air than the lignin.

Table 2.2: Dynamic Thermogravimetric Analysis of Wood and Various Components

Sample[1]	Active Pyrolysis Onset Temperature (°C)	Peak mass loss rate temperature[2] (°C)	Residual Pyrolysis Temperature Range (°C)	Volatilization (%) at temperature in °C							
				200	250	300	350	400	450	500	550
HC (N_2)	193	321	-	1	7	25	71	77	79	81	83
HC (air)	190	314	330-450	1	7	27	68	78	97	99	99
CL (N_2)	231	368	-	0	1	4	26	82	84	86	87
CL (air)	246	346	350-490	0	0	4	64	80	86	99	100
LG (N_2)	120	400	-	2	5	10	18	32	43	47	50
LG (air)	127	425	-	2	5	10	16	30	70	96	97
DF (N_2)	218	370	-	1	2	8	31	73	77	80	82
DF (air)	233	340	350-480	0	1	8	62	73	81	99	100

[1] HC is hemicellulose, CL is cellulose, LG is lignin and DF is Douglas-fir latewood.
[2] Taken as the first peak during active pyrolysis within the differential TGA curves.

Individual component vs. wood pyrolysis

For wood, the individual wood polymeric components have been used to develop models to predict the behavior of the thermal degradation of bulk wood [1, 21, 36]. Often, a volume-weighted average of the component properties are employed in these models. Figure 2.4 compares the normalized mass fraction (MF) for the Douglas-fir latewood to a weighted average of the individual polymers calculated using:

$$MF_{WA} = \frac{\sum x_i MF_i}{\sum x_i} \qquad \text{eq. 2.1}$$

where MF_i is the mass fraction remaining for each, isolated component as a function of time and x_i is the fraction of the total yield from the carbohydrate analysis (Table 2.1) for each polymer species *i* (hemicellulose, cellulose and lignin).

a)

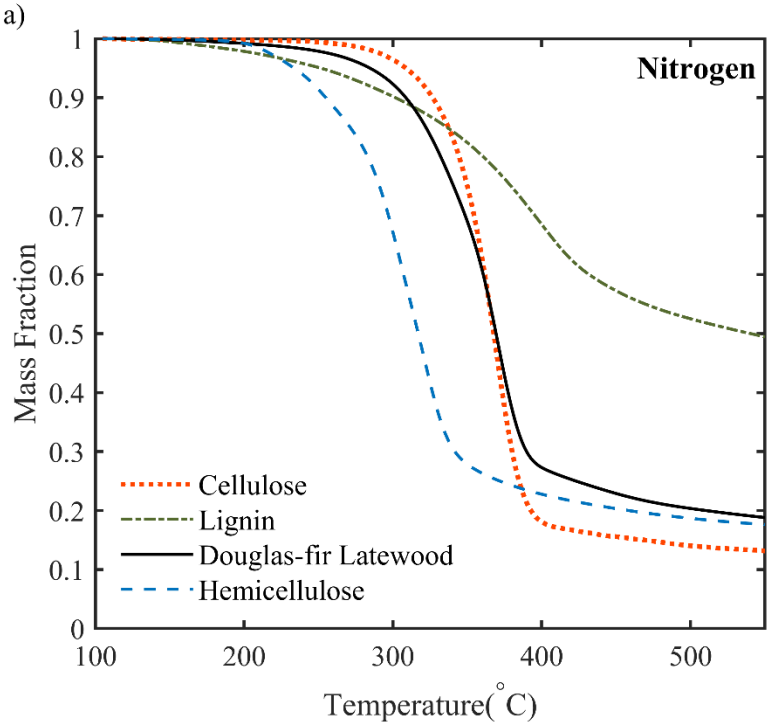
Nitrogen
Mass Fraction
Temperature(°C)
Cellulose
Lignin
Douglas-fir Latewood
Hemicellulose
0
0.1
0.2
0.3
0.4
0.5
0.6
0.7
0.8
0.9
1
100
200
300
400
500

b)

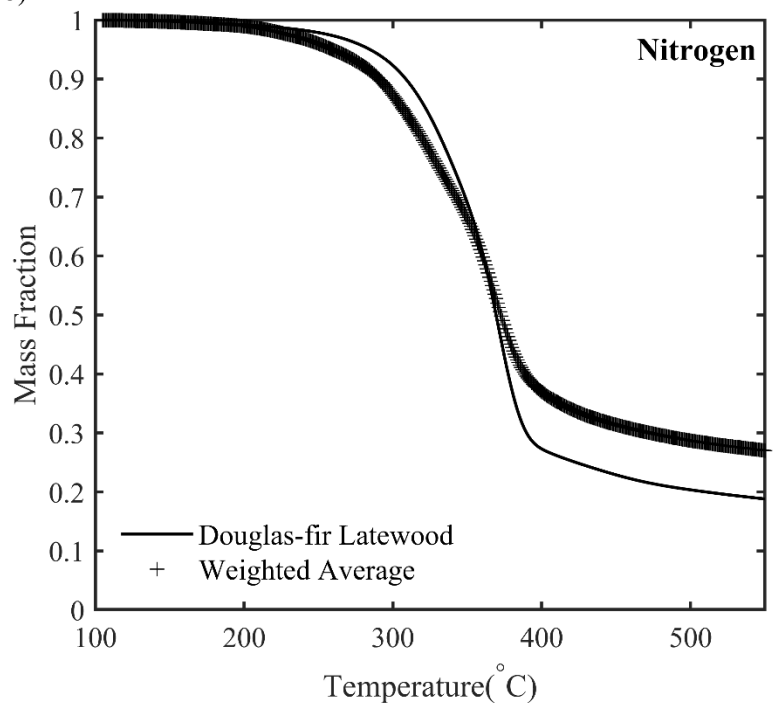
Nitrogen
Mass Fraction
Temperature(°C)
Douglas-fir Latewood
Weighted Average
0
0.1
0.2
0.3
0.4
0.5
0.6
0.7
0.8
0.9
1
100
200
300
400
500

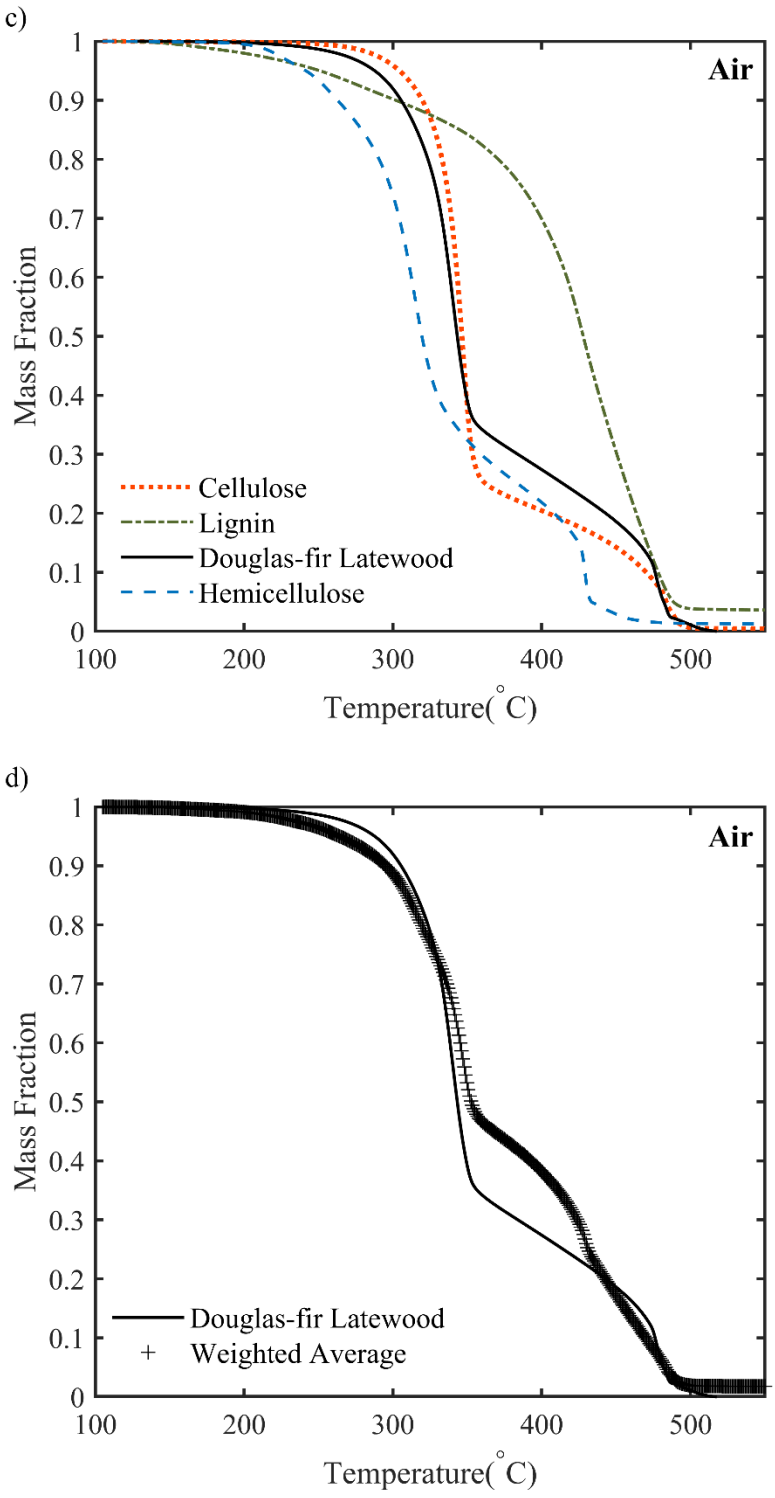

Figure 2.4: Mass fraction of Douglas-fir latewood during dynamic TGA experiments at 10˚C/min compared to individual wood polymers in a) nitrogen c) and air. The Douglas-fir latewood is also compared to a weighted average of the individual components in b) nitrogen and d) air.

In nitrogen, the weighted average represented Douglas-fir latewood up to 380°C. Above 380°C, the weighted average underestimates material volatized in the Douglas-fir latewood. The Douglas-fir latewood samples lost approximately 70% of their mass by 400°C while using the weighted average predicts only 60% of the material being pyrolyzed. This difference is due to the slow thermal degradation of the Kraft lignin component, which causes the weighted average to remain high towards the end of active pyrolysis for both the hemicellulose and cellulose. In air, the weighted average predicts the thermal degradation of the Douglas-fir latewood up to a temperature of 350°C. The general inflections of the weighted average curve in air occur at the same temperatures as the Douglas-fir latewood in air and degrade to the same final mass. However, the curves diverge between 350°C and 440°C with the weighted average, again, underestimating the amount of material volatized in the Douglas-fir latewood by 10% at 400°C. This underestimation of the weighted average is, again, due to the Kraft lignin component given that lignin is the only component with a mass fraction above the Douglas-fir latewood in this temperature range. Ultimately, both the cellulose and the mixture are similar to the Douglas-fir latewood with the areas under each curve provided in Table 2.3. The cellulose slightly over-estimates the thermal degradation while the weighted average mixtures slightly underestimates the thermal degradation.

Table 2.3: Areas under each TGA curve

Material in Nitrogen	Area under curve (Nitrogen)	Material in Air	Area under curve (Air)
Hemicellulose	247.8	Hemicellulose	231.4
Cellulose	281.5	Cellulose	259
Lignin	354.1	Lignin	306.5
Douglas-fir Latewood	288.7	Douglas-fir Latewood	261.8
Weighted Average	299	Weighted Average	269.3

There are several models that currently exist for deriving pyrolysis kinetic parameters from TGA data [1-9]. Slopiecka et al. compared three models using non-isothermal TGA on poplar wood

[10]. They found that the Kissinger–Akahira–Sonuse (KAS) and Flynn–Wall and Ozawa (FWO) [11, 12] models were efficient in the description of the degradation mechanism of solid-state reactions. Using TGA data, the degree of conversion, α, is often calculated as:

$$\alpha = \frac{m_o - m}{m_o - m_\infty} \qquad \text{eq. 2.2}$$

Where m_o is the initial mass and m_∞ is the mass at the end of the pyrolysis stage.

The kinetic model form typically used is:

$$\frac{d\alpha}{dt} = k(T)f(\alpha) \qquad \text{eq. 2.3}$$

Where $k(T)$ is a function carrying the temperature-dependence of the reaction rate and $f(\alpha)$ is the reaction model.

$$f(\alpha) = (1-\alpha)^n \qquad \text{eq. 2.4}$$

Here, n is the reaction order in the remaining solid mass. Typically, the Arrhenius equation is used to model $k(T)$ [18, 37, 38]:

$$k(T) = Aexp\left(-\frac{E}{RT}\right) \qquad \text{eq. 2.5}$$

where A is the pre-exponential factor for each reaction or pyrolysis phase, E is the activation energy and R is the universal gas constant.

Since my experiments were not isothermal, the heating rate of 10°C/min must be included as β such that equation 2.3 combined with equations 2.4 and 2.5 becomes:

$$\frac{d\alpha}{dt} = \frac{A}{\beta} exp\left(-\frac{E}{RT}\right)(1-\alpha)^n$$

Such models might be appropriate for the individual polymer components of wood, after the components have been isolated from each other. However, when the polymers are closely intermingled, as they are inside the cell wall, it is a stretch to expect that the pyrolysis of each will be completely independent of the others. The fact that pyrolysis of Douglas-fir follows most closely the pyrolysis of cellulose (Figure 2.4 a and c) suggests that not all the lignin and hemicellulose pyrolyze independently; instead, the pyrolysis of portions of these two components might be rate-limited by the cellulose. To test this idea, I assume that portions of the lignin and hemicellulose pyrolyze with the cellulose and leave the same residue. A least squares fit is used to determine the best values for the amounts of hemicellulose and lignin that are rate-limited by cellulose. Hemicellulose and lignin content in the Douglas-fir are 0.21 and 0.31, respectively. From the least squares analysis, the best fit to Douglas-fir corresponds to 0.08 hemicellulose and 0.17 lignin rate-limited by cellulose, while 0.13 hemicellulose and 0.14 lignin evaporate as they do in isolated components. Interestingly, the results from the least squares analysis were the same in both nitrogen and air. Figure 2.5 provide the results from this analysis for the specimens in nitrogen and air. In Figure 2.5, the kinetic model is almost indistinguishable from the Douglas-fir mass fraction results. For further details regarding the preliminary co-pyrolysis kinetic model developed here, see Appendix A.

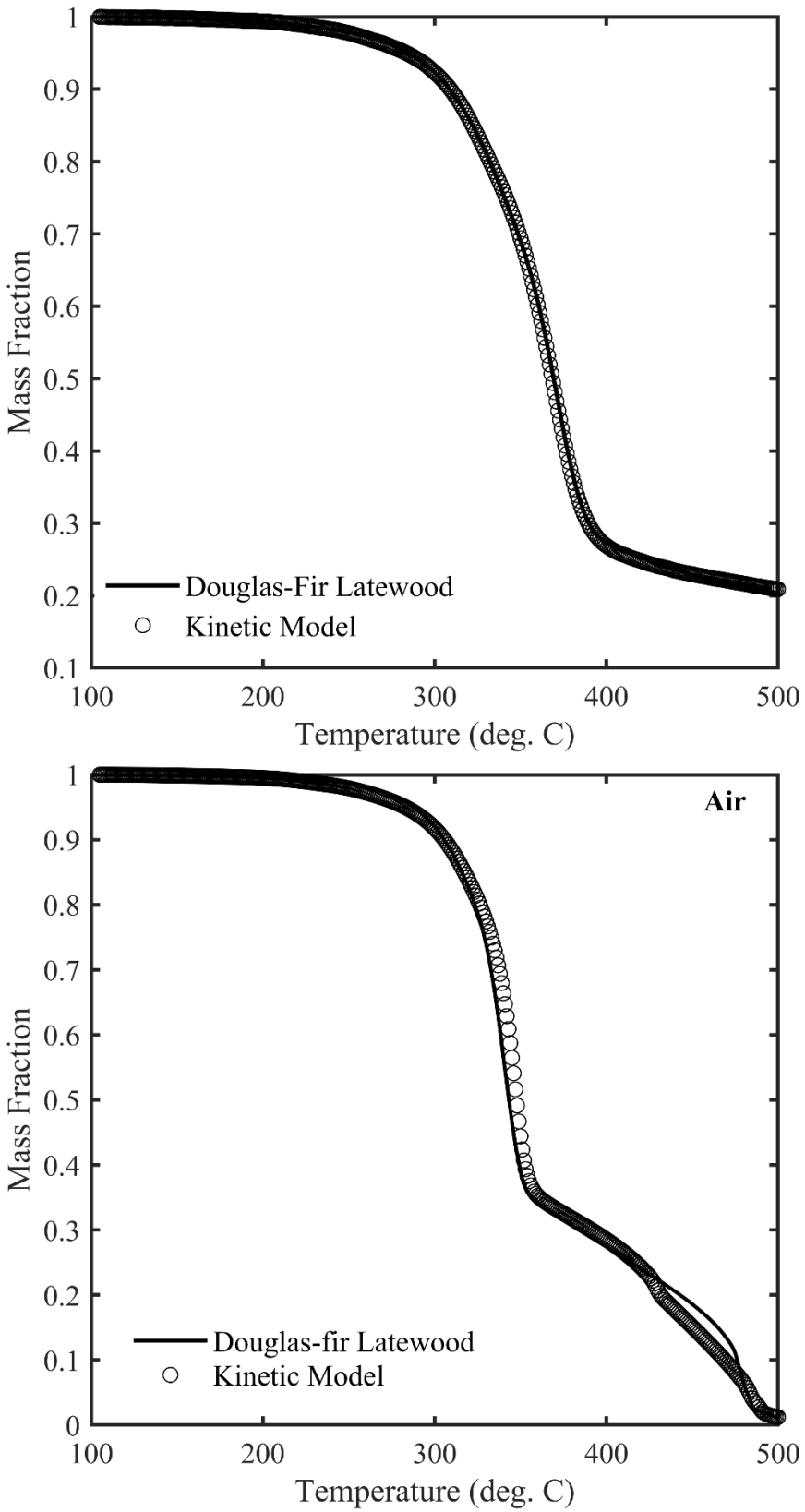

Figure 2.5: Mass fraction of Douglas-fir latewood during dynamic TGA experiments at 10˚C/min compared to individual wood polymers, weighted average, and a kinetic model in nitrogen (top) and air (bottom).

2.5 Discussion

Comparing the temperatures of the active pyrolysis peak, hemicellulose was found to be the least thermally stable with lignin being the most. This agrees with previous studies [9, 13, 39-41] and is also evident in the solid residue left in nitrogen at temperatures above 450°C with 50% of the lignin remaining and 15-20% residue remaining for hemicellulose, cellulose and Douglas-fir latewood.

The arabinogalactan used to represent hemicellulose here, has shorter chains and an amorphous structure rich with side-branches that are easily degraded to volatiles at lower temperatures [36]. For the hemicellulose in air, the trough indicates two consecutive reactions and the shoulder that occurs before the peak may indicate two almost overlapping reactions. The two consecutive reactions are thought to be fragmentation into water-soluble molecules followed by the volatilization of the material [12, 42]. The overlapping reactions causing the shoulder are most likely the depolymerization of the short polymer chains into monomers that leads to volatilization and a more direct and rapid degradation to volatiles without observable monomeric fragments. Since cellulose is a long, unbranched polymer and, when compared to hemicellulose, the onset of thermal degradation takes place at higher temperatures. Lignin is a highly branched polymer with a complex structure and the thermal degradation occurs over a wide temperature range due to the oxygen functional groups with various different thermal stabilities [43]. The TGA curves for lignin included shoulders around 250°C. The first shoulder is believed to represent the cleaving of ether linkages and the breaking of side-chains[9, 12]. The large peak that occurs above 400°C is the residual pyrolysis reaction which includes reactions such as the cleavage of the bonds attached to the aromatic rings [44]. Shoulders that occur as a tail to a peak often represent strong adsorption of volatiles during the formation of a new solid phase [6].

It has long been understood that in thermal analysis of wood components, reactions with oxygen present occur at accelerated rates, which is true here as well. However, Beall noted that, in pure oxygen, the initial degradation temperatures were lower than in nitrogen [12]. In this study air was used and it was found that the onset of degradation temperatures for all materials were within 15°C of the onset of degradation temperatures of specimens in nitrogen. After the initial onset of thermal degradation, the presence of oxygen in the air allowed for the residue to be further volatized and consumed with nearly zero above 500°C for all materials while an unstable residue remained for all materials in nitrogen.

There are similarities between the pyrolysis of the wood polymers and Douglas-fir latewood. For instance, the onset temperature between the cellulose and the Douglas-fir latewood differed by only 13°C in both nitrogen and air. Additionally, the temperatures at which the first peak mass loss rate occurred in cellulose was differed by only 2°C in nitrogen and 6°C in air compared to the Douglas-fir latewood. Despite similarities, the weighted average of the isolated polymers underestimates the amount of thermal degradation based on mass fraction of the Douglas-fir latewood at temperatures above 380°C in nitrogen and 350°C in air. This is because the weighted average model does not consider the interactions of the polymer in situ. The kinetic model illustrates the need to determine how much of the hemicellulose and lignin is rate-limited by the cellulose and that a simple, weighted average of the polymeric components is not applicable to wood.

2.6 Conclusions

Overall, the atmosphere plays an important role on the pyrolysis of wood and its isolated components. In air, the specimens experienced two stages of active pyrolysis (active and residual) with the residual pyrolysis replacing the passive pyrolysis phase that is observed in nitrogen. Active pyrolysis in air occurred with a higher change in mass fraction (mass loss rate) at lower temperatures than observed in nitrogen. In the residual pyrolysis, the degradation of an intermediate material (char) took place above 380°C. Additionally, hemicellulose, cellulose and Douglas-fir latewood all self-ignited above 420°C. The lignin showed signs of an exothermic reaction, but never self-ignited in the temperature range evaluated here. The percent of material remaining above 500°C was much higher in nitrogen (13-50% remaining) than in air (0-4%). This indicates that the material remaining after the initial active pyrolysis is not thermally stable and is subject to solid-phase oxidation.

Comparable to previous studies, the results of the dynamic thermogravimetric analysis on the isolated components show that hemicellulose is the least thermally stable, cellulose is more thermally stable, and lignin is the most thermally stable. The hemicellulose decomposition is almost complete when the accelerated degradation of the cellulose starts, and the lignin decomposition occurs over a large temperature range. Despite the differences in temperatures at which active pyrolysis occurs, the overall thermal degradation of the hemicellulose, cellulose and Douglas-fir latewood were similar in behavior based on the TGA curve shapes that consisted of active pyrolysis, residual (in air) or passive (in nitrogen) pyrolysis. However, the weighted average of the isolated polymers does not accurately predict the thermal degradation of the Douglas-fir latewood and is not recommended for use in pyrolysis models of wood building products. Instead, a rate-limiting model is necessary to describe the thermal degradation of the polymers in situ.

2.7 References

[1] F. Shafizadeh, "The Chemistry of Pyrolysis and Combustion," in *The Chemistry of Solid Wood*. vol. 207, R. M. Rowell, Ed., ed Washington, DC: American Chemical Society, 1984.

[2] F. Richter and G. Rein, "Pyrolysis kinetics and multi-objective inverse modelling of cellulose at the microscale," *Fire Safety Journal,* vol. 91, pp. 191-199, 2017/07// 2017.

[3] C. A. Hill, *Wood modification: chemical, thermal and other processes*. West Sussex, England: John Wiley & Sons, 2006.

[4] A. Garcia-Maraver, D. Salvachúa, M. Martínez, L. Diaz, and M. Zamorano, "Analysis of the relation between the cellulose, hemicellulose and lignin content and the thermal behavior of residual biomass from olive trees," *Waste Management,* vol. 33, pp. 2245-2249, 2013.

[5] M. Fang, D. Shen, Y. Li, C. Yu, Z. Luo, and K. Cen, "Kinetic study on pyrolysis and combustion of wood under different oxygen concentrations by using TG-FTIR analysis," *Journal of analytical and applied pyrolysis,* vol. 77, pp. 22-27, 2006.

[6] A. Coats and J. Redfern, "Thermogravimetric analysis. A review," *Analyst,* vol. 88, pp. 906-924, 1963.

[7] A. Kumar, L. Wang, Y. A. Dzenis, D. D. Jones, and M. A. Hanna, "Thermogravimetric characterization of corn stover as gasification and pyrolysis feedstock," *Biomass and Bioenergy,* vol. 32, pp. 460-467, 2008.

[8] U.-J. Kim, S. H. Eom, and M. Wada, "Thermal decomposition of native cellulose: influence on crystallite size," *Polymer Degradation and Stability,* vol. 95, pp. 778-781, 2010.

[9] M. Ramiah, "Thermogravimetric and differential thermal analysis of cellulose, hemicellulose, and lignin," *Journal of Applied Polymer Science,* vol. 14, pp. 1323-1337, 1970.

[10] K. Slopiecka, P. Bartocci, and F. Fantozzi, "Thermogravimetric analysis and kinetic study of poplar wood pyrolysis," *Applied Energy,* vol. 97, pp. 491-497, 2012.

[11] M. G. Grønli, G. Várhegyi, and C. Di Blasi, "Thermogravimetric analysis and devolatilization kinetics of wood," *Industrial & Engineering Chemistry Research,* vol. 41, pp. 4201-4208, 2002.

[12] F. Beall, "Thermogravimetric analysis of wood lignin and hemicelluloses," *Wood and Fiber Science,* vol. 1, pp. 215-226, 1969.

[13] L. Gašparovič, Z. Koreňová, and Ľ. Jelemenský, "Kinetic study of wood chips decomposition by TGA," *Chemical papers,* vol. 64, pp. 174-181, 2010.

[14] N. Liu, W. Fan, R. Dobashi, and L. Huang, "Kinetic modeling of thermal decomposition of natural cellulosic materials in air atmosphere," *Journal of Analytical and Applied Pyrolysis,* vol. 63, pp. 303-325, 2002.

[15] T. Ohlemiller, T. Kashiwagi, and K. Werner, "Wood gasification at fire level heat fluxes," *Combustion and Flame,* vol. 69, pp. 155-170, 1987.

[16] A. I. Bartlett, R. M. Hadden, and L. A. Bisby, "A Review of Factors Affecting the Burning Behaviour of Wood for Application to Tall Timber Construction," *Fire Technology,* vol. 55, pp. 1-49, 2019/01// 2019.

[17] H. W. Emmons and A. Atreya, "The science of wood combustion," *Proceedings of the Indian Academy of Sciences Section C: Engineering Sciences,* vol. 5, p. 259, 1982.

[18] F. Shafizadeh and A. Bradbury, "Thermal degradation of cellulose in air and nitrogen at low temperatures," *Journal of applied polymer science,* vol. 23, pp. 1431-1442, 1979.
[19] K. Raveendran, A. Ganesh, and K. C. Khilar, "Pyrolysis characteristics of biomass and biomass components," *Fuel,* vol. 75, pp. 987-998, 1996.
[20] J. J. Orfão, F. J. Antunes, and J. L. Figueiredo, "Pyrolysis kinetics of lignocellulosic materials—three independent reactions model," *Fuel,* vol. 78, pp. 349-358, 1999.
[21] T. R. Rao and A. Sharma, "Pyrolysis rates of biomass materials," *Energy,* vol. 23, pp. 973-978, 1998.
[22] S. Wang, X. Guo, K. Wang, and Z. Luo, "Influence of the interaction of components on the pyrolysis behavior of biomass," *Journal of Analytical and Applied Pyrolysis,* vol. 91, pp. 183-189, 2011.
[23] C. Couhert, J.-M. Commandre, and S. Salvador, "Is it possible to predict gas yields of any biomass after rapid pyrolysis at high temperature from its composition in cellulose, hemicellulose and lignin?," *Fuel,* vol. 88, pp. 408-417, 2009.
[24] T. Hosoya, H. Kawamoto, and S. Saka, "Cellulose–hemicellulose and cellulose–lignin interactions in wood pyrolysis at gasification temperature," *Journal of analytical and applied pyrolysis,* vol. 80, pp. 118-125, 2007.
[25] B. T. Bormann, "Douglas-fir," 1984.
[26] Western Wood Products Association. (2002, Douglas Fir & Western Larch. Available: https://www.wwpa.org/docs/default-source/secure/fs-3-douglas-fir.pdf?sfvrsn=2
[27] MilliporeSigma. (2018). *MSDS sheets*. Available: www.sigmaaldrich.com
[28] A. Sluiter, B. Hames, R. Ruiz, C. Scarlata, J. Sluiter, D. Templeton*, et al.*, "Determination of structural carbohydrates and lignin in biomass," *Laboratory analytical procedure,* vol. 1617, pp. 1-16, 2008.
[29] M. W. Davis, "A rapid modified method for compositional carbohydrate analysis of lignocellulosics by high pH anion-exchange chromatography with pulsed amperometric detection (HPAEC/PAD)," *Journal of Wood Chemistry and Technology,* vol. 18, pp. 235-252, 1998.
[30] C. Zhang, J. Zhu, R. Gleisner, and J. Sessions, "Fractionation of forest residues of Douglas-fir for fermentable sugar production by SPORL pretreatment," *Bioenergy Research,* vol. 5, pp. 978-988, 2012.
[31] A. M. Socha, S. P. Plummer, V. Stavila, B. A. Simmons, and S. Singh, "Comparison of sugar content for ionic liquid pretreated Douglas-fir woodchips and forestry residues," *Biotechnology for biofuels,* vol. 6, p. 61, 2013.
[32] R. M. Rowell, "The chemistry of solid wood," in *Advances in Chemistry Series*. vol. 207, ed: American Chemical Society Washington, DC, 1984.
[33] K. Mansaray and A. Ghaly, "Determination of kinetic parameters of rice husks in oxygen using thermogravimetric analysis," *Biomass and Bioenergy,* vol. 17, pp. 19-31, 1999.
[34] S. W. Freiman, S. A. Hooker, K. D. Migler, and S. Arepalli, "Measurement issues in single-wall carbon nanotubes," 2008.
[35] "ASTM E2550 Standard Test Method for Thermal Stability by Thermogravimetry," ed. West Conshohocken, PA: ASTM International, 2017.
[36] H. Yang, R. Yan, H. Chen, D. H. Lee, and C. Zheng, "Characteristics of hemicellulose, cellulose and lignin pyrolysis," *Fuel,* vol. 86, pp. 1781-1788, 2007.
[37] C. Lautenberger, "A Generalized Pyrolysis Model for Combustible Solids (PhD. thesis) University of California," ed: Berkeley, 2007.

[38] C. Di Blasi, "Physico-chemical processes occurring inside a degrading two-dimensional anisotropic porous medium," *International journal of heat and mass transfer,* vol. 41, pp. 4139-4150, 1998.
[39] A. G. Barneto, J. A. Carmona, J. E. M. Alfonso, and R. S. Serrano, "Simulation of the thermogravimetry analysis of three non-wood pulps," *Bioresource technology,* vol. 101, pp. 3220-3229, 2010/05// 2010.
[40] A. K. Chambers, "Application of TGA-FTIR Analysis to Study the Ignition Properties of Lignite Chars," *International Journal of the Society of Materials Engineering for Resources,* vol. 7, pp. 267-272, 2015/11/01/2016-08-03 2015.
[41] Z. Z. Zhang, M. M. Zhu, P. Hobson, W. Doherty, and D. K. Zhang, "Contrasting the Pyrolysis Behavior of Selected Biomass and the Effect of Lignin," *Journal of Energy Resources Technology-Transactions of the Asme,* vol. 140, 2018/06// 2018.
[42] D. Fengel, "On changes of wood and its components within the temperature range up to 200C- Part I: Hot and cold water extracts of thermlaly treated spruce wood.," *Holz als Roh- und Werkstoff,* vol. 24, pp. 9-14, 1966.
[43] M. Brebu and C. Vasile, "Thermal degradation of lignin—a review," *Cellulose Chemistry & Technology,* vol. 44, p. 353, 2010.
[44] H. Kawamoto, "Lignin pyrolysis reactions," *Journal of Wood Science,* vol. 63, pp. 117-132, 2017.

Chapter 3. Chemical Changes in Wood Due to Pyrolysis

3.1 Introduction

Pyrolysis models have multiple practical applications such as the energy recovery from biofuels and the ability to design structures with advanced materials, the latter being the main focus of this dissertation. Pyrolysis is often modeled using numeric techniques and typically uses one of two approaches to simplify the pyrolysis reactions for modelling [1]. The first simplification is often referred to as a char model and is used in structural fire resistance calculations. The char model assumes infinitely fast kinetics which is implemented by a fixed temperature at which the conversion of virgin wood into char occurs. This results in a model with an infinitely-thin pyrolysis front that calculates the velocity at which that front propagates into the wood using a heat balance at the front [2-8]. A second approach uses a global reaction model that typically include primary and secondary reactions and lump the pyrolysis products into three groups (char, tar and gas) [6, 7, 9-11]. Typically, the primary reaction consists of wood decomposing into the three pyrolysis products and the secondary reaction includes further degradation of the tar into char and gas. Although wood is a heterogenous material, the global reaction models often consider wood as a homogeneous material for the primary reaction by assuming its physical properties, such as density, are uniformly distributed [10]. The global reaction models are used predict product yields and rely on the Arrhenius equation to determine the velocity of the pyrolysis front into the wood.

The degradation kinetics used in the models are obtained from experimental techniques that use small samples (on the order of mg), such as thermogravimetric analysis (TGA) [12-15]. The small samples are used so all gradients become negligible and the sample can be treated as “thermally thin.” However, the relevance of TGA-measured kinetics to the pyrolysis of the polymers in wood

building products under fire-level heating rates is unknown [16]. This is because the heat transfer for thermally thick specimens differs from the heat transfer for thermally thin specimens used in TGA. Other simplifications for the prediction of wood pyrolysis include using the degradation kinetics of just cellulose or a weighted average of the three main polymeric components [17, 18]. Thorough reviews of the current modeling capabilities can be found elsewhere [1, 10].

While valuable, these models have limitations (e.g., only applicable for specific heat flux levels and oxygen concentrations, and materials that don't change volume) that must be understood by the user prior to implementation. These models also do not predict the chemical changes within the wood due to pyrolysis; instead, the degradation of wood is often described by a series of reactions corresponding to the pyrolysis of the main polymeric components [19, 20]. As Lautenberger noted, methods exist for measuring the rate constants of elementary gas phase reactions, but equivalent techniques have not yet been developed for kinetics in solids [1]. In order to advance towards determining kinetic rates in solid wood, a better understanding of the effects of pyrolysis on the chemical bonds must be gained.

Here, the use of X-ray photoelectron spectroscopy (XPS) is used to better understand the bond scission caused by pyrolysis in thermally thick wood. XPS is a surface-sensitive, quantitative spectroscopic technique that measures the elemental composition, chemical state and electronic state of the elements that exist within a material. XPS detects all elements except for hydrogen and helium and is, therefore, well-suited for chemical state identification and local bonding information of atoms within the surface of complex organic materials.

Soft X-rays from a photon source are irradiated onto a material's surface and can penetrate to a depth of 10 nm [21]. When the source X-rays hit the material's surface, photoelectrons are ejected and their kinetic energy (KE) is measured by an analyzer. The binding energy (BE) of the electrons

is deduced from the KE and incident photon energy. The binding energy of an electron will be affected by the element, the orbital from which the electron was ejected, and the chemical state of the element (i.e. bonding environment). The core level from which an electron is ejected is limited by the source energy such that electrons are ejected from different subshells for different elements.

3.2 Background on X-ray Photoelectron Spectroscopy (XPS) of Wood

In this chapter, XPS is utilized to evaluate bond scission caused by pyrolysis in charred Douglas-fir. Previous studies have used XPS to study the surface chemistry of black cherry, red oak and pine wood surfaces [22], heat-treated wood surfaces [23, 24], mechanically treated wood surfaces [25, 26], and weathered wood and wood-plastic composites[27, 28].

Based on the measured binding energies and the types of bonds found in wood polymers, it has been accepted in the wood XPS literature that the assignment of deconvoluted C1s peaks correspond to four types of carbon atom bonds in wood [29, 30]. The first carbon peak, C1, is a carbon atom bound only to other carbon atoms and/or hydrogen atoms (C-C, C=C, or C-H) [29]. The aromatic carbon (C=C) is attributed specifically to the lignin with the aromatic ring and the aliphatic carbon (C-C) being attributed to extractives and adventitious carbon, respectively. Adventitious carbon is a thin layer of carbonaceous material that forms on the surface of most air-exposed materials and is generally comprised of hydrocarbons [31]. The second carbon peak, C2, is a carbon bound to a single non-carbonyl oxygen atom (C-O) and is mainly caused by cellulose and hemicellulose, although lignin can contribute to this peak as well. The third carbon peak, C3, represents a carbon atom bound to one carbonyl oxygen or two noncarbonyl oxygen atoms (C=O and/or O-C-O). The fourth carbon peak, C4, represents a carbon atom linked to one carbonyl oxygen and one noncarbonyl oxygen (O-C=O) [32]. While the models typically have four carbon peaks for wood, others found using five [33] or six peaks [24] was appropriate. In this dissertation,

the C1 peak was split into two peaks representing the C-C aliphatic carbon bonds and C=C aromatic carbon bonds. Additionally, a sixth peak for the π-π* transition was included to account for the small contribution from the satellite structure due to the aromatic rings [34, 35]. In this dissertation, six peaks were used for Douglas-fir and lignin specimens where C=C and π-π* are expected. For cellulose, the four-peak model was used.

It has been reported that the O1s peaks of woody materials are difficult to predict because of the electronegativity and the polarizability of substituents that may interact with the oxygen atoms [29]. While tentative assignments for two bond types within the O1s peak are provided in the literature, the data related to this peak is sparse compared to the C1s peak [36]. Because of this, the total O1s spectrum is typically used to calculate O/C ratios rather than deconvoluting the peaks.

Bañuls-Ciscar et al. produced reference spectra for cellulose and lignin to enable easier identification of the composition of pine wood strands [35, 37]. They identified four C1s carbon peaks and one O1s peak for both cellulose (Sigma-Aldrich CAS Registry #9004-34-6) and organosolv lignin (Fibria Innovations CAS Registry #8068-03-9). In addition to providing reference peak binding energies, their experiments also provided valuable information about the characteristic shape of the spectra. For cellulose, the spectra had a weak aliphatic carbon peak and a strong carbon-oxygen peak due to the alcohol groups. Whereas, lignin can be characterized by an intense aliphatic peak and a π-π* transition [35, 37]. In 1997, Nishimiya et al. used XPS to study the relationship between the wood chemical structure and the carbonization temperature [24]. They carried out XPS experiments on wood carbonized in inert environments at temperatures ranging from 300°C to 2400°C. The results of these experiments showed that the hydroxyl (OH) and carbonyl (C=O) groups decreased with increasing temperatures. Additionally, the aromatic carbon to the aliphatic carbon ratio increased with carbonization temperature indicating the growth

of a graphite crystalline structure. Inari et al. characterized the chemical changes after heating beech wood in inert atmosphere up to 240°C and found that heating induced a substantial decrease of the O/C ratio as well as the C-O contribution to the C1s spectrum. While these studies provided baseline information for conducting XPS on wood, inconsistencies in the experimental methods existed. For instance, dwell times, pass energies, the use of surface etching and specimen preparation varied between studies. These inconsistencies are addressed further in Section 3.3. Additionally, for studies by Nishimiya et al. [24] and Inari et al. [23], the specimens were exposed to high temperature under inert atmospheres for longer exposure times and slower heating rates than would be expected in a structure fire.

The number of XPS studies related to biochar and wood charcoal continues to grow [38-41]. However, research relating to changes in chemical bonds (via bond scission) caused by pyrolysis in wood exposed to a fire in atmospheric conditions is nonexistent. Evaluating the chemical bonds present in uncharred wood, through the pyrolysis zone and into the charred layer of thermally thick wood can ultimately be used for verification of pyrolysis models that are currently based on mass loss of thermally thin materials.

3.3 Materials and Methods

Materials

Charred Isolated Polymers

The same two reference materials obtained from Sigma Aldrich used in Chapter 2 were also used here: α–cellulose (CAS Registry #: 9004-34-6) and Kraft lignin (CAS Registry #: 8068-05-1). The same cellulose used by Bañuls-Ciscar et al. was used here to verify the spectra obtained [35]. The lignin was not the same as previously used in the literature, but Kraft lignin accounts for 85% of

lignin production worldwide [42, 43]. Sulfur is used during the Kraft pulping process and may be present in the spectra whereas, sulfur is not used in the processing to develop the organosolv lignin used by Bañuls-Ciscar et al. [44]. However, only the C1s and O1s peaks were examined in this study and sulfur is expected to have a negligible impact on the presented spectra.

While cellulose is a long-chain polymer made of glucose monomers and hemicellulose is a short-chain polymer made of many monomers, they are both polysaccharides made up of sugar monomers and have similar chemical formulae and O/C ratios (~0.8). Since XPS characterizes the elements present in the wood and the bonding environment of those elements, the results cannot differentiate between cellulose and hemicellulose (together referred to as holocellulose). Because of this, XPS on reference hemicellulose was not conducted.

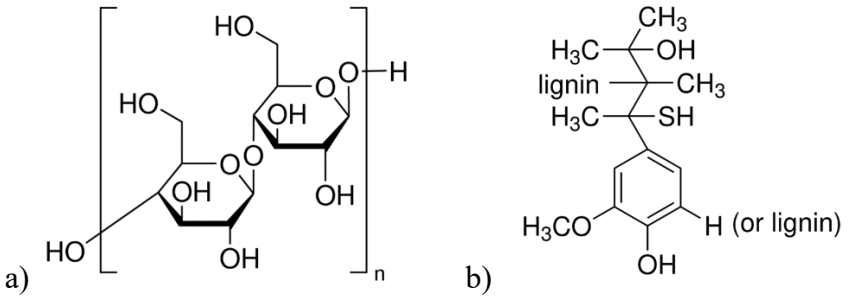

Figure 3.1. Chemical structure of a) both α-cellulose and cellulose from spruce and b) lignin precursor Images from [45].

To determine the effect of thermal degradation on the cellulose and lignin, the isolated polymeric materials were heated to specific temperatures using a differential scanning calorimeter (DSC) (TA Instruments Q2000) with air as the purge gas. While DSC is typically used to detect phase changes in materials, here the DSC instrument was used as a controlled and repeatable heating source for specimen preparation. Cellulose and lignin reference materials were weighed and placed in aluminum T-zero pans with lids (TA Instruments 901683.901/901671.901) and exposed to a specified heating/cooling sequence. The sequence included drying the specimen at 105°C for 5

minutes, ramping at 42°C/minute to a specific hold temperature for 20 seconds and then cooling at the maximum rate of 200°C/minute. The ramp rate was chosen based on the heating rate of a thermocouple at 4 mm below the surface of Douglas-fir exposed to heat flux of 50 kW/m^2, which is discussed further in the next section. The hold temperatures were every 25°C from 200°C to 400°C with 10 replicates for both cellulose and lignin at 350°C. Overall, a total of 18 heat-treated specimens for both cellulose and lignin were produced using the DSC.

Charred Wood

To use XPS as a tool to study how wood changed during pyrolysis, it was necessary to study a wood surface that exhibited a gradient from unmodified wood to char. To develop such surface, one board of Douglas-fir (*Pseudotsuga menziesii*) that had been cut parallel to the longitudinal direction of the trunk was chosen and a specimen with final dimensions of 100 mm x 100 mm x 20 mm was cut from the board (Figure 3.2). Prior to exposure in the cone calorimeter, the specimen was conditioned in an oven at 105°C for 24 hours to remove moisture

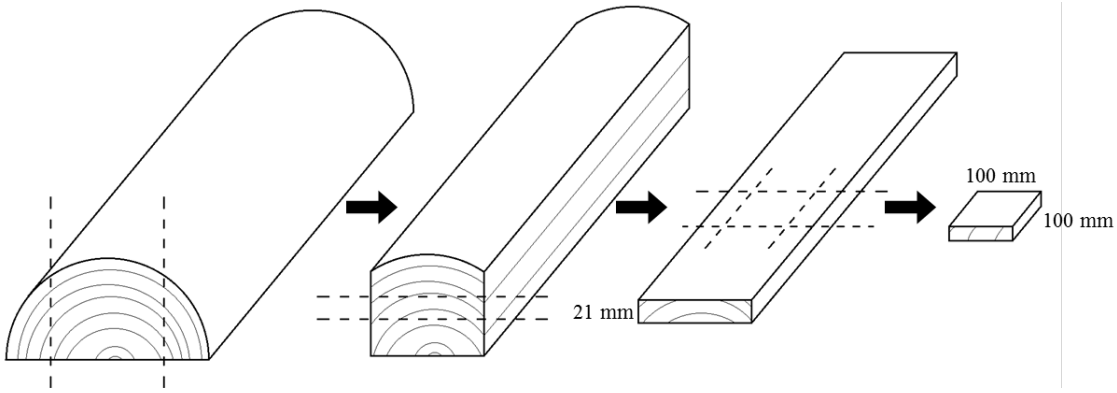

Figure 3.2. Schematic of wood specimen prior to charring.

Then, the radial-longitudinal surface of the wood specimen was exposed to a constant heat flux using a cone calorimeter, such that all subsequent XPS measurements on the pyrolyzed wood could be performed on a single latewood growth ring, which would reduce variability. The cone

calorimeter is a bench-scale test typically used to measure key flammability modeling properties such as time to ignition, heat release rate and mass loss rate while exposed to a known heat flux. The cone calorimeter (FTT iCone Mini, East Grinstead, West Sussex, UK) is located at the Forest Products Laboratory and can irradiate the test specimen with fluxes up to 100 kW/m^2. For these tests, a constant heat flux of 50 kW/m^2 was applied.

To measure the thermal profile through the Douglas-fir specimen, four thermocouples made from 30 gauge, type K thermocouple wire (Omega Engineering, GG-K-30-SLE) were inserted into the holes parallel to the exposed surface as well as one on the unexposed surface (0 mm) and one on the top surface (20 mm). One horizontal hole with a diameter of 0.2mm and a length of 30 mm was drilled on each edge of the specimen at 4 mm, 8 mm, 12 mm, or 16 mm from the unexposed surface (Figure 3.3). When the temperature of the unexposed surface reached 100°C, the test was terminated, the specimen was removed, and the fire was extinguished with water.

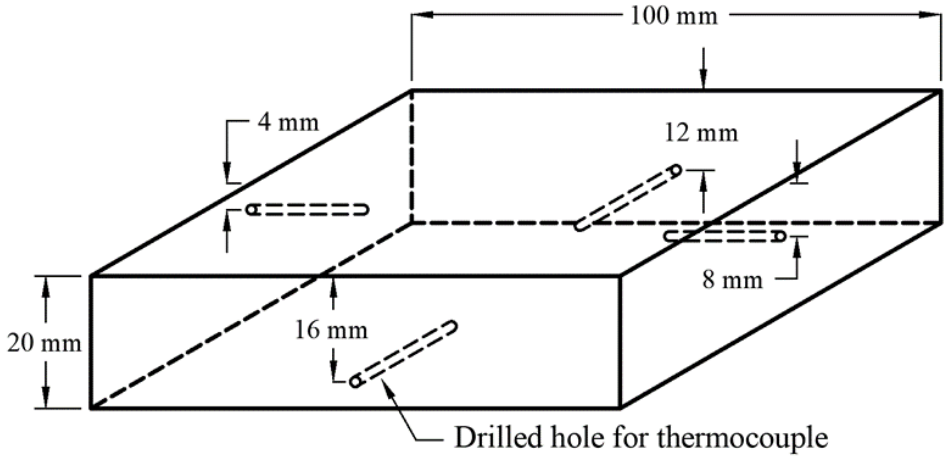

Figure 3.3: Schematic of thermocouple locations in Douglas-fir specimen prior to exposure in the cone calorimeter.

The final temperatures in the charred wood specimen at the measured depths are provided in Table 3.2.

Table 3.2: Final measured temperatures in charred wood specimen

Distance from Unexposed surface (mm)	Temperature at test termination (°C)
20	685
16	428
12	266
8	186
4	121
0	100

The temperatures between thermocouple locations were calculated using Fire Dynamics Simulator (FDS), which is a computational fluid dynamics model of fire-driven fluid flow and includes heat conduction models [46, 47]. Figure 3.4 shows the measured temperatures from the thermocouples and the calculated temperatures from FDS. While the temperature measured at the exposed surface (20 mm) is slightly higher than the calculated value, the remainder of the calculated temperatures were in close agreement with the measured values. The standard limits of error for the thermocouples used is ±2.2°C, which is smaller than the marker used and, therefore, not provided in Figure 3.4.

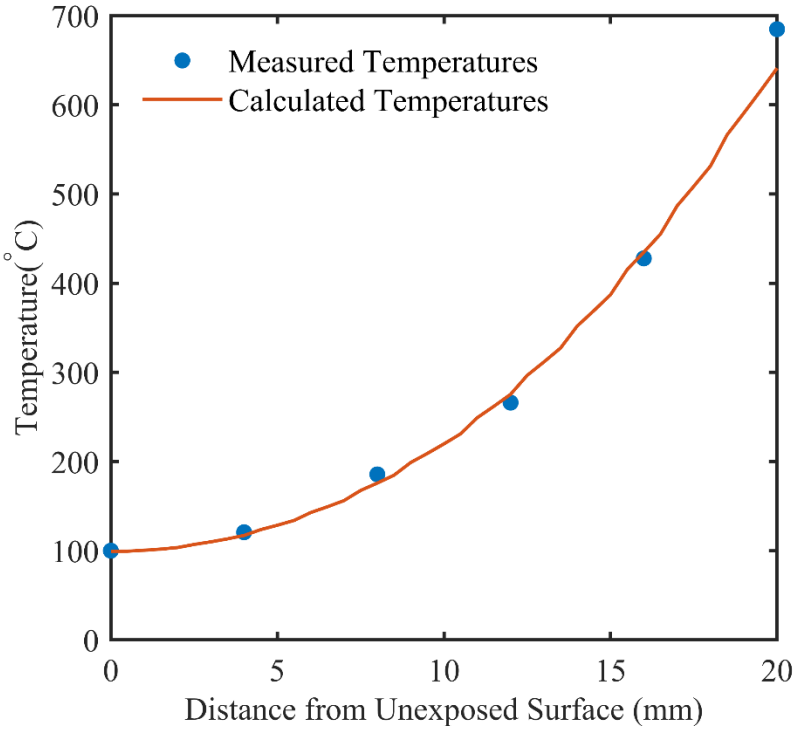

Figure 3.4: Final temperature profile in the charred wood specimen from embedded thermocouples (measured) compared to calculated temperatures from FDS program.

After exposure in the cone calorimeter, the charred wood specimen was cut in the radial direction into 4 mm sections (Figure 3.5). To avoid edge effects caused by the cone calorimeter holder, a 4 mm slice from the center of the specimen was selected for further analysis. Within this section, a specific latewood growth ring was chosen to conduct XPS analysis on. This latewood growth ring was also used for the nano-indentation experiments in Chapter 4.

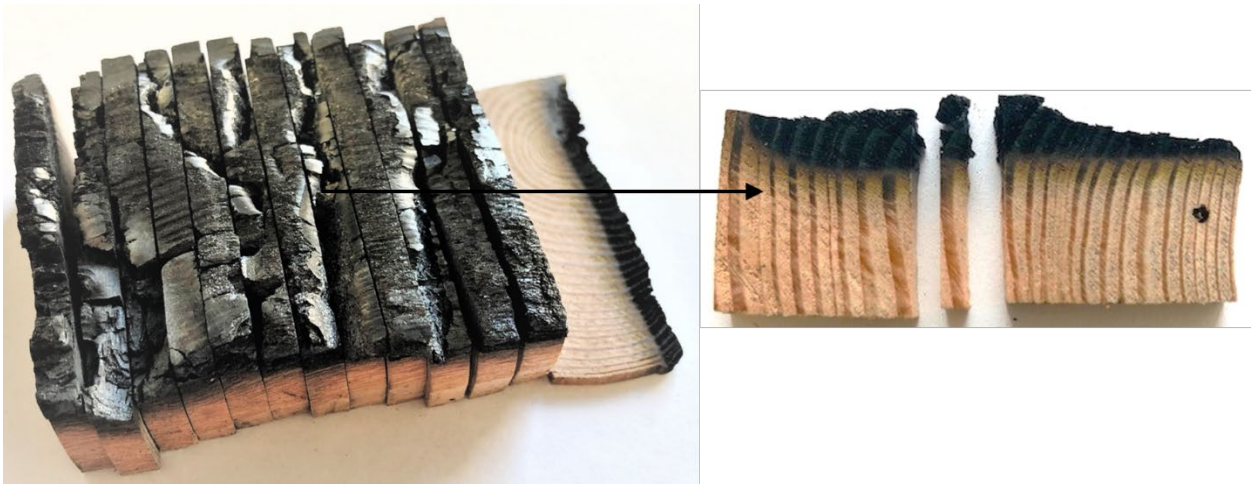

Figure 3.5: Charred wood specimen cut into 4 mm sections and selected latewood growth ring for XPS analysis.

The final length of the charred latewood specimen was 17 mm, with 3 mm from the original dimension lost due to char formation and contraction [48, 49].

Material Preparation for XPS Analysis

Since XPS is sensitive and susceptible to even trace contaminants, specimen preparation must be carried out with care [50, 51]. To ensure no contamination of the heat-treated cellulose and lignin, degreased stainless-steel tools were used to remove the material from the DSC pans and compress the material into the XPS powder sample holder (Figure 3.6) prior to analysis.

To reduce contamination to the surface of the charred latewood specimen, degreased tweezers were used to handle the specimen. Immediately prior to XPS analysis, the transverse surface of the charred specimen was pulled across six inches of 2000 grit sandpaper once in the radial direction to avoid char contaminating the uncharred wood. After sanding, the sawdust was removed from the surface with pressurized nitrogen. In addition to the handling of the material, Banuls-Ciscar et al. and Inari et al. recommend removing extractives prior to conducting XPS on wood [37, 50] although other studies did not remove extractives prior to XPS analysis [24, 32, 52].

The effects of removing the extractives from the charred Douglas-fir latewood on the XPS spectra was unknown and investigated here. To remove the extractives, the charred latewood specimen was soaked in acetone (reagent grade, minimum purity of 99.5% CH_3COCH_3 by volume, with a residue after evaporation of less than 0.001%) for 48 hours, removed, and oven-dried at 100°C for 24 hours prior to surface preparation and XPS analysis. Acetone was chosen as the solvent because it is a common and effective solvent for removing resinous extractives and does not leave a water residue [53-55]. Additionally, the acetone soak was employed to avoid breaking the fragile char layer. However, it is likely that the acetone did not remove all extractives and, if not for the fragile char layer, another more complete extraction method [56] would have been used.

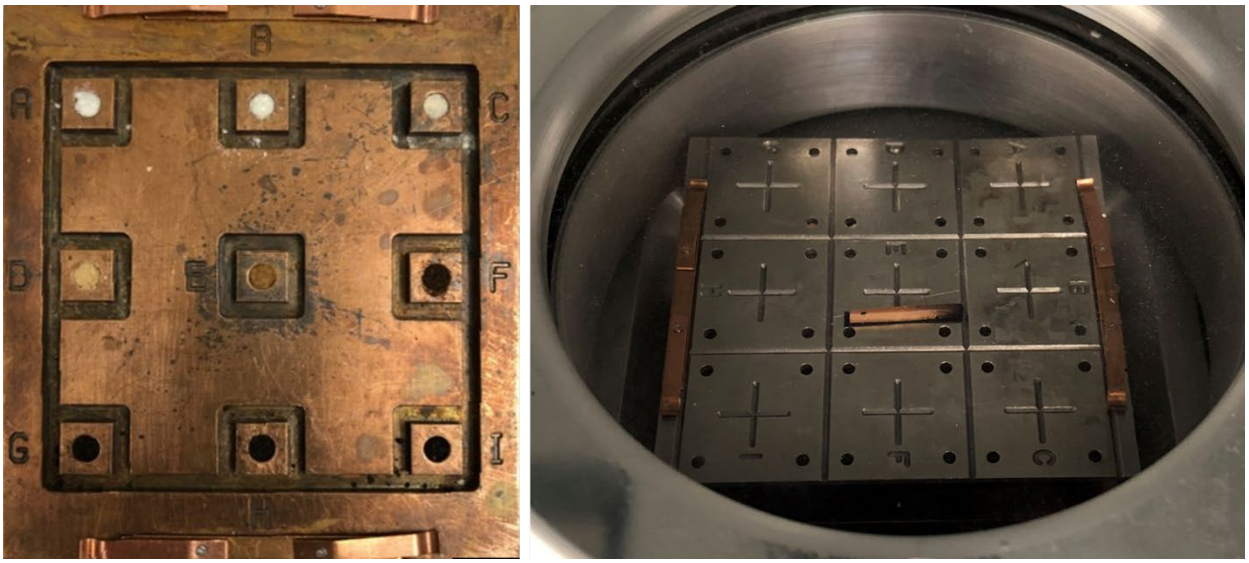

Figure 3.6: Left: Heat-treated cellulose (from 200°C to 400°C) compressed in dimples A to I on the XPS powder sample holder. Right: Charred latewood specimen on sample holder in loading chamber prior to analysis.

Methods

Instrument Settings

The XPS instrumentation acquisition settings found throughout the literature were inconsistent regarding pass energies, argon etching, and spot sizes. Some of those variations are compiled in

the Table 3.3 and compared to the settings used here. A dashed line indicates that the information was not provided.

Table 3.3: Comparison of XPS settings used for analysis of wood

	Inari [23]	**Nishimiya [24]**	**Banuls-Ciscar [37]**	**Hasburgh (Present work)**
X-Ray Source	Al Kα	Mg Kα	Al Kα	Al Kα
Spot Size	700 μm	---	400 μm	50 μm
Survey Step Size	1 eV	---	0.4 eV	1 eV
Survey Pass Energy	160 eV	---	300 eV	200 eV
Hi-Res Step Size	0.05 eV	---	0.2 eV	0.05
Hi-Res Pass Energy	20 eV	---	50 eV	20 eV
Flood Gun Used	Yes	---	Yes	Yes
Dwell time	---	---	---	100 ms
Surface Etch (Argon)	---	Yes, no energy provided	---	Varied (0-2000 eV)[1]
Surface Etch Time	---	30 seconds	---	10 seconds[1]

[1] Argon energy varied from 0 to 2000 eV to evaluate the effect. When used, a 10 second etch time was applied.

Compared to others, a smaller spot size of 50 microns was used to limit effects from the pyrolysis gradient present but still ensure that at least one wood cell was measured per scan. Line scans were used to conduct multiple single scans from the unmodified wood through to the char while individual single measurements were conducted on the cellulose and lignin. For each spot, the initial, low resolution scan occurred with an analyzer pass energy of 200 eV and a step size of 1 eV to obtain the survey spectra between zero and 1230 eV. Then, additional passes occurred with the analyzer pass energy at 20 eV with a step size of 0.5 eV to increase the spectral resolution. For the high-resolution C1s scans, the binding energy range was 279 to 298 eV and for the high-resolution O1s scans, the binding energy range was 525 to 545 eV. A charge neutralizing flood gun was used as recommended for XPS analysis on nonconductive materials to reduce the build-up of a positive charge which ultimately affects the spectral resolution leading to line broadening and energy shifts [57]. To ensure enough sampling was conducted without causing damage to the surface, a dwell time of 100 ms was used for each pass.

The use of argon etching to remove the adventitious carbon was recommend by Nishimiya et al. [24]. However, the argon (Ar) energy used in their study was not provided and other sources note that the use of argon etching on organic polymers may cause damage and affect the measurements [58]. To investigate if, and at what energy, argon etching should be used for the charred wood, experiments were carried out with increasing argon beam energies and compared to wood without surface etching.

XPS Data Analysis

The spectra obtained from XPS analysis can be used to quantify the types of chemical bonds present in a sample's surface. However, quantitative analysis of the XPS spectra is not trivial and requires accurate measurements of the spectral lines that correspond to different elements or chemical states of one element [59]. Two factors complicate the determination of the intensities. First, at high binding energies, the measured signal represents a combination of the real photoelectrons as well as inelastically scattered photoelectrons and there is not an explicit procedure to separate these two contributions [60-62]. Second, the spectral line profile itself cannot be described by an analytical function and, instead, a deconvolution procedure is necessary [59, 63, 64]. Historically, the deconvolution has been carried out via a Lorentzian and Gaussian function. The Lorentzian function represents the core-hole lifetime, which is the finite time between the ejection of a core electron and the decay of an electron from the valence band to the core level. The Gaussian function includes the transmission properties of the spectrometer and the line shape of the monochromatic X-rays [65]. More recently, an asymmetric Pseudo-Voigt function with a sigmoidal step function has been used for analysis of XPS data [65].

Here, the elemental composition of the sample was determined by evaluating the binding energies where peaks occurred in the low-resolution survey spectra. Then, high-resolution scans were

conducted in the binding energy ranges for the elements present. Each peak from the high-resolution spectra was corrected for background using the Shirley baseline [66] and then fitted to obtain the area under the peak (A_P) using the trapezoid function. The normalized areas were then obtained using equation 3.1.

$$A_N = \frac{A_P}{TXFN*SF*ECF} \quad \text{eq. 3.1}$$

TXFN is the transmission function and describes the efficiency of the measurement of electrons of a given energy, and for the Al K_α instrument it equals 1 because the data is corrected for transmission efficiency during acquisition. SF is the sensitivity factor, which deals with the inherent intensity of a peak from a given element. ECF is the energy correction factor that describes the scattering from electrons in the sample and is defined in equation 3.2.

$$ECF = (1486.6 - BE)^{0.6} \quad \text{eq. 3.2}$$

Here, the x-ray source used had an energy of 1486.6 eV and the BE is the binding energy of the peak of interest, and the exponent is based on Schofield's correction. The atomic percentage was then obtained from the ratio of the normalized areas as shown in equation 3.3.

$$Atomic\ \% = \frac{A_N}{\Sigma A_N} * 100 \quad \text{eq. 3.3}$$

To determine the type of chemical bonds present and their contribution to the total spectra, the high-resolution spectra were deconvoluted into either four (cellulose) or six peaks (lignin and wood) using a Python routine [67]. The Shirley background of each curve was calculated and subtracted from the data, which were then fitted. Each peak was fitted to a Pseudo-Voigt and the area under each peak was calculated using the trapezoid function written in NumPy. The integrated

areas were then normalized according to equation 3.3, and the percentage of each bond type was calculated using equation 3.4.

$$Bond\ Type\ \% = \frac{A_N}{\Sigma A_N} * 100 \qquad \text{eq. 3.4}$$

An electron flood gun was used during analysis to compensate for the positive change that can build-up on non-conducting samples, such as wood. Additionally, a charge compensation was applied, post-analysis, to ensure proper peak assignments. The charge compensation is determined by using a known species within the specimen as an internal reference and shifting the spectra to the appropriate binding energy for the internal reference. Typically, the C1s adventitious carbon peak is used as an internal reference and the shift required to move this peak to 285 eV is known as the charge compensation. This method has received criticism [68] and alternative approaches to binding energy referencing for non-conducting samples include depositing a noble metal either in situ [69] or on the surface [70, 71], intentionally depositing organic layers [72], and implanting noble gas atoms [73]. However, each of these methods has shortcomings, particularly when taking into consideration the rough surface of the wood specimen used here. Ultimately, to avoid introducing an additional species that could overpower the spectra from the wood polymers the C-C adventitious/aliphatic peak was used as the internal reference. With this method for charge compensation the position of the six carbon peaks is given in Table 3.4.

Table 3.4: Classification of carbon peak components for wood materials

Carbon bond	Origin in Wood	Binding Energy (Peak Center)
C-C or C-H	Hemicellulose, adventitious carbon, and extractives	285 eV
C=C	Lignin (aromatic carbons)	284.6 eV
C-O or C-O-C	Cellulose and hemicellulose (from alcohols and ether functional groups), lignin (alcohol and methoxy groups) and C-O-C in extractives	286.1 eV
C=O or O-C-O	Cellulose (ketone group) and lignin (ketones and aldehydes)	287.6 eV
COOH	Lignin (carboxylic acid) and cellulose due to X-ray opening a ring forming an aldehyde group that is easily oxidized	290.1 eV
π-π*	Lignin (aromatic carbons)	289.6 eV

3.4 Results

The first half of the results section evaluates the effects of removing extractives from the specimen and the effects of using a monatomic argon ion beam to etch the surface of the Douglas-fir. The second section provides the results for the change in chemical bonding environments in both the polymers exposed to high temperatures and through the pyrolysis zone, after the appropriate experimental conditions were set.

Experimental Considerations

Extraction of Extractives

To evaluate the effect of extractives, a line scan was first conducted on the prepared, transverse surface of the charred latewood specimen without the extractives removed. Figure 3.7a provides an example of the C1s spectrum (fit and deconvoluted) in the Douglas-fir at the unexposed surface prior to an acetone soak, O/C ratios versus exposure temperature, and the C1s peak ratios and peak areas versus exposure temperature. The O/C ratios are calculated as the total area under the O1s peak to the total area under the C1s spectrum. The C1s peak ratios are calculated as the area under the individual peaks from each bond type to the total area under the C1s spectrum.

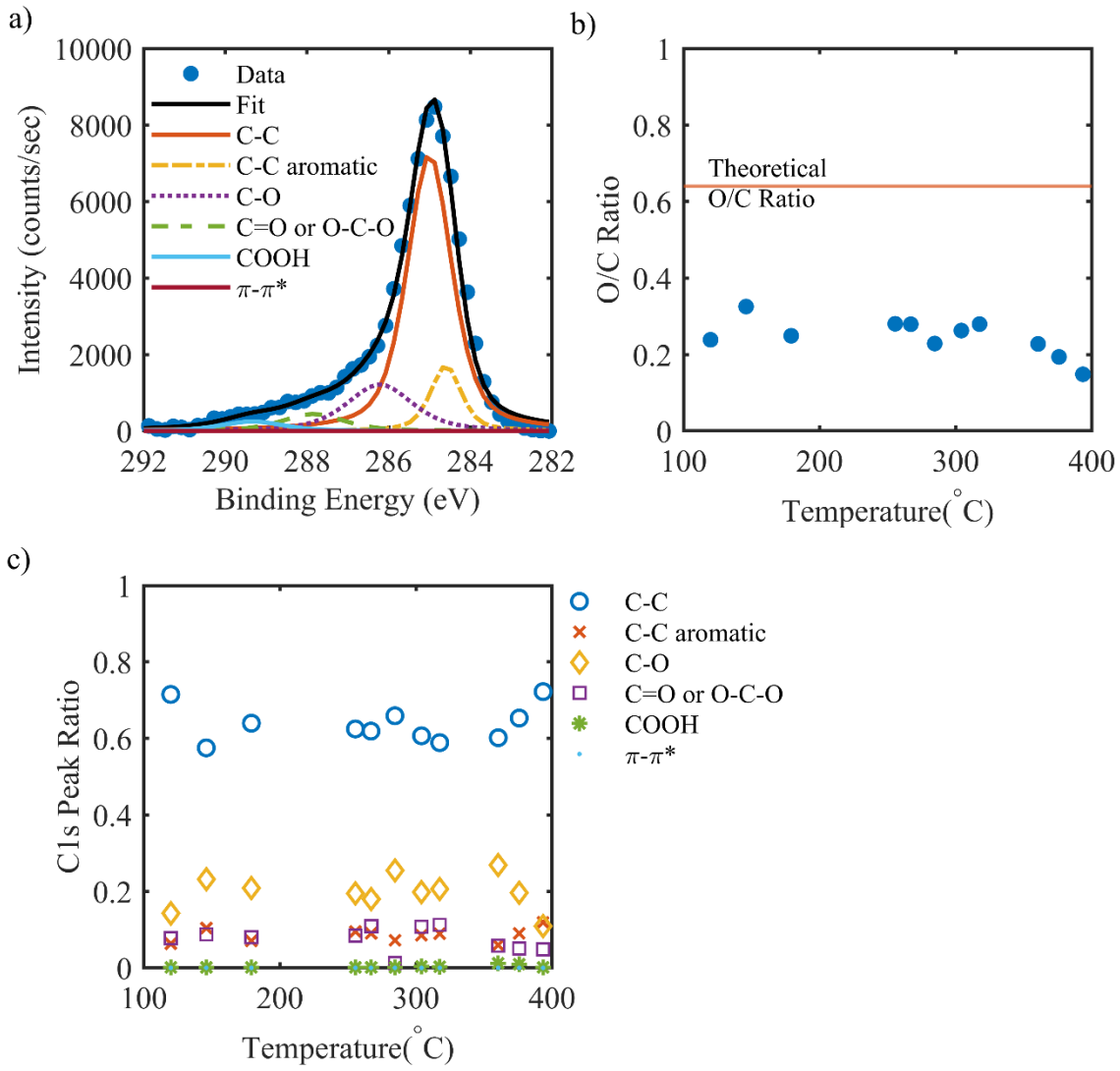

Figure 3.7: Results from charred Douglas-fir prior to removal of extractives: a) C1s data with fit and deconvoluted peaks at a temperature of 100°C, b) O/C ratio versus exposure temperature of charred Douglas-fir prior to removal of extractives, and c) C1s peak ratios.

While the C1s data appears similar to the results found by others [24, 32], it is not indicative of what would be expected in wood. Given the chemical structures of the polymers, the theoretical O/C ratios for cellulose, hemicellulose and lignin are 0.83, 0.8 and 0.33, respectively [50]. From these values and using the polymer composition for Douglas-fir previously shown in Section 2.4, the expected O/C ratio would be approximately 0.65. From Figure 3.7b, the O/C ratio averages

much lower at 0.24 throughout the specimen. Additionally, based on the structure of the wood polymers, the peak due to the carbon atoms bound to a single oxygen atom (C-O) should be larger than the C-C peak. From Figure 3.7c, it is evident that the C-C bond is artificially higher and accounts for 65% of the C1s spectrum. Furthermore, a change in the peak ratios is expected as the polymers thermally degrade at higher temperatures. However, the peak ratios within the C1s carbon spectra remain relatively constant throughout the specimen. This is potentially due to the migration of extractives during exposure to temperatures greater than 60°C [74] or under the influence of the ultrahigh vacuum (UHV) (~10^{-8} mbar) necessary to conduct XPS experiments [50].

After the acetone soak to remove extractives from the surface, XPS was conducted on ten spots on the Douglas-fir in the latewood at 2 mm from the unexposed surface. Figure 3.8 provides a comparison of the C1s peaks for the Douglas-fir before and after the extractives were removed.

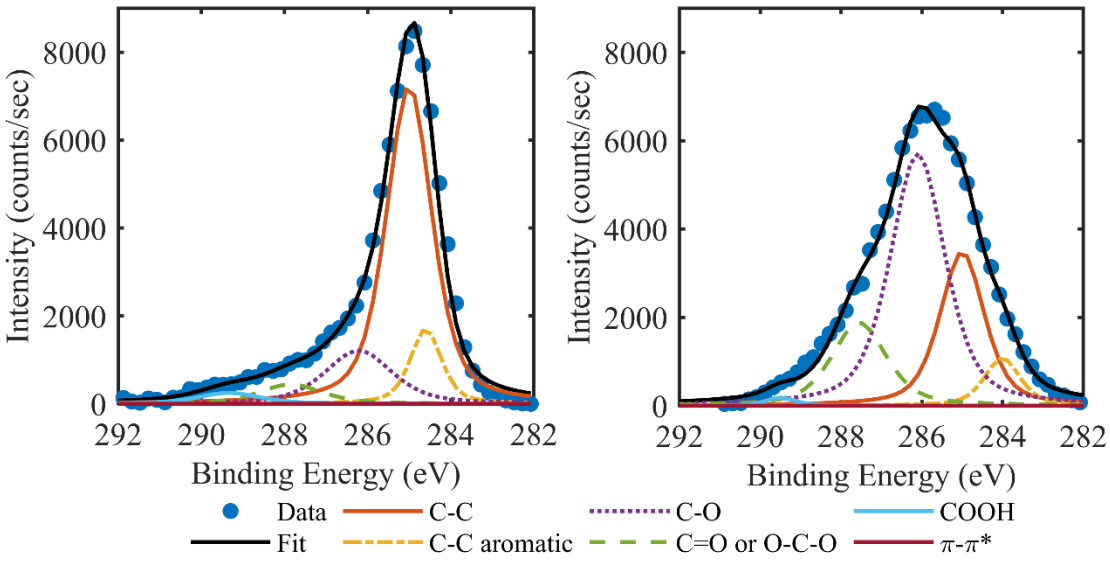

Figure 3.8: Fit and deconvoluted C1s peaks from Douglas-fir latewood without extractives removed (left) and with extractives removed (right).

Figure 3.9 is a box plot for the ten replicates showing the minimum, maximum, sample median, and the first and third quartiles for each C1s peak. The C-O peak ratio is meaningfully higher going from a peak ratio of 0.14 prior to extraction to an average of 0.4 in the specimen with extractives removed. Additionally, the C-C peak jumped from having a peak ratio of 0.7 prior to extraction to an average of 0.14 in the specimen with extractives. These results are consistent with what we would expect given the polymeric constituents of wood, and are similar to findings from Inari et al. [50].

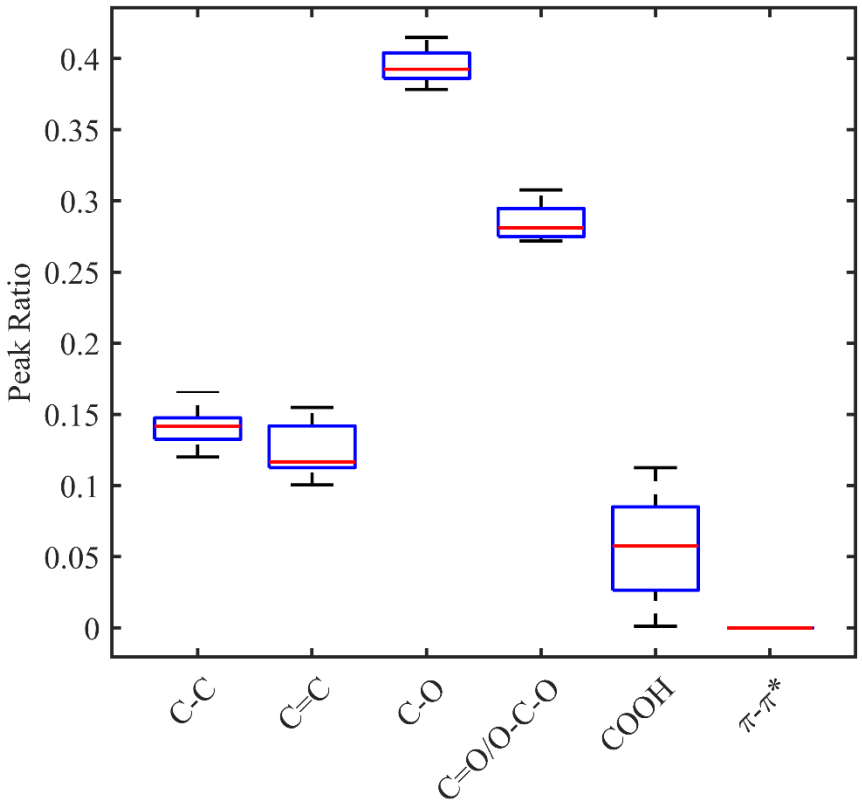

Figure 3.9: C1s peak ratios from ten replicate spots on 2 mm from the unexposed surface of the Douglas-fir latewood with extractives removed.

The final peak ratios in the specimen with extractives removed were closer to the theoretical values and, in terms of the repeatability, the peak ratios remained ordered despite the slight variance in

values. For this reason, the remainder of the XPS analysis was conducted on the charred wood specimen with the extractives removed.

Surface etching with argon

Another experimental parameter that may affect the XPS results is the use of an argon etch. Argon etching is often used for depth profiling to reveal subsurface information and to remove surface contamination on materials such as semiconductor films. Nishimiya et al. utilized argon etching for 30 seconds to exclude the effects of impurities present on the surfaces of their wood charcoal specimens, but did not note the argon energy used [24]. Hofstetter et al. demonstrated that, even with etching at the lowest available monatomic ion energy for a short amount of time, polymeric materials undergo damage that distorts the compositional information obtained with XPS [58].

To determine the effects and applicability of argon surface etching, the prepared transverse surface of the charred latewood at 1 mm from the unexposed surface was etched with an argon monatomic ion beam set to 0, 200, 500, 1000 and 2000 eV for 30 seconds each prior to XPS analysis. From Figure 3.10c, the O/C ratio is immediately affected by the argon etching decreasing from 0.5 with no etching to 0.21 with the argon energy set to 200 eV, which was the lowest setting available.

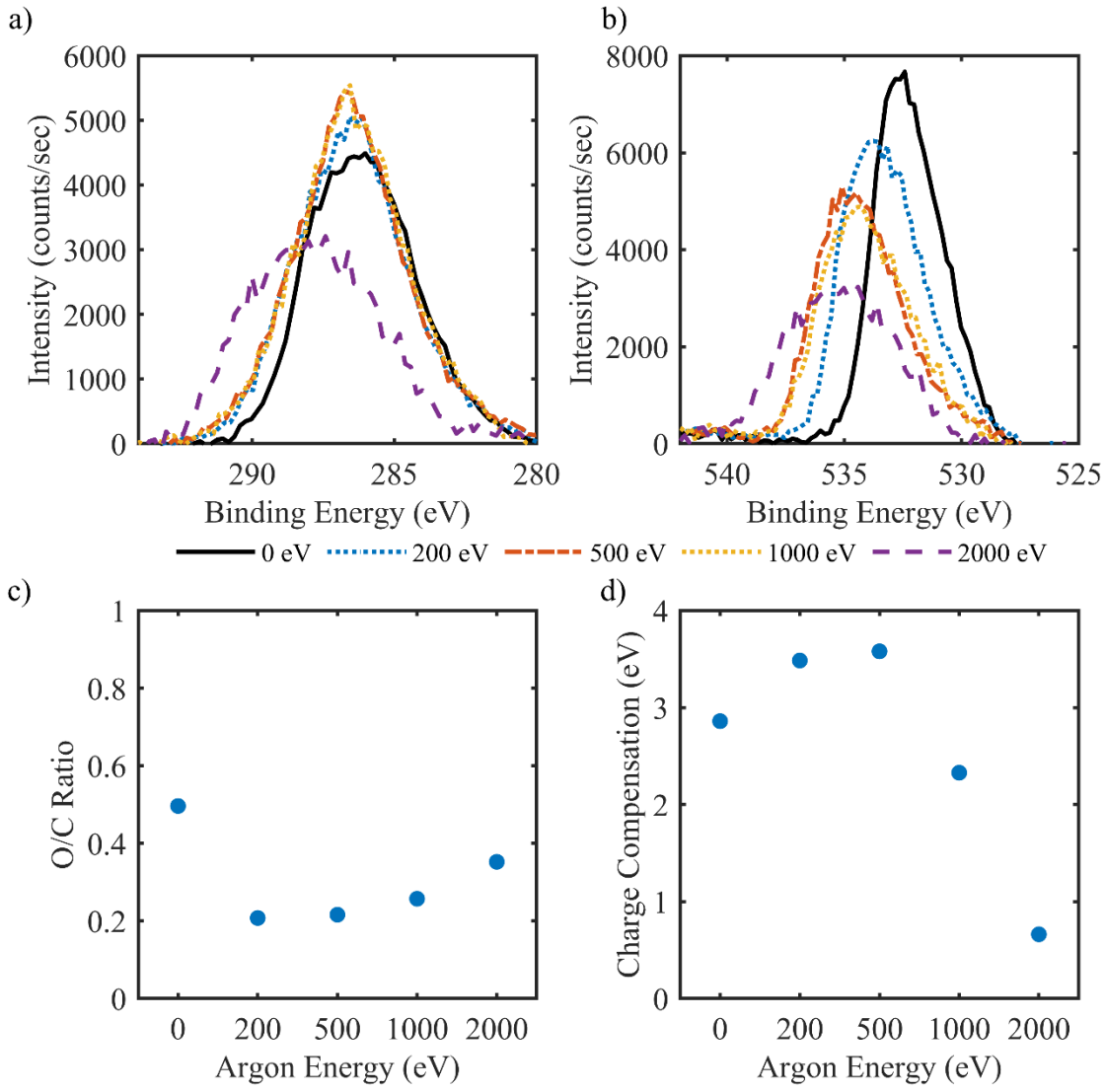

Figure 3.10: Results from surface etching with an argon monatomic ion beam energy at 1 mm from unexposed surface in charred latewood: a) C1s peaks before processing, b) O1s peaks before processing. c) O/C ratios and d) charge compensations.

Additionally, the changes in the C1s and O1s peak shapes illustrate the potential distortion caused by the argon exposure. For the C1s peak (Figure 3.10a), the shape becomes slightly sharper with increased argon monatomic ion beam energy until substantial degradation at 2000 eV is observed with a low, broad C1s peak. Also, there is a substantial change in the peak position causing the charge compensation constant (Figure 3.10d) to decrease from an average of 3 eV for argon

energies of 0 eV to 1000 eV to 0.6 at 2000 eV occurs. The O1s peak (Figure 3.10b) intensity decreases and the binding energy of the peak center increases by 1 eV with the lowest possible increase in argon energy from 0 eV to 200 eV. This trend continues with increasing argon monatomic ion beam energies and results in a low and broad O1s peak at an argon etching setting of 2000 eV. Because of the observed degradation and distortion to the XPS measurements, surface etching with argon was not used for further investigation of the charred latewood section.

With the specimen preparation methods and the instrumentation configuration set, XPS analysis of the heat-treated cellulose and lignin as well as the charred latewood from Douglas-fir was carried out.

Charred Material

Reference spectra for the cellulose and lignin exposed to high temperatures were required to compare to the thermal degradation results presented in Chapter 2. The results from the charred reference material can then be used to evaluate the thermal degradation of the polymers observed via XPS in charred wood.

Cellulose

Figure 3.11 is the high-resolution scan of the XPS spectra of C1s for cellulose exposed to 200°C with the deconvolution into four peaks. The first peak component at 285 eV corresponds to the aliphatic carbon bonding. Carbon contamination from exposure in air and the extraction process are the main contributors for this peak since all carbon atoms in cellulose are linked to an oxygen atom. However, since this cellulose was also exposed to 200°C, early stages of thermal degradation may also contribute to this peak. The C-O peak is the largest at this temperature, indicating that most of the alcohol and ether functional groups are still intact.

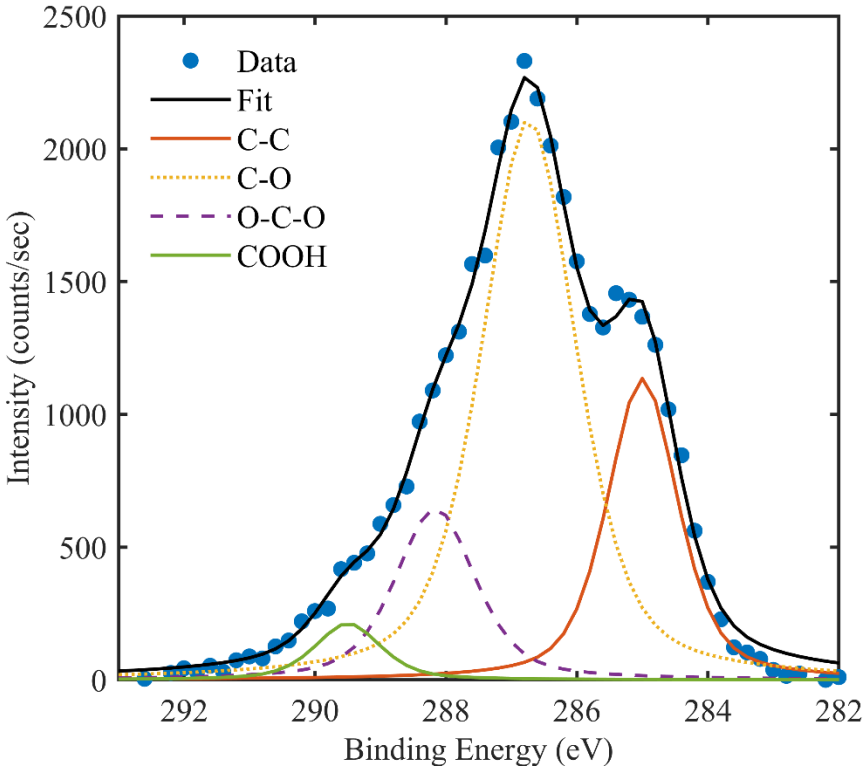

Figure 3.11: C1s data with fit and deconvoluted peaks from cellulose at a temperature of 200°C.

The repeatability of the experimental methods was evaluated by producing ten replicates of cellulose exposed to 350°C in the DSC. Figure 3.12 provides the distribution in the C1s peak ratios from each specimen. The maximum spread for the peak ratios in the fit data was negligible at 0.09 for the C-O peak, indicating that the experimental methods from the development of the charred material in the DSC to the XPS analysis result in repeatable data.

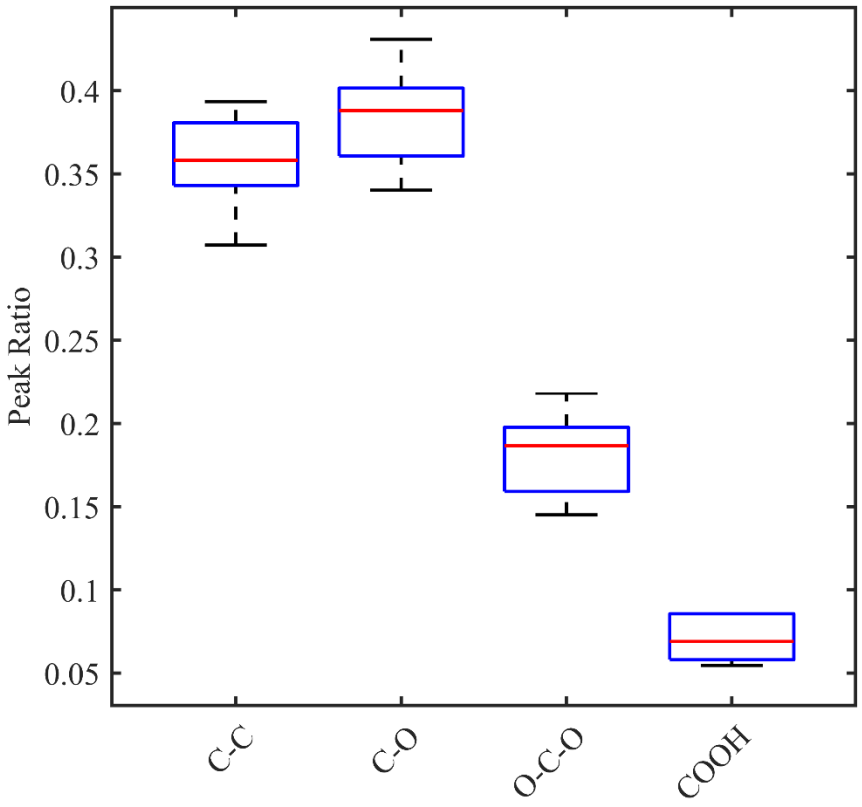

Figure 3.12: C1s peak ratios from ten replicates of cellulose exposed to a temperature of 350°C.

Cellulose has five carbon atoms of C-O and one of O-C-O, leading to a theoretical C-O peak ratio of 0.83 and O-C-O peak ratio of 0.16. While the measured C1s peak component ratios are quite different from the theoretical values, they are comparable to those obtained by Bañuls-Ciscar et al. on Avicel PH-101 cellulose [35]. This is likely due to the changes that occur during the isolation process. Figure 3.13a provides the C1s component peak ratios, versus temperature for the cellulose. The C-O peak ratio decreases while the C-C peak ratio increased with increasing temperature. Figure 3.13b is the same as Figure 3.13a, but only shows peak ratios for the C-C and C-O components with a second order polynomial fit as guide for the reader. These two bond types are typically the most significant in the C1s peak determined by peak ratio and happen to be where most substantial changes occur. From this figure we see that the C-C peak component begins to

increase around 300°C and that the components are almost equal around 350°C and beyond 365°C the dominant component changes from C-O to C-C at 400°C. C_C is calculated at the sum of the C-C, C=C and π-π* peak ratios and C_O is calculated at the sum of C-O, C=O and COOH peak ratios. C_C to C_O versus exposure temperature is presented in Figure 3.13c. This graph illustrates the distinct increase in C-C bonds compared to the other components, indicating the scission of carbon to oxygen bonds and the condensing of C-C bonds.

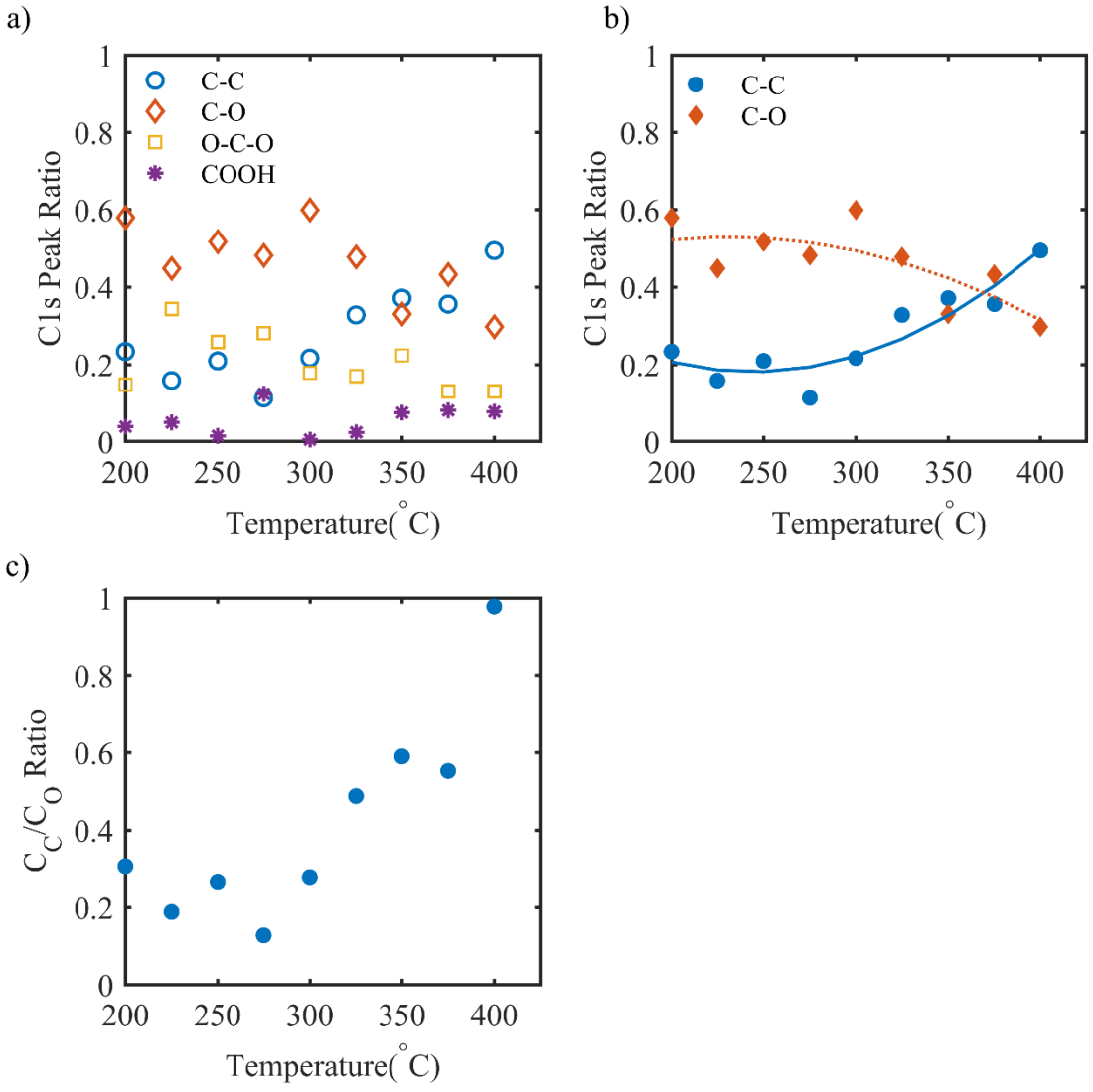

Figure 3.13: Results for heat-treated cellulose: a) C1s peak ratios, b) C-C and C-O peak ratios and d) ratio of C_C to C_O versus temperature.

Lignin

Figure 3.14 is the high-resolution scan of the XPS spectra of C1s for lignin exposed to 200°C with the deconvolution into six peaks. From the lowest binding energy to the highest, the first two peaks are associated with the aromatic and aliphatic carbon bonds found within lignin. Combined, these peaks are the most intense within the lignin, which aligns with both the theoretical expectations and XPS results on organosolv lignin [35].

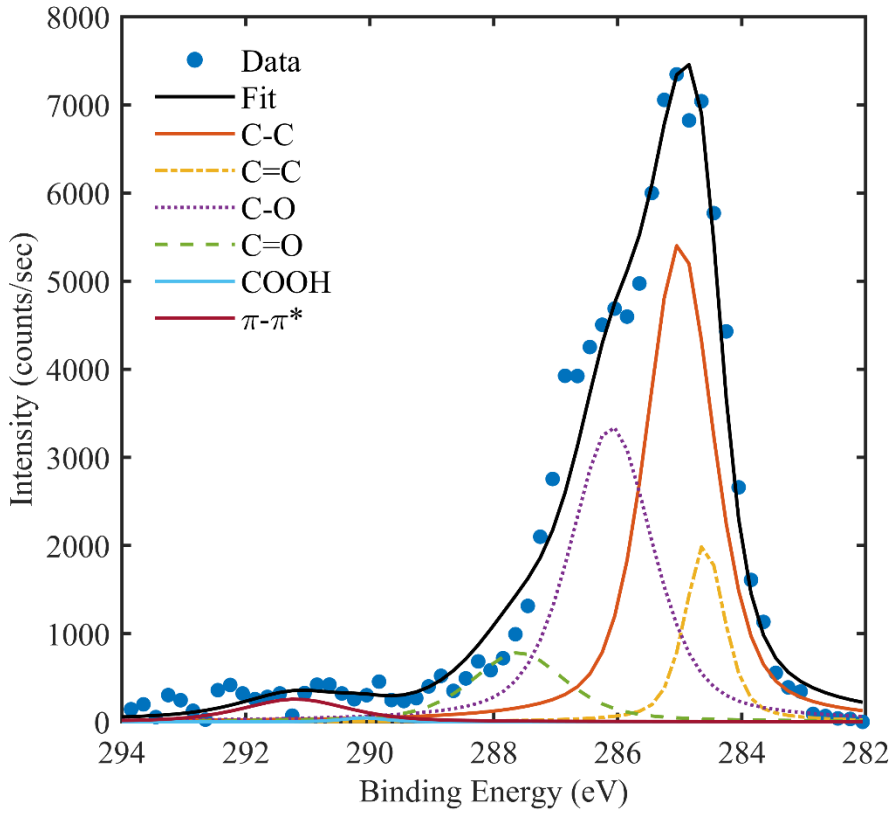

Figure 3.14: C1s data with fit and deconvoluted peaks from lignin at a temperature of 325°C.

Figure 3.15 provides the distribution in the C1s peak ratios from ten replicates of lignin exposed to 350°C. Like the cellulose, the spread in the fit data was trivial with a maximum spread for the

peak ratios of 0.07 occurring for the C-C peak. This indicates that the experimental methods used for the development of the charred material in the DSC and the XPS analysis result in repeatable data.

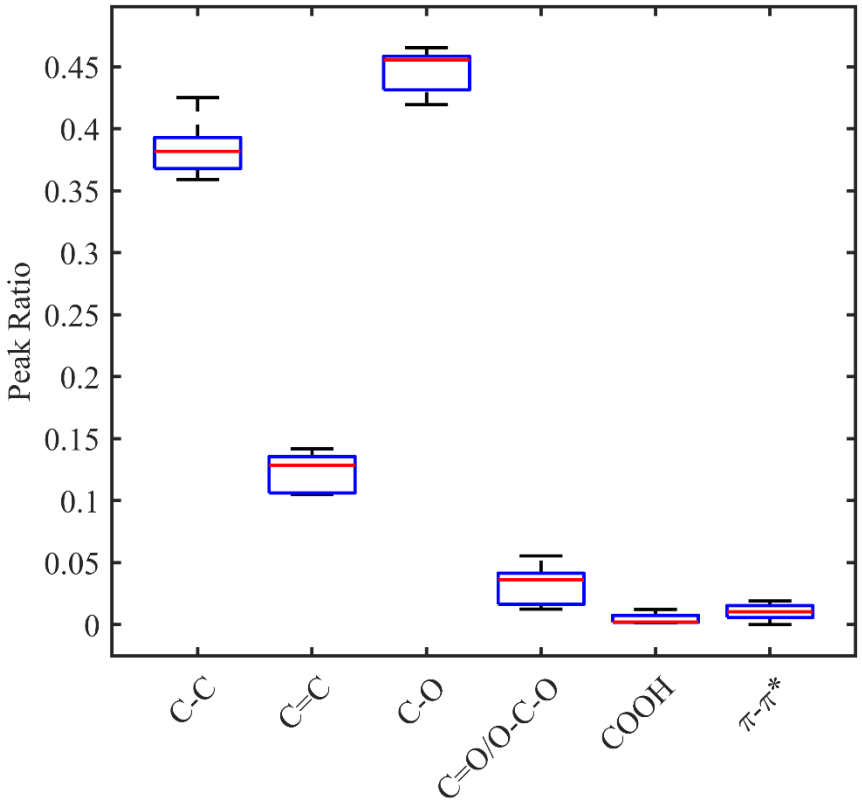

Figure 3.15: C1s peak ratios from ten replicates of lignin exposed to a temperature of 350°C.

Figure 3.16a provides the lignin C1s component peak ratios with Figure 3.16b focusing on the C-C and C-O components only with second order polynomial fits. Figure 3.16c provides the ratio of C_C to C_O versus exposure temperature for the lignin. The C-C peak ratio fluctuates between 0.21 and 0.44 below 325°C with an average of 0.34. At 325°C and higher, the C-C peak increases with an average peak ratio of 0.50. The C-O peak ratio changes in the same temperature range as the C-C peak. The average peak ratio for C-O below 325°C is 0.44 with a decrease to an average of 0.28 for temperatures of 325°C and higher. The C=C peak remains relatively constant until a

temperature of 400°C with a sudden and substantial increase to 0.33 from an average of 0.1 for temperatures below 400°C.

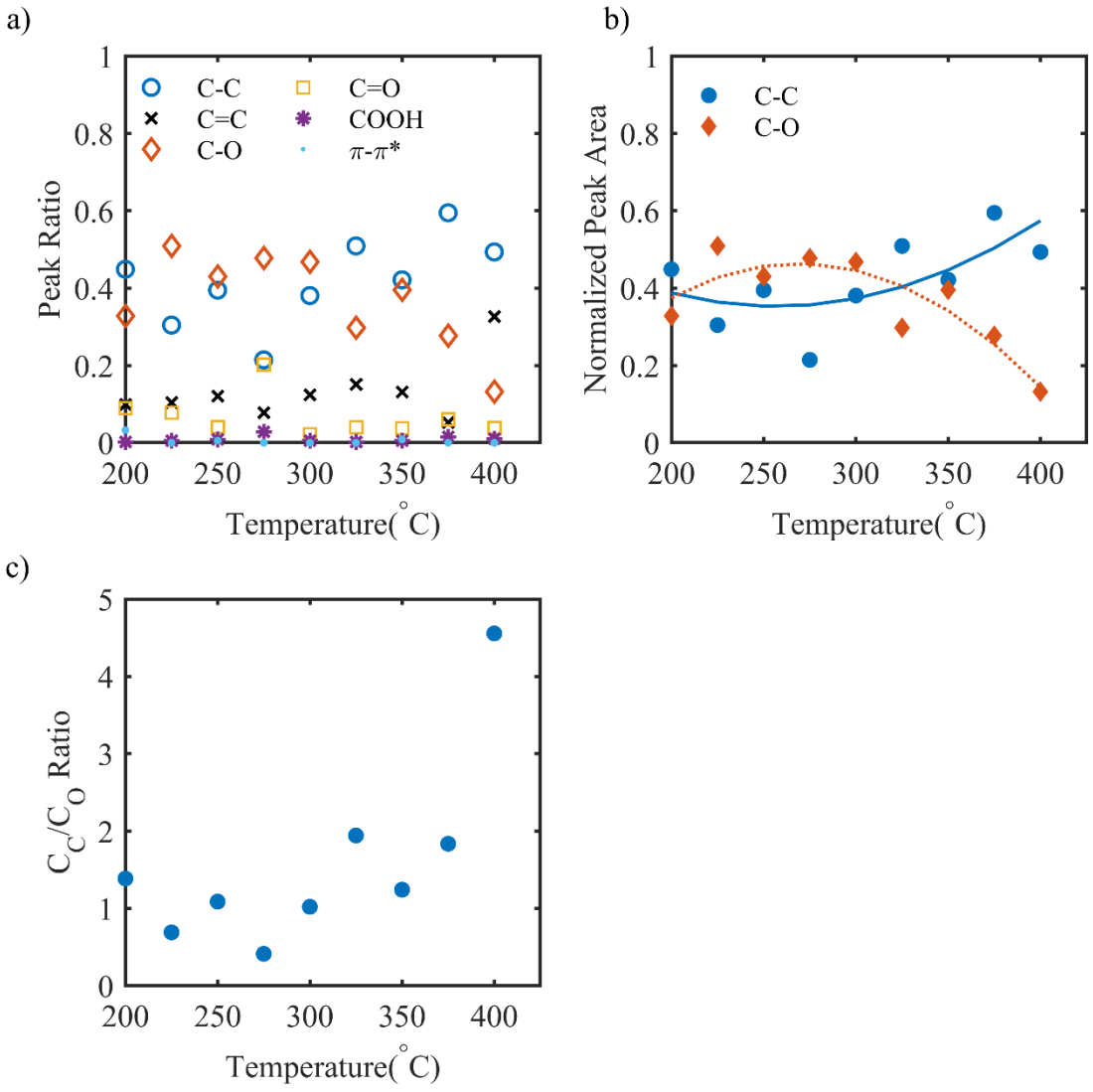

Figure 3.16: Results for heat-treated lignin: a) C1s peak ratios, b) C-C and C-O peak ratios and d) ratio of C_C to C_O versus temperature.

The ratio of C_C to C_O further illustrates the slight increase in the amount of carbon atoms bound to only other carbon atoms at temperatures above 300°C in the lignin. This indicates when the carbon to oxygen bonds in the lignin begin to break and that substantial thermal degradation of the carbon

bound to oxygen above 375°C occurs, which is highlighted by the large increase in the ratio at 400°C.

Wood

Figure 3.17 shows the locations and calculated temperatures for each spot where XPS analysis was conducted on the prepared, transverse surface of the charred latewood specimen with the extractives removed.

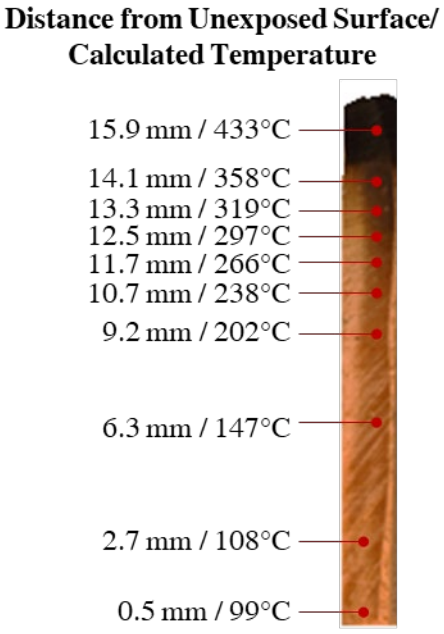

Figure 3.17: Charred latewood specimen with XPS analysis locations (distance from unexposed surface given in mm) and calculated temperatures.

Figure 3.18 provides an example of the C1s spectrum (fit and deconvoluted) in the uncharred portion of the Douglas-fir specimen. The peak shape and components are comparable to those found by Inari et al. after extraction of Norway Spruce [50].

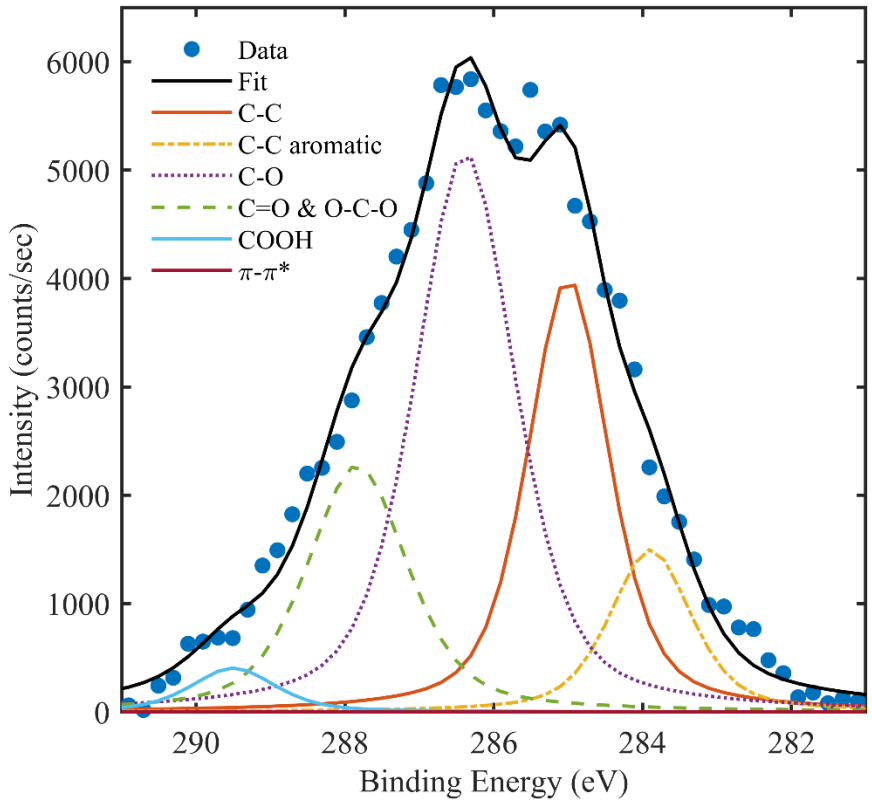

Figure 3.18: C1s data with fit and deconvoluted peaks from the uncharred edge of the latewood specimen.

Fitting six peaks to the C1s high-resolution spectra, the peak ratios and peak areas for each C1s component were obtained and presented in Table 3.5 and Figure 3.19a. The initial peak ratios at 100°C are similar to the peak ratios found by Inari et al. for Norway spruce with extractives removed [50]. The C-O peak is the most significant peak component and is attributed to the holocellulose. The C-C and C=C peak ratios remain consistent with averages of 0.23 and 0.08, respectively, until temperatures above 350°C when the peak ratios increase by at least twofold.

Table 3.5: C1s peak ratios obtained at a depth/temperature in the charred Douglas-fir latewood

Temperature (°C)	C-C	C=C	C-O	C=O O-C-O	COOH	π-π*
99	0.25	0.06	0.51	0.17	0.01	0.00
108	0.29	0.10	0.43	0.18	0.00	0.00
147	0.27	0.10	0.42	0.19	0.03	0.00

202	0.19	0.04	0.38	0.34	0.05	0.00
238	0.23	0.09	0.36	0.26	0.06	0.00
266	0.20	0.08	0.35	0.30	0.06	0.00
297	0.25	0.10	0.36	0.26	0.04	0.00
319	0.16	0.08	0.32	0.35	0.07	0.02
358	0.19	0.09	0.27	0.38	0.06	0.01
433	0.42	0.25	0.22	0.09	0.02	0.00

Between 100°C and 200°C, the C-O peak ratio decreases slightly and is then steady until another decrease begins at 300°C and continues to above 400°C. For temperatures of 350°C and lower, the C=O and O-C-O peak ratio increases as the C-O decreases, but ultimately is reduced to 0.9 at 433°C. This likely due to the C-O bond having a lower bond dissociation energy than the C=O, allowing it to degrade at lower temperatures than required to break the C=O bond.

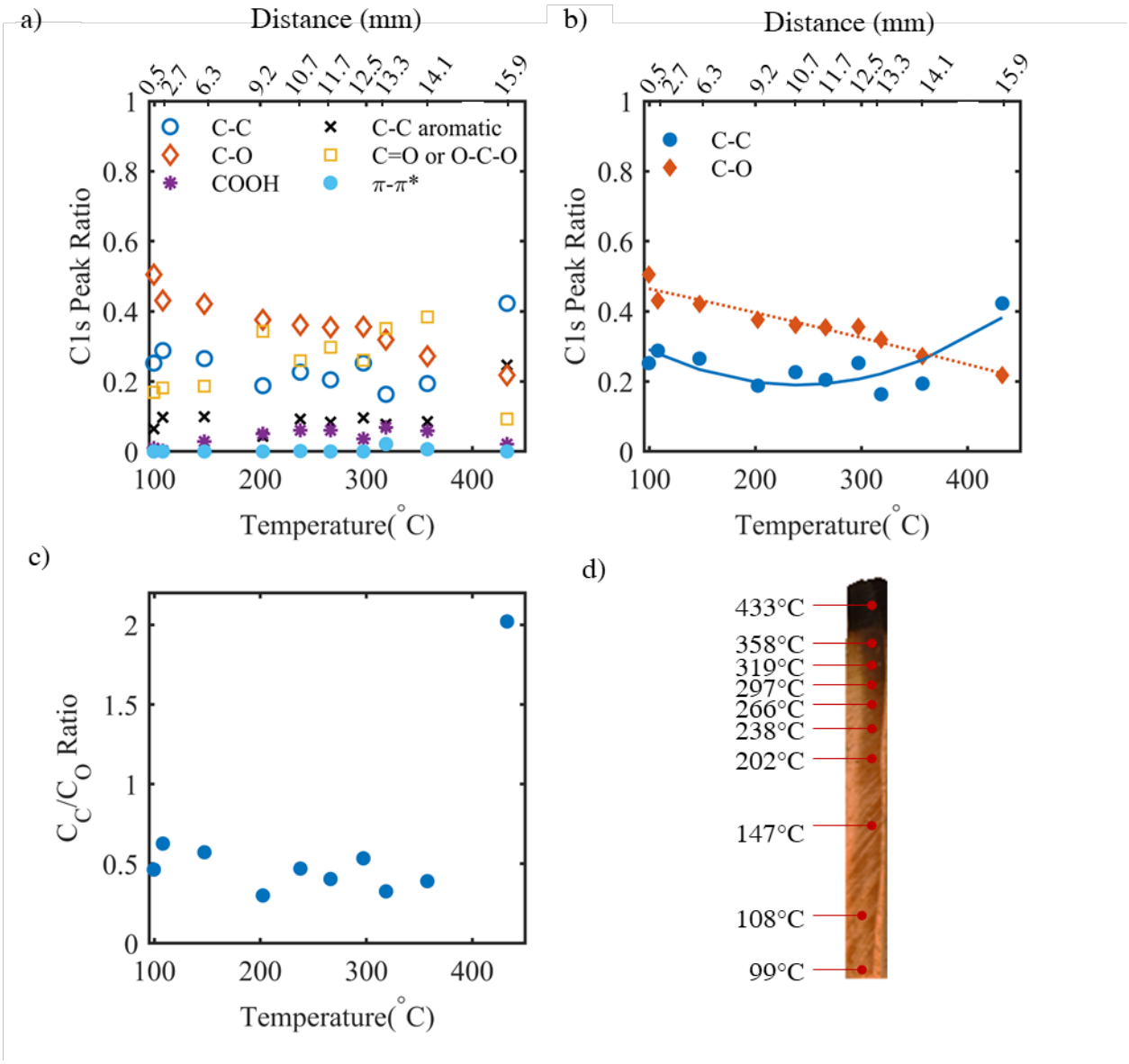

Figure 3.19: Results for charred Douglas-fir latewood: a) C1s peak ratios, b) C-C and C-O peak ratios, c) ratio of C_C to C_O versus temperature and d) XPS analysis locations in charred Douglas-fir latewood for visual comparison.

The O/C ratios are calculated as the total area under the O1s peak to the total area under the C1s peak. The O/C ratios calculated for the charred wood as a function of temperature are plotted in Figure 3.20. The calculated results are much lower than the theoretical value of 0.65 as discussed earlier in this section, but are similar to those found by Inari et al. for Norway spruce with extractives removed [50]. The low O/C ratio is potentially due to experimental artefacts from the

x-ray beam cleaving oxygen bonds or from the sanding used for surface preparation [26] and, while outside the scope of this dissertation, warrants further investigation. However, despite the values being lower than expected, the decreasing trend in the O/C ratio signifies that the overall oxygen content is decreasing temperature.

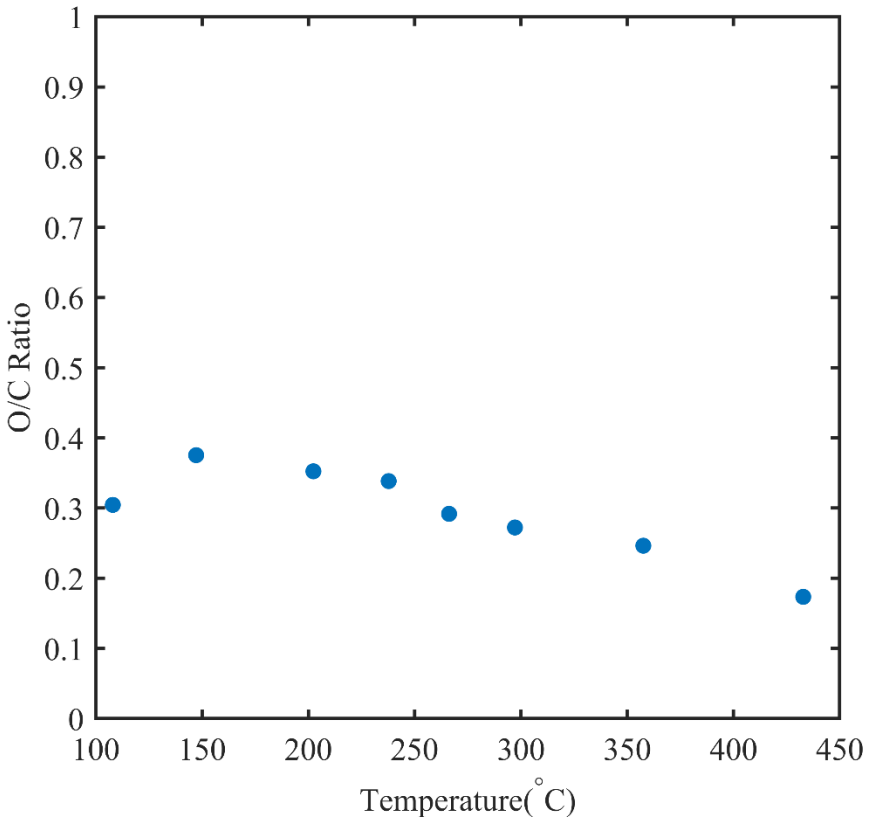

Figure 3.20: O/C ratios as a function of temperature in the charred Douglas-fir latewood specimen.

3.5 Discussion

Both experimental considerations for XPS analysis on wood and the changes in the chemical environment of cellulose, lignin and wood post-pyrolysis are presented in this chapter.

Prior to an acetone soak, high C-C peak ratios, low O/C ratios and an unchanging chemical environment with increasing temperature were observed for Douglas-fir. Inari et al. postulated the

extractives migrate through resin canals to the specimen surface under the influence of UHV necessary to conduct XPS experiments [50], causing the artificially high C-C peak and stressed the importance of removing extractives from wood specimens prior to XPS. However, they did not record consecutive XPS spectra of the specimen under UHV to see if the C-C peak continues to increase over time under UHV conditions. This work must be carried out to determine if, in fact, the extractives migrate under the influence of UHV. Here, it is more likely that the extractives are present in higher quantities on the surface due to exposure to high temperatures. It has been shown that, kiln-dried (~60°C) wood has higher extractive content at the surface when compared to air-dried lumber [74]. To remove the extractives at the surface without causing damage to the char layer, an acetone soak was used. While it is likely that this acetone soak did not remove all extractives from the charred Douglas-fir specimen, it is probable that the acetone removed extractives in the first 10 nm of the specimen, where XPS analysis occurs. The effects of the acetone soak are observed in the changes in the deconvoluted C1s peak. After the acetone soak, C-O became the most significant C1s peak component in the uncharred Douglas-fir instead of the C-C component and the C1s peak ratios were comparable to expected values in literature.

Variations of the XPS instrument settings will affect either the spectral intensity and shape or the resolution without affecting the elemental composition of the material. The use of argon etching was recommended by Nishimiya et al. to remove adventitious carbon on wood charcoal. However, etching the surface with argon poses a threat to the actual elemental composition measured and the etching process can result in various types of damage such as: molecular fragmentation, reduction, and cross-linking [58]. Applying different monatomic argon ion beam energies, it was found that the O/C ratio decreased with increasing energy. The O1s peak was heavily degraded by increasing the argon energy when compared to the C1s peak. This is likely due to preferential sputtering,

where the oxygen atoms are more rapidly removed by the argon beam than the carbon. Preferential sputtering arises from different puttering yields of the individual components in multicomponent samples [75]. The oxygen atom has been shown to be preferentially sputtered from some oxides (e.g., aluminum oxide, titanium oxide, and zirconium oxide) and is attributed to either atomic mass differences and surface binding effects [76]. Since carbon and oxygen masses are so close to each other, preferential sputtering of oxygen in wood may be attributed to surface binding effects. However, this has not been observed in wood and warrants further investigation. Additionally, increasing the argon energy leads to a decrease in the peak intensities and a shift in the peak positions of the O1s and the C1s spectra. The distortion in the compositional information obtained on the Douglas-fir is comparable to that noted by Hofstetter et al. on various polymeric materials [58]. The shift of the peak centers resulted in the charge compensation decreasing with increasing argon ion beam energy. This decrease is likely due to the change in bonding environment as the oxygen was considerably degraded by the monoatomic argon ion beam. As the material left at the surface was mostly carbon, it was slightly more conductive and a positive charge did not build up on the surface, requiring a smaller charge compensation to shift the data based on the adventitious carbon internal reference. Ultimately, the use of a monatomic argon ion beam was not used and is not recommended on wood, charred or uncharred.

Evaluating the chemical changes that occur in cellulose, lignin and wood exposed to high temperatures in air had not been completed prior to this body of work. As the temperature increased, the thermal degradation of hydroxyl groups in the cellulose began to degrade around 300°C. Above this temperature, the contributions from the C-O and O-C-O peaks decrease while the C-C peak increases. At temperatures above 350°C, the C-C component dominates the C1s spectrum, indicating the scission of carbon to oxygen bonds and the condensing of C-C bonds.

The thermal degradation, detected via changes in C1s peak component ratios, was not observed until 325°C in the isolated lignin material. Below 325°C, the C1s peak component ratios remained relatively constant. Above this temperature, the C-C peak began to slowly increase while the C-O peak decreased. Additionally, the C=C peak component began increasing at 350°C, indicating that the aromatic rings were still intact up to this temperature with major thermal degradation of the lignin occurring above 375°C.

Ultimately, the purpose of this work was to describe, for the first time, the pyrolysis in wood based on the chemical bonding environment present. For the charred Douglas-fir latewood specimen, the initial C1s peak at 100°C was similar to previous results on softwood with extractives removed [23, 37, 50]. Deconvolution of this peak results in the C-O peak as the most significant peak component, which is attributed to the holocellulose. Based on the bond scission measured using XPS, the onset of thermal degradation begins at low temperatures (<200°C). This is observed as the C-O peak component decreases between 100°C and 200°C and is likely due to the sidechains of the in situ hemicellulose cleaving [77-79]. From 200°C to 300°C, the C-O peak component remains steady and then decreases again for temperatures above 300°C. This decrease is likely due to the thermal degradation of the in situ cellulose and aligns with the temperature at which a decrease in the C-O peak for the isolated cellulose was observed. The C=C peak in the isolated lignin did not increase until it reached temperatures above 350°C, because the aromatic rings are thermally stable. Similarly, the C=C peak component in the Douglas-fir did not increase until above 350°C, indicating that similar chemical changes in the isolated lignin and the in situ lignin are occurring around the same temperature. The temperature range for the condensation of C=C bonds corresponds to the degradation of carbonyl groups (O-C-O and C=O).

3.6 Conclusions

The results obtained in this study demonstrate the importance of specimen preparation when conducting XPS analysis on wood. Using an acetone soak on the Douglas-fir resulted in C1s peak ratios in closer agreement with theoretical values for wood. This suggests that the removal of some extractives reduces their effect on the C1s spectrum. However, it is proposed that further investigation include analysis of the extractive residue from the acetone soak and continuous XPS analysis to determine if extractives migrate over time under UHV.

The XPS instrument settings also affected the results and it was shown that the use of a monoatomic argon ion beam at any energy is not appropriate for wood as it causes distortion in the data. Even the lowest possible increase in argon ion beam energy caused a shift in peak centers to higher binding energies and a decrease in the O/C ratio. Also, for the first time, preferential sputtering was observed in wood as the O1s peak was substantially affected by increasing argon energy when compared to the C1s peak.

Using XPS, the spectra for pyrolyzed, isolated cellulose and lignin as well as charred Douglas-fir were obtained. The C1s spectra of the uncharred Douglas-fir agreed with values reported in the literature by others, although the O/C ratio was lower than theoretical values. For charred Douglas-fir, the XPS analysis occurred from the virgin wood through to the char layer to observe changes in chemical composition. The results show the thermal degradation of the holocellulose in the Douglas-fir occurred at lower temperature ranges than those observed in the isolated cellulose. Additionally, the double carbon bonds found in the lignin aromatic rings were unchanging in both the isolated polymers and the Douglas-fir until temperatures above 350°C, when the carbonyl groups degraded, and carbon condensed. Further investigation on other charred wood of other species and verification using complementary techniques, such as x-ray diffraction that can

distinguish between the cellulose and hemicellulose, are recommended. Nevertheless, if the thermal degradation of the polymers is further confirmed, the information obtained from XPS analysis could become crucial in verifying pyrolysis models for thermally thick wood.

3.7 References

[1] C. Lautenberger, "A Generalized Pyrolysis Model for Combustible Solids (PhD. thesis) University of California," ed: Berkeley, 2007.

[2] M. Spearpoint and J. Quintiere, "Predicting the burning of wood using an integral model," *Combustion and Flame,* vol. 123, pp. 308-325, 2000.

[3] Y. Chen, M. Delichatsios, and V. Motvalli, "Material pyrolysis properties, part I: an integral model for one-dimensional transient pyrolysis of charring and non-charring materials," *Combustion Science and Technology,* vol. 88, pp. 309-328, 1993.

[4] B. Moghtaderi, V. Novozhilov, D. Fletcher, and J. Kent, "An integral model for the transient pyrolysis of solid materials," *Fire and Materials,* vol. 21, pp. 7-16, 1997.

[5] F. Jia, E. Galea, and M. K. Patel, "Numerical simulation of the mass loss process in pyrolizing char materials," *Fire and materials,* vol. 23, pp. 71-78, 1999.

[6] C. Di Blasi, "Modeling chemical and physical processes of wood and biomass pyrolysis," *Progress in Energy and Combustion Science,* vol. 34, pp. 47-90, 2008.

[7] C. Di Blasi, "Modeling and simulation of combustion processes of charring and non-charring solid fuels," *Progress in energy and combustion science,* vol. 19, pp. 71-104, 1993.

[8] A. Galgano and C. D. Blasi*, "Infinite-versus finite-rate kinetics in simplified models of wood pyrolysis," *Combustion science and technology,* vol. 177, pp. 279-303, 2005.

[9] K. M. Bryden, K. W. Ragland, and C. J. Rutland, "Modeling thermally thick pyrolysis of wood," *Biomass and Bioenergy,* vol. 22, pp. 41-53, 2002.

[10] C. Di Blasi, "The state of the art of transport models for charring solid degradation," *Polymer international,* vol. 49, pp. 1133-1146, 2000.

[11] F. Shafizadeh, "The Chemistry of Pyrolysis and Combustion," in *The Chemistry of Solid Wood*. vol. 207, R. M. Rowell, Ed., ed Washington, DC: American Chemical Society, 1984.

[12] H.-C. Kung, "A mathematical model of wood pyrolysis," *Combustion and flame,* vol. 18, pp. 185-195, 1972.

[13] H. Yang, R. Yan, H. Chen, D. H. Lee, and C. Zheng, "Characteristics of hemicellulose, cellulose and lignin pyrolysis," *Fuel,* vol. 86, pp. 1781-1788, 2007.

[14] L. Yang, Y. Wang, X. Zhou, J. Dai, and Z. Deng, "Experimental and numerical study of the effect of sample orientation on the pyrolysis and ignition of wood slabs exposed to radiation," *Journal of Fire Sciences,* vol. 30, pp. 211-223, 2012/05/04/2015- -09 2012.

[15] Y. Lizhong, Z. Yupeng, W. Yafei, and G. Zaifu, "Predicting charring rate of woods exposed to time-increasing and constant heat fluxes," *Journal of Analytical and Applied Pyrolysis,* vol. 81, pp. 1-6, 2008.

[16] C. Lautenberger, G. Rein, and C. Fernandez-Pello, "The application of a genetic algorithm to estimate material properties for fire modeling from bench-scale fire test data," *Fire safety journal,* vol. 41, pp. 204-214, 2006.

[17] S. Wang, X. Guo, K. Wang, and Z. Luo, "Influence of the interaction of components on the pyrolysis behavior of biomass," *Journal of Analytical and Applied Pyrolysis,* vol. 91, pp. 183-189, 2011.

[18] S. D. Stefanidis, K. G. Kalogiannis, E. F. Iliopoulou, C. M. Michailof, P. A. Pilavachi, and A. A. Lappas, "A study of lignocellulosic biomass pyrolysis via the pyrolysis of cellulose, hemicellulose and lignin," *Journal of analytical and applied pyrolysis,* vol. 105, pp. 143-150, 2014.

[19] S. Alves and J. Figueiredo, "A model for pyrolysis of wet wood," *Chemical Engineering Science,* vol. 44, pp. 2861-2869, 1989.

[20] C. A. Hill, *Wood modification: chemical, thermal and other processes*. West Sussex, England: John Wiley & Sons, 2006.

[21] J. Chastain, R. C. King, and J. Moulder, *Handbook of X-ray photoelectron spectroscopy: a reference book of standard spectra for identification and interpretation of XPS data*: Physical Electronics Division, Perkin-Elmer Corporation Eden Prairie, Minnesota, 1992.

[22] P. Nzokou and D. Pascal Kamdem, "X-ray photoelectron spectroscopy study of red oak-(Quercus rubra), black cherry-(Prunus serotina) and red pine-(Pinus resinosa) extracted wood surfaces," *Surface and interface analysis,* vol. 37, pp. 689-694, 2005.

[23] G. N. Inari, M. Petrissans, J. Lambert, J. Ehrhardt, and P. Gérardin, "XPS characterization of wood chemical composition after heat-treatment," *Surface and interface analysis,* vol. 38, pp. 1336-1342, 2006.

[24] K. Nishimiya, T. Hata, Y. Imamura, and S. Ishihara, "Analysis of chemical structure of wood charcoal by X-ray photoelectron spectroscopy," *Journal of Wood Science,* vol. 44, pp. 56-61, 1998.

[25] G. Sinn, M. Gindl, A. Reiterer, and S. Stanzl-Tschegg, "Changes in the surface properties of wood due to sanding," *Holzforschung,* vol. 58, pp. 246-251, 2004.

[26] G. Sinn, A. Reiterer, and S. Stanzl-Tschegg, "Surface analysis of different wood species using X-ray photoelectron spectroscopy (XPS)," *Journal of materials science,* vol. 36, pp. 4673-4680, 2001.

[27] N. M. Stark and L. M. Matuana, "Surface chemistry changes of weathered HDPE/wood-flour composites studied by XPS and FTIR spectroscopy," *Polymer Degradation and Stability,* vol. 86, pp. 1-9, 2004.

[28] L. M. Matuana and D. P. Kamdem, "Accelerated ultraviolet weathering of PVC/wood-flour composites," *Polymer Engineering & Science,* vol. 42, pp. 1657-1666, 2002.

[29] D. Kamdem, B. Riedl, A. Adnot, and S. Kaliaguine, "ESCA spectroscopy of poly (methyl methacrylate) grafted onto wood fibers," *Journal of applied polymer science,* vol. 43, pp. 1901-1912, 1991.

[30] X. Hua, S. Kaliaguine, B. Kokta, and A. Adnot, "Surface analysis of explosion pulps by ESCA Part 1. Carbon (1s) spectra and oxygen-to-carbon ratios," *Wood Science and Technology,* vol. 27, pp. 449-459, 1993.

[31] T. L. Barr and S. Seal, "Nature of the use of adventitious carbon as a binding energy standard," *Journal of Vacuum Science & Technology A: Vacuum, Surfaces, and Films,* vol. 13, pp. 1239-1246, 1995.

[32] C.-M. Popescu, C.-M. Tibirna, and C. Vasile, "XPS characterization of naturally aged wood," *Applied Surface Science,* vol. 256, pp. 1355-1360, 2009.

[33] R. Bodîrlău, C.-A. Teacă, D. Roşu, L. Roşu, C.-D. Varganici, and A. Coroabă, "Physico-chemical properties investigation of softwood surface after treatment with organic anhydride," *Central European Journal of Chemistry,* vol. 11, pp. 2098-2106, 2013.
[34] H. Darmstadt, C. Roy, and S. Kaliaguine, "ESCA characterization of commercial carbon blacks and of carbon blacks from vacuum pyrolysis of used tires," *Carbon,* vol. 32, pp. 1399-1406, 1994.
[35] J. Bañuls-Ciscar, M.-L. Abel, and J. F. Watts, "Characterisation of cellulose and hardwood organosolv lignin reference materials by XPS," *Surface Science Spectra,* vol. 23, pp. 1-8, 2016.
[36] X. Hua, S. Kaliaguine, B. Kokta, and A. Adnot, "Surface analysis of explosion pulps by ESCA Part 2. Oxygen (1s) and sulfur (2p) spectra," *Wood Science and Technology,* vol. 28, 1993.
[37] J. Bañuls-Ciscar, D. Pratelli, M. L. Abel, and J. F. Watts, "Surface characterisation of pine wood by XPS," *Surface and Interface Analysis,* vol. 48, pp. 589-592, 2016.
[38] G. C. Smith, "20 X-ray photoelectron spectroscopy analysis of biochar," *Biochar: A Guide to Analytical Methods,* p. 229, 2017.
[39] G. Sorrenti, C. A. Masiello, B. Dugan, and M. Toselli, "Biochar physico-chemical properties as affected by environmental exposure," *Science of the total Environment,* vol. 563, pp. 237-246, 2016.
[40] S. Wang, L. Wu, X. Hu, L. Zhang, T. Li, S. Jiang*, et al.*, "Changes in the Biochar Chemical Structure during the Low-Temperature Gasification of Mallee Biochar in Air as Revealed with Fourier Transform Infrared/Raman and X-ray Photoelectron Spectroscopies," *Energy & fuels,* vol. 32, pp. 12545-12553, 2018.
[41] S. Yoo, S. S. Kelley, D. C. Tilotta, and S. Park, "Structural characterization of loblolly pine derived biochar by X-ray diffraction and electron energy loss spectroscopy," *ACS Sustainable Chemistry & Engineering,* vol. 6, pp. 2621-2629, 2018.
[42] H. Chen, *Biotechnology of lignocellulose*: Springer, 2005.
[43] H. Chen and H. Chen, "Lignocellulose biorefinery feedstock engineering," *Lignocellulose Biorefinery Engineering, 1st ed.; Woodhead Publishing: Cambridge, UK,* pp. 37-86, 2015.
[44] A. Shrotri, H. Kobayashi, and A. Fukuoka, "Catalytic conversion of structural carbohydrates and lignin to chemicals," in *Advances in Catalysis*. vol. 60, ed: Elsevier, 2017, pp. 59-123.
[45] MilliporeSigma. (2018). *MSDS sheets*. Available: www.sigmaaldrich.com
[46] K. B. McGrattan, H. R. Baum, R. G. Rehm, A. Hamins, G. P. Forney, J. Floyd*, et al.*, *Fire dynamics simulator--Technical reference guide*: National Institute of Standards and Technology, Building and Fire Research Laboratory, 2000.
[47] K. McGrattan, S. Hostikka, R. McDermott, J. Floyd, C. Weinschenk, and K. Overholt, "Fire dynamics simulator user's guide," *NIST special publication,* vol. 1019, 2013.
[48] R. H. White and E. V. Nordheim, "Charring rate of wood for ASTM E 119 exposure," *Fire Technology,* vol. 28, pp. 5-30, 1992.
[49] "Calculating the Fire Resistance of Wood Members and Assemblies, Technical Report No. 10," American Wood Council, Leesburg, VA2018.
[50] G. N. Inari, M. Pétrissans, S. Dumarcay, J. Lambert, J. Ehrhardt, M. Šernek*, et al.*, "Limitation of XPS for analysis of wood species containing high amounts of lipophilic extractives," *Wood Science and Technology,* vol. 45, pp. 369-382, 2011.
[51] M. Sernek, "Comparative analysis of inactivated wood surfaces," Virginia Tech, 2002.

[52] D. Kocaefe, X. Huang, Y. Kocaefe, and Y. Boluk, "Quantitative characterization of chemical degradation of heat-treated wood surfaces during artificial weathering using XPS," *Surface and interface analysis,* vol. 45, pp. 639-649, 2013.
[53] E. Sjöström and R. Alén, *Analytical methods in wood chemistry, pulping, and papermaking*: Springer Science & Business Media, 2013.
[54] T. L. Eberhardt and L. J. Samuelson, "Collection of wood quality data by X-ray densitometry: a case study with three southern pines," *Wood Science and Technology,* vol. 49, pp. 739-753, 2015.
[55] T. L. Eberhardt, C.-L. So, and D. J. Leduc, "Wood variability in mature longleaf pine: Differences related to cardinal direction for a softwood in a humid subtropical climate," *Wood and Fiber Science,* vol. 50, pp. 323-336, 2018.
[56] C. Santos, M. Gomes, L. Colodette, M. Resende, G. Lino, and V. Zanuncio, "A Comparison Of Methods For Eucalypt Wood Removal Extractive," *5th International Colloqium on Eucalyptus Pulp,* 2011.
[57] G. Barth, R. Linder, and C. Bryson, "Advances in charge neutralization for XPS measurements of nonconducting materials," *Surface and Interface Analysis,* vol. 11, pp. 307-311, 1988.
[58] Y. J. Hofstetter and Y. Vaynzof, "Quantifying the damage induced by x-ray photoelectron spectroscopy depth profiling of organic conjugated polymers," *ACS Applied Polymer Materials,* vol. 1, pp. 1372-1381, 2019.
[59] S. Hüfner, *Photoelectron spectroscopy: principles and applications*: Springer Science & Business Media, 2013.
[60] H. Hansen, S. Tougaard, and H. Biebuyck, "The adsorption of alkanethiols on gold studied quantitatively by XPS inelastic background analysis," *Journal of electron spectroscopy and related phenomena,* vol. 58, pp. 141-158, 1992.
[61] S. Tougaard, "Quantitative analysis of the inelastic background in surface electron spectroscopy," *Surface and Interface Analysis,* vol. 11, pp. 453-472, 1988.
[62] M. Repoux, "Comparison of background removal methods for XPS," *Surface and interface analysis,* vol. 18, pp. 567-570, 1992.
[63] G. Wertheim and L. Walker, "Many-body effects in transition metals: role of the density of states," *Journal of Physics F: Metal Physics,* vol. 6, p. 2297, 1976.
[64] Y. Yafet, "Y. Yafet and GK Wertheim, J. Phys. F 7, 357 (1977)," *J. Phys. F,* vol. 7, p. 357, 1977.
[65] M. Schmid, H. P. Steinrück, and J. M. Gottfried, "A new asymmetric Pseudo-Voigt function for more efficient fitting of XPS lines," *Surface and Interface Analysis,* vol. 46, pp. 505-511, 2014.
[66] A. Herrera-Gomez, "The peak-Shirley background," Internal Report. CINVESTAV-Unidad Queretaro2011.
[67] N. Plaza, "Automated Peak Fitting Routine for XPS data from wood (Version Version from March 2019)," ed, 2019.
[68] G. Greczynski and L. Hultman, "X-ray photoelectron spectroscopy: Towards reliable binding energy referencing," *Progress in Materials Science,* p. 100591, 2019.
[69] D. Hnatowich, J. Hudis, M. Perlman, and R. Ragaini, "Determination of charging effect in photoelectron spectroscopy of nonconducting solids," *Journal of Applied Physics,* vol. 42, pp. 4883-4886, 1971.

[70] D. Stephenson and N. Binkowski, "X-ray photoelectron spectroscopy of silica in theory and experiment," *Journal of Non-Crystalline Solids,* vol. 22, pp. 399-421, 1976.
[71] M. Edgell, D. Baer, and J. Castle, "Biased referencing experiments for the XPS analysis of non-conducting materials," *Applied Surface Science,* vol. 26, pp. 129-149, 1986.
[72] C. Vesely and D. Langer, "Electronic core levels of the II B− VI A compounds," *Physical Review B,* vol. 4, p. 451, 1971.
[73] P. Citrin and D. Hamann, "Measurement and calculation of polarization and potential-energy effects on core-electron binding energies in solids: X-ray photoemission of rare gases implanted in noble metals," *Physical Review B,* vol. 10, p. 4948, 1974.
[74] O. Myronycheva, O. Karlsson, M. Sehlstedt-Persson, M. Öhman, and D. Sandberg, "Distribution of low-molecular lipophilic extractives beneath the surface of air-and kiln-dried Scots pine sapwood boards," *PloS one,* vol. 13, 2018.
[75] S. Oswald, "X-Ray Photoelectron Spectroscopy in Analysis of Surfaces," *Encyclopedia of Analytical Chemistry: Applications, Theory and Instrumentation,* 2006.
[76] J. Malherbe, S. Hofmann, and J. Sanz, "Preferential sputtering of oxides: A comparison of model predictions with experimental data," *Applied surface science,* vol. 27, pp. 355-365, 1986.
[77] A. Sinha, R. Gupta, and J. A. Nairn, "Thermal degradation of bending properties of structural wood and wood-based composites," *Holzforschung,* vol. 65, pp. 221-229, 2011.
[78] F. Shafizadeh and A. Bradbury, "Thermal degradation of cellulose in air and nitrogen at low temperatures," *Journal of applied polymer science,* vol. 23, pp. 1431-1442, 1979.
[79] F. C. Beall and H. W. Eickner, "Thermal degradation of wood components: a review of the literature," *Research Papers. United States Forest Products Laboratory,* 1970.

Chapter 4. Changes in Cell Wall Mechanical Properties Caused by Pyrolysis

4.1 Introduction

The pyrolysis process causes substantial chemical changes to the wood cell wall as the polymers thermally degrade [1, 2]. Because of these chemical changes, the physical and mechanical properties are modified. The modifications become greater at higher exposure temperatures and longer exposure times. In bulk wood, the effect of temperature on the various mechanical properties, such as modulus of elasticity (MOE), are well studied and compiled. Green et al. noted that the strength of lumber is inversely related to the temperature [3]. Similarly, Sinha et al. found the MOE of wood exposed to elevated temperatures was lower than that of a non-exposed control [4]. To study the effects while exposed to flames, Firmanti et al. developed a bench-scale four-point bending test with a continuous flame applied in the shear-free region of the specimen between the applied load points [5]. They found that the time to failure was exponentially affected by the stress levels. Recently, Zelinka et al. developed a bench-scale test method to quantify the strength loss in wood adhesive below the char temperature of wood and, as part of that work, also quantified the strength loss in solid wood [6]. For Douglas-fir, they found that, as the temperature increased, the strength, modulus, and strain at failure all decreased.

Microstructural changes in wood caused by pyrolysis have been evaluated by Brandt et al. using transmission electron microscopy (TEM) and atomic force microscopy (AFM) imaging. They showed that the layered microstructure of the wood cell wall disappears with exposure to temperatures above 250°C and is replaced by a homogeneous structure. Paris et al. conducted a detailed microstructural study of softwood pyrolysis using small- and wide-angle X-ray scattering

measurements to evaluate the cellulose crystallinity and found that between 250°C and 350°C, the crystal structure of the cellulose is fully deteriorated [2].

To evaluate the mechanical properties on the length scale required to compare the thermo-chemical changes found in Chapters 2 and 3, nanoindentation (NI) was used. Since Wimmer et al. first demonstrated the utility of nanoindentation to probe wood cell wall layer mechanical properties, nanoindentation has become a valuable tool in wood science research [7, 8]. Jakes et al. developed improved protocols and methods for nanoindentation experiments on wood [9, 10]. Youssefian et al. focused on the effect of moisture on the elastic moduli within the cell walls of bamboo fiber [11]. While not related to the effect of high temperature on the cell wall mechanical properties, the moisture content will be extremely low during pyrolysis, and the findings of Youssefian et al. are applicable to this work. They found that, at low moisture contents (<2%), the elastic modulus in the transverse and longitudinal direction were 8 GPa and 19 GPa, respectively. These values are slightly higher than obtained at higher moisture contents. For instance, at a moisture content of 8%, elastic modulus in the transverse and longitudinal direction were 5 GPa and 16 GPa, respectively. Zickler et al. studied the changes of mechanical properties of spruce wood pyrolyzed in an inert atmosphere as a function of temperature up to 2400°C. Their pyrolyzed wood was embedded in polymethyl methacrylate (PMMA) prior to conducting nanoindentation experiments. They found that hardness increased by more than one order of magnitude to 4.5 GPa at 700°C and that deformation induced by the indenter was largely visco-plastic in native wood, but it was almost purely elastic in the charred region, with particularly low values of the indentation ductility index around 700°C [12]. Brandt et al. used Scots pine pyrolyzed at temperatures up to 325°C in inert atmosphere and embedded in an epoxy resin. They found that the development of the mechanical properties with increasing temperature can be explained by alterations in the structure but that

hardness follows no clear trend through pyrolytic conversion up to 325°C [1]. Wang et al. set out to evaluate the effects of on the wood cell walls of Masson pine that was thermally modified in nitrogen at 150, 170 and 190°C for 2, 4 and 6 hours, respectively [13]. Their work using nanoindentation conducted at a relative humidity of 50% showed that the reduced MOE and the hardness of the cell wall increased with thermal modification. However, 190°C for 6 hours proved to be detrimental to the cell wall properties and not only caused degradation of hemicelluloses, but also damaged the crystalline cellulose. Recently, Lindstrom conducted experiments conducted at 50% relative humidity on red oak pyrolyzed 400°C, 450°C and 500°C [14] and, similar to Zickler et al., found the reduced MOE and hardness of the cell walls increased with increasing temperature. Xing et al. conducted nanoindentation experiments equipped with a hot stage to investigate the temperature-dependent real-time mechanical behavior of Larix wood cell walls heat-treated at 180°C and 210°C [15]. Conducting the experiments in the longitudinal direction, they found that the average reduced modulus of the cell wall decreased from 20.8 GPa at 20°C to 17.8 GPa at 180°C. The hardness initially increased between 20°C and 100°C and then decreased greatly from 100°C to 180°C, resulting in a hardness lower than its original hardness.

The current literature does not address over what dimension the microfibrils decompose during pyrolysis or the changes of mechanical responses of cell walls in wood exposed to fire in an oxidative environment. Here, nanoindentation conducted in a dry environment is used to evaluate these changes in charred Douglas-fir with measurements in unmodified wood, through the pyrolysis zone and into the char layer.

4.2 Materials and Methods

Materials

The same board of Douglas-fir (*Pseudotsuga menziesii*) used for the x-ray photoelectron experiments (XPS) in Chapter 3 was used for the nanoindentation experiments. A brief description of the specimen fire exposure technique is given here, for a more detailed description, refer to Section 3.3. A 100 mm by 100 mm specimen was exposed to a heat flux of 50 kW/m^2 using a cone calorimeter (FTT iCone mini, East Grinstead, West Sussex, UK). The thermal wave through the Douglas-fir specimen was obtained via embedded thermocouples located at heights of 4 mm, 8 mm, 12 mm, and 16 mm from the bottom, unexposed surface as well as one on the top surface and one on the unexposed surface of the specimen. The final measured temperatures are provided in Table 4.1. To determine the temperatures at locations other than those measured by the thermocouples, Fire Dynamics Simulator was used as described in more detail in Section 3.3. The calculated temperatures at the nanoindentation locations are also provided in Figure 4.1.

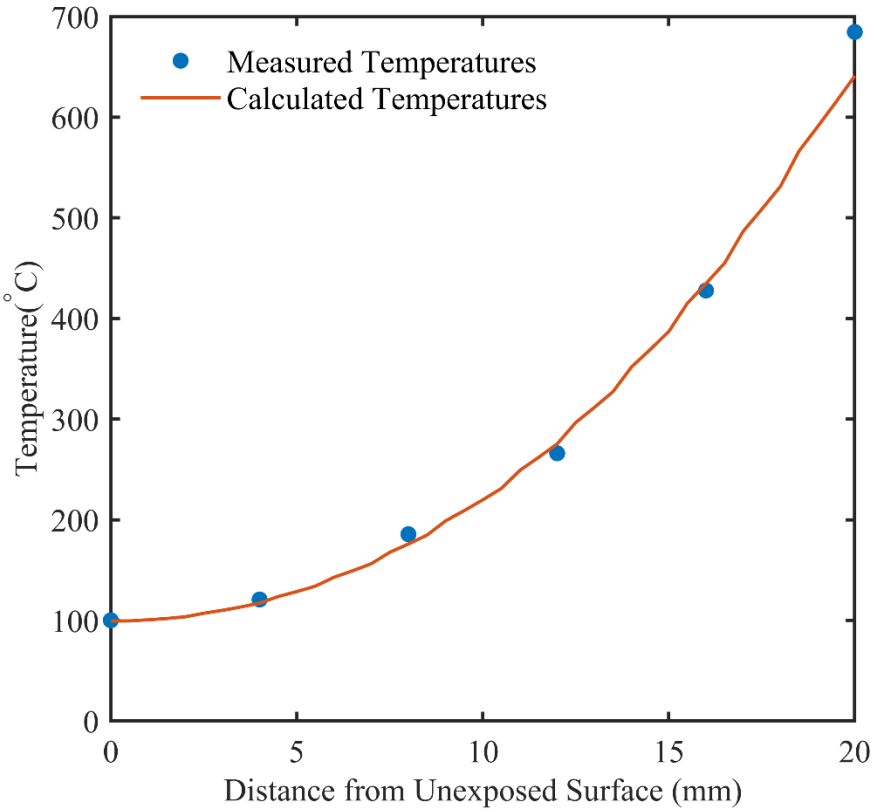

Figure 4.1: Final temperature profile in the charred wood specimen from embedded thermocouples (measured) compared to calculated temperatures from FDS program.

After exposure, the charred wood specimen was cut along the transverse plane into 4 mm thick sections (Figure 4.2a). To create the nanoindentation specimens, consecutive, 4 mm slices were used with the same latewood growth ring cutout of each section (Figure 4.2b). The latewood growth rings were then cut into smaller blocks to allow for nanoindentation at distances of 2, 9, 11, 13, 15 and 17 mm from the unexposed surface in both the longitudinal and transverse directions (Figure 4.2c). The direction refers to the direction the probe travels such that the measurements in the longitudinal direction were taking on the transverse surface and those in the transverse direction occurred on the tangential-longitudinal plane.

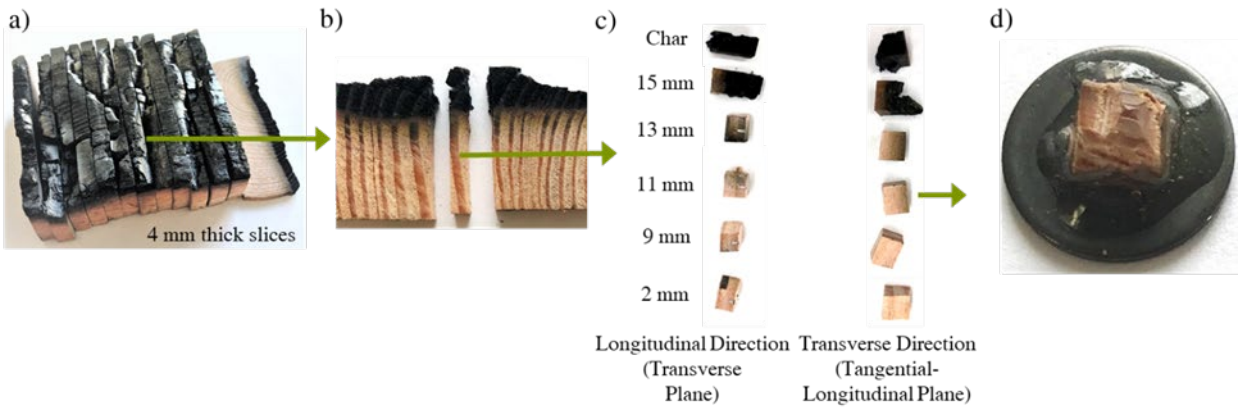

Figure 4.2: a) Specimen after fire exposure and sectioning. b) Section used for nanoindentation with chosen latewood ring cut out. c) Cut latewood ring in both transverse and longitudinal planes with depths from unexposed surface given and d) example of final nanoindentation specimens mounted in epoxy with prepared surfaces.

The wood specimens were mounted on a metal disc with epoxy (Figure 4.2d) but were not embedded to avoid any potential effects of the epoxy on the nanoindentation surface. Nanoindentation surfaces were prepared on both transverse and tangential-longitudinal planes following previously established procedures [9, 16]. In brief, a hand razor was used to carefully trim a pyramid with an apex in the region of interest. Then, the oriented blocks were fitted into Leica EM UC7 ultramicrotome (Wetzlar, Germany) equipped with a diamond knife. Surfaces were prepared by removing 200 nm thick sections from the apex until an appropriately sized, ultra-smooth surface was prepared, typically about 100 microns on a side.

Methods

A Bruker-Hysitron (Minneapolis, Minnesota, USA) TriboIndenter® equipped with a Berkovich probe was used. The machine compliance, probe area function, and tip roundness effects were determined from a series of 80 nanoindents in a fused silica standard using the load function and the procedures in [10, 17]. Following the calibration reporting procedure prescribed in [10]: Values for the square root of the Joslin-Oliver parameter of 1.2 $\mu m/N^{1/2}$, elastic modulus of 72.0 ± 0.3

GPa, and Meyer's hardness of 8.9 ± 0.1 GPa (uncertainties are standard errors) were assessed for fused silica calibration nanoindentations with contact depths between 57 and 200 nm; no systematic variations of machine compliance or Joslin-Oliver parameter were observed in the systematic SYS plot analysis over this range of contact depths.

To replicate moisture conditions in wood during pyrolysis, the nanoindentation experiments were performed under dry conditions. The relative humidity (RH) inside of the nanoindentation enclosure was maintained near zero by conditioning the enclosure with dry laboratory air. Prepared specimens were placed inside of the nanoindenter enclosure at least 60 hours before experiment commencement and the dry atmosphere was maintained during the experiments. In the longitudinal direction, nanoindentations were placed in the tangential side of the S2 to avoid the pits that are sometimes in the radial side. In the transverse direction, nanoindentations were placed inside of an S2 next to an exposed lumen. In each specimen, four to seven nanoindentations were performed in four different cell walls. From scanning probe microscopy images of residual nanoindentations, any nanoindentation that was not completely contained within the S2 was excluded from analysis. The multiload load function described in [11] was used in this study. The maximum load for all specimens not including the char was 0.3 mN. For experiments in char, the maximum loads were varied between 0.5 and 0.8 mN. The structural compliance method [9, 18] was employed to remove artifacts caused by edge effects and specimen-scale flexing at each nanoindentation location. Unloading segments with contact depths less than 57 nm were excluded from the structural compliance analysis because they were affected by tip roundness effects in fused silica calibrations. After correcting the data for structural compliance, the Meyer hardness (H) was calculated using

$$H = \frac{P_0}{A_0} \qquad \text{eq. 4.1}$$

where P_0 and A_0 are the is the maximum load and contact area calculated using the probe area function, respectively, immediately prior to each unloading segment. The effective modulus (E_{eff}) of contact was calculated using:

$$E_{\text{eff}} = \frac{S}{A_0^{1/2}} \qquad \text{eq. 4.2}$$

where S is the contact stiffness calculated by fitting the Oliver–Pharr [19] power law function from to 40-95% of the maximum load of each unloading segment. The diamond probe contributions to E_{eff} are accounted for and assess the nanoindentation elastic modulus E_s^{NI} using:

$$\frac{1}{E_{\text{eff}}} = \frac{1}{\beta}\frac{\pi^{1/2}}{2}\left(\frac{1-\upsilon_s^2}{E_s} + \frac{1-\upsilon_d^2}{E_d}\right) \qquad \text{eq. 4.3}$$

where E_d is the Young's modulus of diamond (1137 GPa), ν_d is the Poisson's ratio of diamond (0.1), and ν_s is the Poisson's ratio assumed for the S2 cell wall layer (0.5) [8]. The numerical factor β was assumed to be 1. The "NI" superscript is included to indicate that the elastic modulus assessed here is not the Young's modulus typically calculated. The H and E_s^{NI} were calculated for each unloading segment in the multiload nanoindentations. After excluding data affected by tip roundness, no data exhibited any systematic size dependence. Therefore, for each specimen, all results from the remaining unloading slopes were averaged and used to calculate standard deviation.

A Quesant (Agoura Hills, California, USA) atomic force microscope (AFM) incorporated in the TriboIndenter was used for imaging. The AFM was operated in contact mode and calibrated in the lateral directions using an Advanced Surface Microscopy (Indianapolis, Indiana, USA) calibration standard as described previously [9].

4.3 Results

Load-displacement curves from the nanoindentation experiments on the cell walls from fire exposed Douglas-fir are provided in Figure 4.3. Figures 4.3a and 4.3b are the load-displacement curves in the uncharred wood in the longitudinal direction and transverse direction, respectively. Figures 4.3c and 4.3d are the load-displacement curves in the wood char in the longitudinal direction and transverse direction, respectively. These curves have more noise than typical load displacement curves, which is attributed to running the nanoindentor in dry conditions. Despite the noise, the plastic and elastic behavior of the material are clearly displayed for the different temperature-affected regions. The nanoindentations performed in the uncharred wood show typical plastic behavior expected from wood with a hysteresis loop enclosed by the paths of loading and unloading. In this region, the P_0 is approximately 300 μN. In contrast to the uncharred wood, the slope of the unloading curve for the charred region decreases, the hysteresis loops are smaller, and the P_0 was approximately 500 μN to achieve the same nanoindentation sizes for each region. The load-displacement curves for the charred region show elastic behavior with the unloading curve more closely following the loading path back to the origin of the curve with no significant amount of plastic deformation (Figures 4.4c and 4.4d).

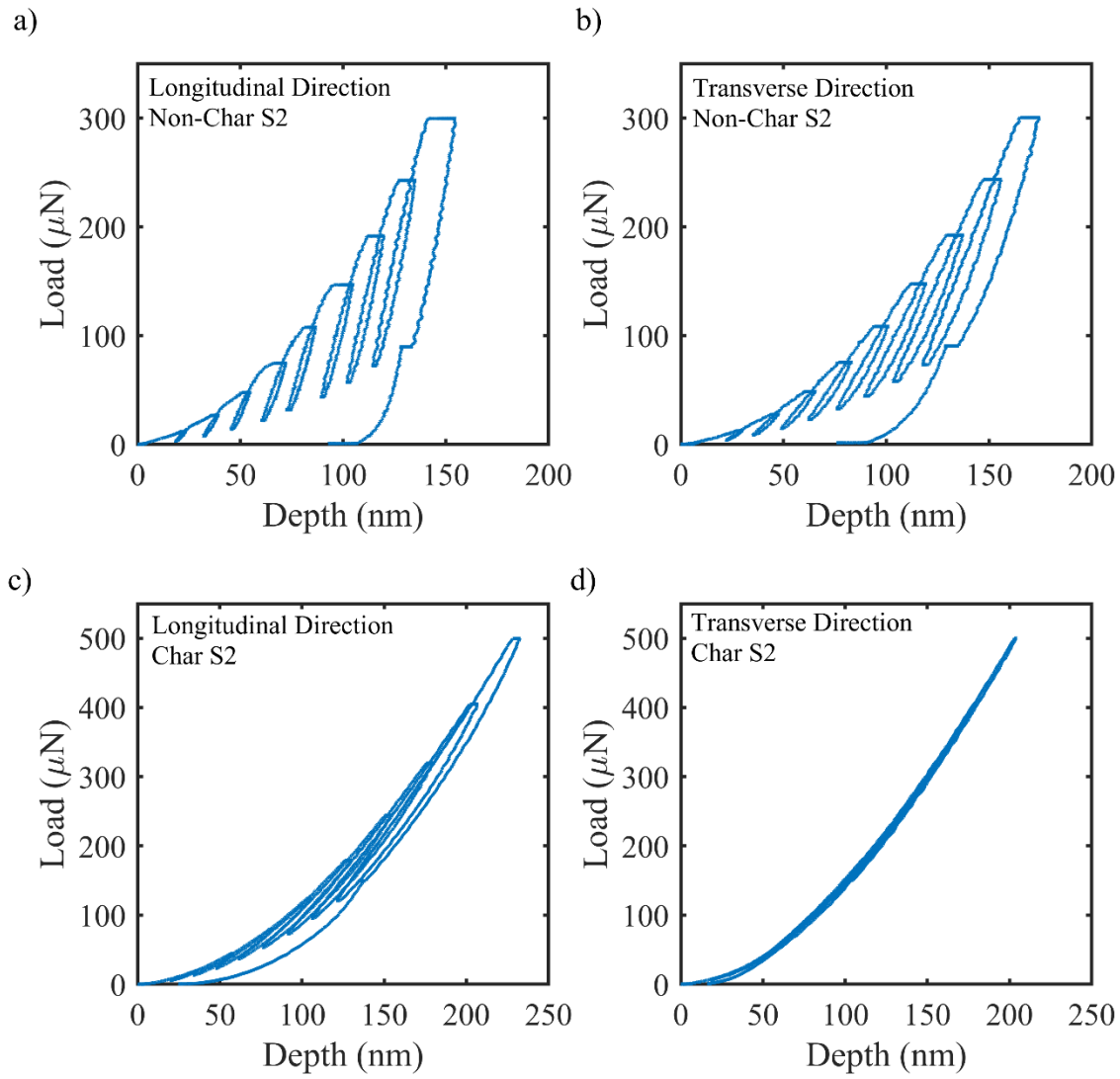

Figure 4.3: Load-displacement curves from nanoindentation experiments in the a) longitudinal direction of the uncharred wood, b) the transverse direction of the uncharred wood, c) longitudinal direction of the char and, d) the transverse direction of the char.

From the AFM images, the S2 cell wall lamina (SCWL) and the compound middle lamella (CML) are visible in the uncharred wood and, after complete unloading, residual indents remain at the surface and are visible in Figures 4.4a and 4.4b. The transverse direction is considered slightly more elastic with the indents not as pronounced as those that remain in the longitudinal direction. In the char (Figures 4.4c and 4.4d), the cell wall features are no longer discernible and no residual

indents remain, indicating the char is mostly elastic, which aligns with the findings of Zickler et al. [12].

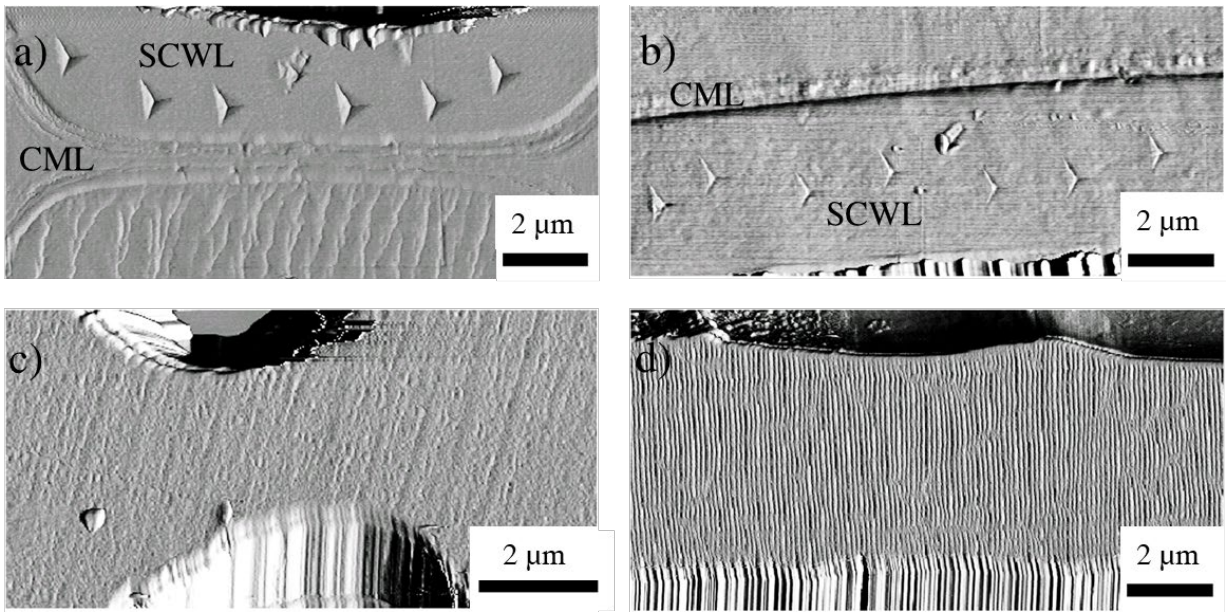

Figure 4.4: AFM images of nanoindentations in Douglas-fir wood cell walls in the a) longitudinal direction of the uncharred wood, b) the transverse direction of the uncharred wood, c) longitudinal direction of the char and, d) the transverse direction of the char.

The summary of the nanoindentation measurements are provided in Table 4.1 and plotted in Figure 4.5. A quantitative analysis of the nanoindentation tests reveal an average longitudinal E_s^{NI} in the region between 2 and 15 mm from the unexposed surface to be 14.7 ± 1.7 GPa and a hardness (H) of 562 ± 35 MPa. Hardness evaluates plasticity of the cell walls and is primarily influenced by the polymer matrix properties in the secondary cell wall [20, 21]. In the char layer, which was exposed to temperatures over 400°C, the longitudinal E_s^{NI} drop rapidly to less than half of the original value while the longitudinal H increased by 20%. An average transverse E_s^{NI} in the uncharred wood was 7.6 ± 0.3 GPa and an average transverse H of 529 ± 59 MPa, which are in agreement with previous work at low moisture contents [11]. The char layer's transverse E_s^{NI} decreased less dramatically than the longitudinal E_s^{NI} with the value being approximately 85% of the original value. The transverse H in the char layer increased by over 200%.

Table 4.1: Nanoindentation results for each specimen

Direction	Distance (mm)	Calculated Temp. (°C)	Number of indentations	Number of unloading slopes	E_s^{NI} Avg. GPa	E_s^{NI} σ GPa	H Avg. MPa	H σ MPa
Longitudinal	2	104	24	143	13.5	1.6	527.3	38.0
	9	199	23	133	14.4	1.0	556.9	41.4
	11	249	21	121	16.3	1.2	562.9	35.1
	13	312	20	112	14.7	0.9	586.3	40.5
	15	387	22	125	14.5	1.1	579.6	39.1
	Char (17)	487	25	173	5.3	0.1	679.0	39.1
Transverse	2	104	20	120	7.3	0.2	499.6	33.8
	9	199	21	126	7.6	0.2	508.8	28.6
	11	249	25	150	7.9	0.2	520.7	26.2
	13	312	25	148	7.3	0.3	525.2	60.7
	15	387	23	132	7.8	0.3	587.9	40.3
	Char (17)	487	35	191	6.5	0.5	1191.6	162.6

[1] σ is the standard deviation

The differences in the longitudinal and transverse elastic moduli indicate the wood is anisotropic up to 400°C because the longitudinal modulus is higher than the transverse modulus. From Figure 4.5, the difference in longitudinal and transverse E_s^{NI} is minimal in the char, indicating that the material is a mostly isotropic carbonaceous residue and that the cellulose has pyrolyzed. The increase in the transverse hardness indicates an increase in resistance to plastic deformation and a transition to elastic behavior.

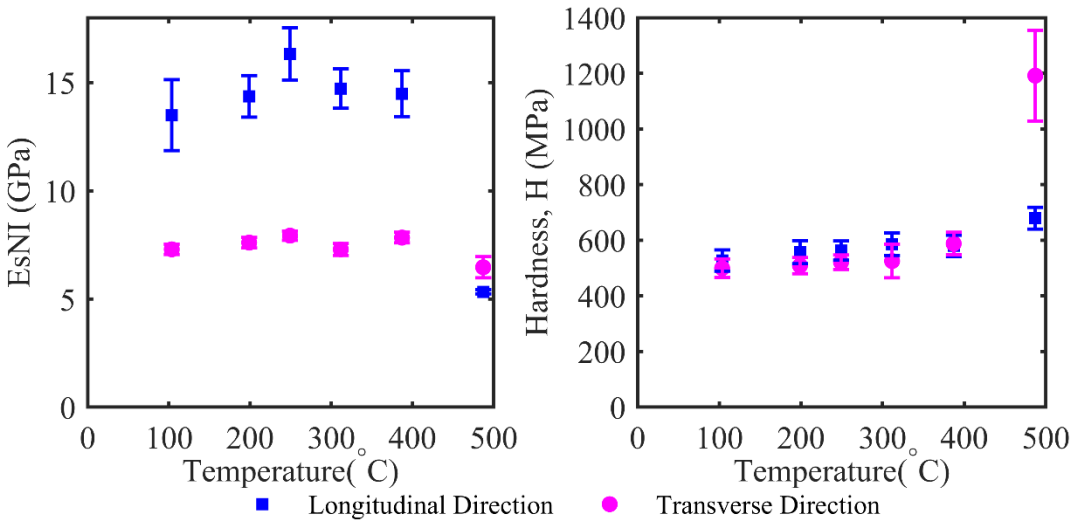

Figure 4.5: Experimental longitudinal and transverse nanoindentation elastic moduli (left) and hardness (right) of Douglas-fir cell walls as a function of calculated temperature.

4.4 Discussion

The intention of this work was to investigate the mechanical response of the material (E_s^{NI} and H) through the gradient found in charred wood. As previously found, the stiff cellulose microfibrils, which are oriented close to parallel with the longitudinal direction, cause the longitudinal elastic moduli to be consistently higher than the transverse elastic moduli in the uncharred wood [11]. Below temperatures of 400°C, the longitudinal E_s^{NI} was nearly twice that in the transverse direction, which is in good agreement with previously published works on the mechanical properties of the wood cell wall [10, 11, 16, 20-22].

Compared to studies on pyrolyzed wood, the E_s^{NI} are consistent with the values from Zickler et al. and Brandt et al. at temperatures below 275°C, but the decrease in E_s^{NI} measured here occurs at a higher temperature than observed by Zickler et al. and Brandt et al. [1, 12]. The difference may be due to the type of wood, whether or not embedment was used, the thermal modification method and the relative humidity (RH) humidity during nanoindentation experiments. It has been shown that the elastic modulus is highly sensitive to moisture content [11]. Unfortunately, both Zickler et al. and Brandt et al. did not discuss the RH conditions during the nanaoindentation experiments. However, Lindstrom conducted experiments on pyrolyzed red oak at 50% RH and found that the nanoindentation elastic modulus and hardness in the transverse direction increased after thermal deconstruction likely due to the reduced water sorption capacity [14]. Here, since water was not introduced to the cell walls, no notable difference in the elastic modulus and hardness is observed in the material properties until the charred region.

The nanoindentation results provide valuable information on the changes on the cell wall mechanical properties during pyrolysis after the moisture has been driven off. However, the temperature during nanoindentation experiments may affect the results. Future work will focus on

developing a hot stage to use with the nanoindentation equipment to observe the effects of temperature in dry conditions. Additionally, further investigation is recommended on additional wood species with varying fire exposures. Nevertheless, the results here show that, regardless of the chemical changes, the largest effect in the secondary cell wall mechanical properties occurs when the stiff cellulose microfibrils are broken down at high temperatures and that this occurs in a narrow region of approximately 2 mm.

4.5 Conclusions

The mechanical properties of the secondary cell wall in charred wood exposed to fire have been measured through the gradient caused by pyrolysis. Overall, the decomposition of wood cell walls exposed to temperatures above 400°C is visible by the loss of the distinct cell wall features. Additionally, the exposure to high temperatures alters the anisotropy of the latewood cell wall to an almost isotropic behavior in the char. The longitudinal elastic modulus does not change at temperatures below 400°C under dry conditions with a drastic change noted at a calculated temperature of 487°C. This suggests that, for wood exposed to fire with a gradient from the unmodified wood to the char, a change in the stiff cellulose microfibrils occurs in a narrow, 2 mm, region and temperature range.

4.6 References

[1] B. Brandt, C. Zollfrank, O. Franke, J. Fromm, M. Göken, and K. Durst, "Micromechanics and ultrastructure of pyrolysed softwood cell walls," *Acta biomaterialia,* vol. 6, pp. 4345-4351, 2010.

[2] O. Paris, C. Zollfrank, and G. A. Zickler, "Decomposition and carbonisation of wood biopolymers—a microstructural study of softwood pyrolysis," *Carbon,* vol. 43, pp. 53-66, 2005.

[3] D. Green, J. Winandy, and D. Kretschmann, "Mechanical properties of wood-wood as an engineering material," *General Technical Report FPL-TR,* vol. 113, 1999.

[4] A. Sinha, R. Gupta, and J. A. Nairn, "Thermal degradation of bending properties of structural wood and wood-based composites," *Holzforschung,* vol. 65, pp. 221-229, 2011.

[5] A. Firmanti, B. Subiyanto, S. Takino, and S. Kawai, "The critical stress in various stress levels of bending member on fire exposure for mechanical graded lumber," *Journal of wood science,* vol. 50, pp. 385-390, 2004.

[6] S. L. Zelinka, K. Sullivan, S. Pei, N. Ottum, N. J. Bechle, D. R. Rammer*, et al.*, "Small scale tests on the performance of adhesives used in cross laminated timber (CLT) at elevated temperatures," *International Journal of Adhesion and Adhesives,* vol. 95, p. 102436, 2019.

[7] R. Wimmer and B. N. Lucas, "Comparing mechanical properties of secondary wall and cell corner middle lamella in spruce wood," *Iawa Journal,* vol. 18, pp. 77-88, 1997.

[8] R. Wimmer, B. Lucas, W. Oliver, and T. Tsui, "Longitudinal hardness and Young's modulus of spruce tracheid secondary walls using nanoindentation technique," *Wood Science and Technology,* vol. 31, pp. 131-141, 1997.

[9] J. E. Jakes, C. R. Frihart, J. F. Beecher, R. J. Moon, and D. Stone, "Experimental method to account for structural compliance in nanoindentation measurements," *Journal of Materials Research,* vol. 23, pp. 1113-1127, 2008.

[10] J. E. Jakes, "Improved methods for nanoindentation Berkovich probe calibrations using fused silica," *Journal of materials science,* vol. 53, pp. 4814-4827, 2018.

[11] S. Youssefian, J. Jakes, and N. Rahbar, "Variation of nanostructures, molecular interactions, and anisotropic elastic moduli of lignocellulosic cell walls with moisture," *Scientific reports,* vol. 7, p. 2054, 2017.

[12] G. Zickler, T. Schöberl, and O. Paris, "Mechanical properties of pyrolysed wood: a nanoindentation study," *Philosophical Magazine,* vol. 86, pp. 1373-1386, 2006.

[13] X. Wang, X. Chen, X. Xie, Y. Wu, L. Zhao, Y. Li*, et al.*, "Effects of thermal modification on the physical, chemical and micromechanical properties of Masson pine wood (Pinus massoniana Lamb.)," *Holzforschung,* vol. 72, pp. 1063-1070, 2018.

[14] J. K. Lindstrom, "Analyzing and exploiting biomass thermal deconstruction," *Ann Arbor,* vol. 1001, 2019.

[15] D. Xing, J. Li, X. Wang, and S. Wang, "In situ measurement of heat-treated wood cell wall at elevated temperature by nanoindentation," *Industrial crops and products,* vol. 87, pp. 142-149, 2016.

[16] J. E. Jakes, C. G. Hunt, D. J. Yelle, L. Lorenz, K. Hirth, S.-C. Gleber*, et al.*, "Synchrotron-based X-ray Fluorescence Microscopy in Conjunction with Nanoindentation to Study Molecular-Scale Interactions of Phenol–Formaldehyde in Wood Cell Walls," *ACS applied materials & interfaces,* vol. 7, pp. 6584-6589, 2015.

[17] D. Stone, K. Yoder, and W. Sproul, "Hardness and elastic modulus of TiN based on continuous indentation technique and new correlation," *Journal of Vacuum Science & Technology A: Vacuum, Surfaces, and Films,* vol. 9, pp. 2543-2547, 1991.

[18] J. Jakes, D. Yelle, J. Beecher, C. Frihart, and D. Stone, "Characterizing pMDI reactions with wood cell walls: 2. Nanoindentation," in *International Conference on Wood Adhesives. Forest Products Society, Harveys Resort & Casino, Lake Tahoe, Nevada, USA*, 2009, pp. 366-373.

[19] W. C. Oliver and G. M. Pharr, "An improved technique for determining hardness and elastic modulus using load and displacement sensing indentation experiments," *Journal of materials research,* vol. 7, pp. 1564-1583, 1992.

[20] W. Gindl and T. Schöberl, "The significance of the elastic modulus of wood cell walls obtained from nanoindentation measurements," *Composites Part A: Applied Science and Manufacturing,* vol. 35, pp. 1345-1349, 2004.

[21] W. Gindl, H. Gupta, T. Schöberl, H. Lichtenegger, and P. Fratzl, "Mechanical properties of spruce wood cell walls by nanoindentation," *Applied Physics A,* vol. 79, pp. 2069-2073, 2004.

[22] W. Gindl, H. Gupta, and C. Grünwald, "Lignification of spruce tracheid secondary cell walls related to longitudinal hardness and modulus of elasticity using nano-indentation," *Canadian Journal of Botany,* vol. 80, pp. 1029-1033, 2002.

Chapter 5. Discussion

This chapter brings together the combined results from XPS, TGA, and nanoindentation to construct a more complete picture of pyrolysis in wood.

5.1 Summary of Experimental Results

Thermogravimetric Analysis

The first experiments, described in Chapter 2, focused on the traditional method of thermogravimetric analysis (TGA) to assess thermal degradation of isolated wood polymers and Douglas-fir latewood. However, unlike previous studies, effects of atmosphere (nitrogen versus air with $P_{O_2} = 0.2\ Atm$) within a single set of specimens were explored. Additionally, the thermal degradation of Douglas-fir was compared to the weighted average of the thermal degradation of the isolated polymers. Similar to what has been reported in previous studies [1-3], the samples in air experienced two stages of active pyrolysis: degradation of the wood polymers then degradation of the residue. Additionally, for all materials except the isolated lignin, the rate of mass-loss peaked at lower temperatures in air than in nitrogen, suggesting that a component of air (e.g., oxygen) not present in nitrogen plays a role in breaking up the polymer networks. Overall, mass loss of Douglas-fir resembles the weighted average of the mass loss exhibited by individual polymers but does not exactly duplicate this average. Instead, thermal degradation of the Douglas-fir most closely follow that of cellulose, suggesting that degradation of cellulose has the greatest influence on the degradation of wood during pyrolysis (Figure 5.1), even though cellulose only makes up approximately 36% of the mass of the Douglas-fir specimens studied here.

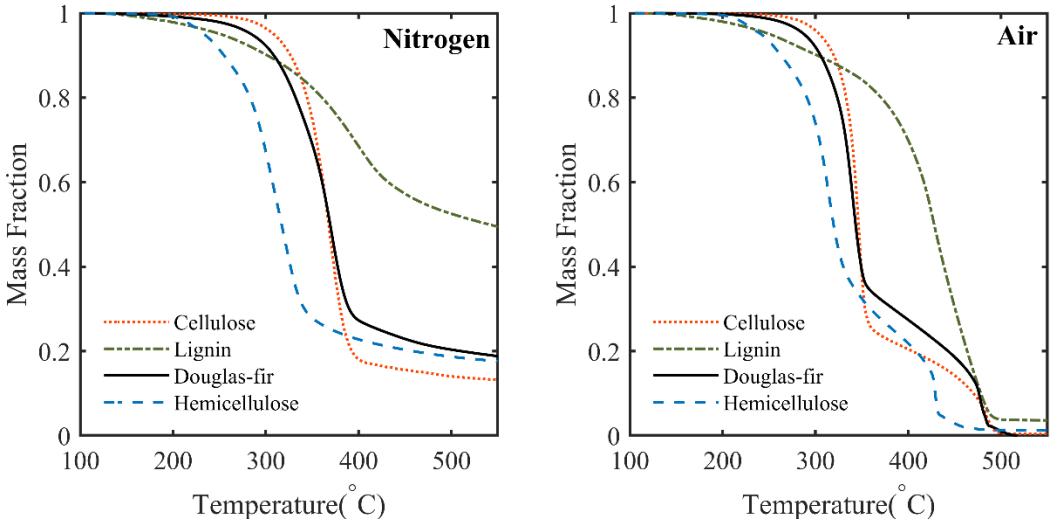

Figure 5.1: Mass fraction of Douglas-fir latewood during dynamic TGA experiments at 10˚C/min compared to individual wood polymers in nitrogen (left) *and air* (right).

X-ray Photoelectron Spectroscopy

To evaluate the chemical changes through charred Douglas-fir latewood, x-ray photoelectron spectroscopy (XPS) was conducted and discussed in Chapter 3. While XPS is a common surface analysis technique, it has not been extensively used on wood, and the experimental methods are not well-established. Not surprisingly, the preliminary experiments conducted showed a range of results depending on sample preparation and instrument settings. It took concerted effort to find the optimal method for measuring wood pyrolysis. Since XPS analysis requires ultra-high vacuum during the experiments, the lipophilic extractives in the wood can migrate to the surface, causing an artificially high C-C peak and a low O/C ratio. Removing the extractives was a necessary step in specimen preparation to remove this artifact. Secondly, the use of an argon ion energy beam to etch the surface to remove adventitious carbon was not appropriate for wood as it causes distortion in the spectra.

After establishing a tight experimental protocol, XPS was used to investigate how the chemical bonds present in cellulose and lignin evolve under exposure to high temperatures. Measurements

of the changes in bonding along the temperature gradient normal to the surface of charred Douglas-fir were also taken. For both isolated cellulose and lignin, the predominate C1s peak component belonged to the C-O bond until higher temperatures, where it was replaced by the C-C bond. For cellulose, the C-C peak became more prominent at higher temperatures beginning at approximately 365°C. For the lignin, the C-C bonds were more prevalent at temperatures above 300°C. The XPS results provide the first measurements of the changes in chemical bonds present through the gradient caused by pyrolysis in wood.

Nanoindentation

The last set of experiments employed nanoindentation to measure secondary cell wall hardness (H) and modulus (E_s^{NI}) as functions of exposure temperature in charred Douglas-fir latewood. Properties of wood exposed to temperatures below 275°C were found to be anisotropic as reported by others [4, 5]. However, above 275°C the results of others showed a decrease in EsNI around 300°C while the decrease was not observed until 400°C in the work conducted here. Above 400°C the transverse hardness increased, indicating an increase in resistance to plastic deformation and a transition to elastic behavior. The mechanical changes observed occurred across a narrow range in the specimen, about 2 mm in thickness, spanned by a 100°C difference (from 387°C to 487°C) in temperature.

5.2 Advancing the Understanding of Pyrolysis

Mass Loss versus Bond Scission

TGA and XPS data from cellulose, lignin, and solid wood are combined in Figures 5.2, 5.3, and 5.4, respectively, as functions of temperature. The XPS data presented is the C_C/C_O ratio. C_C is calculated at the sum of the C-C, C=C and π-π* peak ratios and C_O is calculated at the sum of C-

O, C=O and COOH peak ratios (see Chapter 3). From the TGA results for exposure to air, the rate of mass fraction loss (MF') exhibits a peak in the range 300°C to 350°C. This is the same range of temperature across which the C-O bond peak ratios diminish, while the C-C bond peak ratios grow. These changes are observed in the C_C/C_O ratio shown in Figure 5.2. Notably, the TGA peak for exposure to nitrogen, also shown, falls at a higher temperature. The bond scission and changes in peak ratios correlates best to the rate of change in the mass fraction in air because the specimens were pyrolyzed in air.

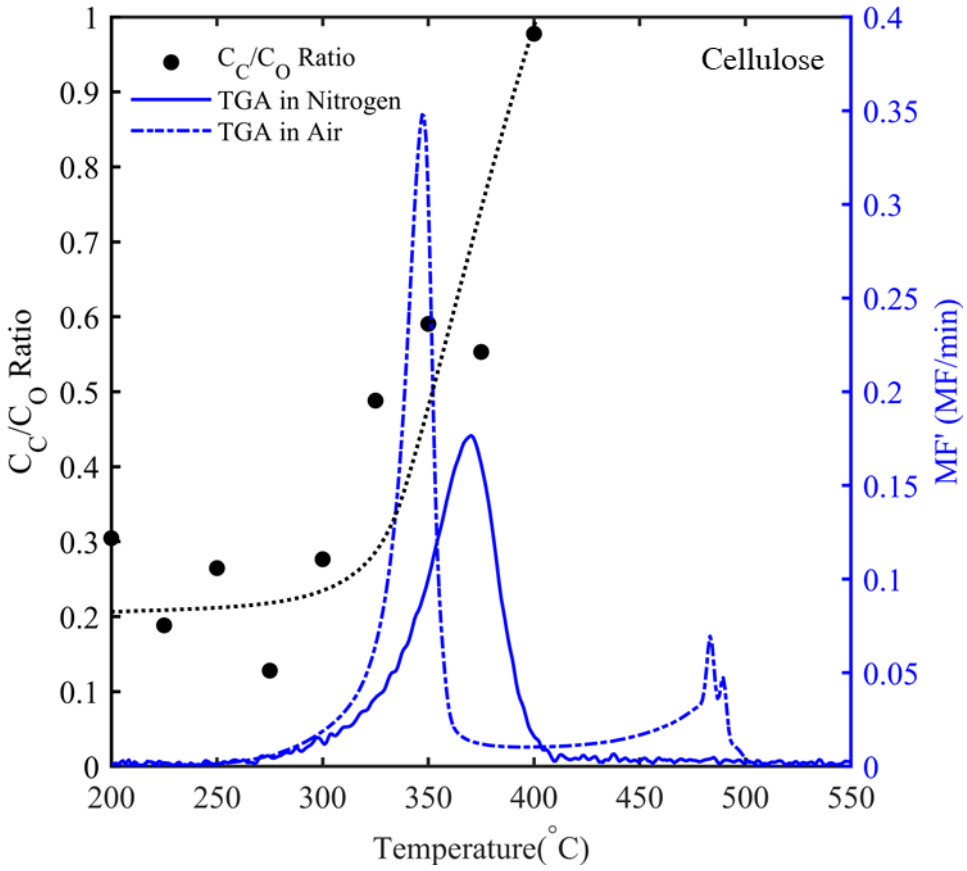

Figure 5.2: XPS and TGA results for cellulose. The black dotted lines have been added to help guide the eye.

For the isolated lignin, the onset of thermal degradation from TGA begins at 127°C in air (below the limits shown in Figure 5.3) but the rate of mass loss only peaks above 400°C. Given that

structure of lignin is more complex [6] than that of cellulose, it is not surprising that lignin exhibits a more complex mass loss spectrum than cellulose. Like the cellulose, the lignin specimens for XPS analysis were exposed to high temperatures in air. Because of this, specific focus is given to the TGA curve in air. Between 250°C and 300°C, there is a gentle peak in mass loss superimposed above a broad background. Just beyond this shoulder, at approximately 312°C, the C_C/C_O ratio begins to increase as the C-O bond peak ratio decreases. Additionally, above 312°C, an increase in the C-C peak ratio is observed just before the peak mass loss rate at 425°C. Unlike the cellulose, the C_C/C_O ratio trends upward before the peak mass loss rate. This is likely due to the fact that there are less hydroxyl groups in the lignin to cleave. Past the peak mass loss rate, it would be expected that the C-C and C=C bonds would be most prevalent, and the C-O bonds would be removed.

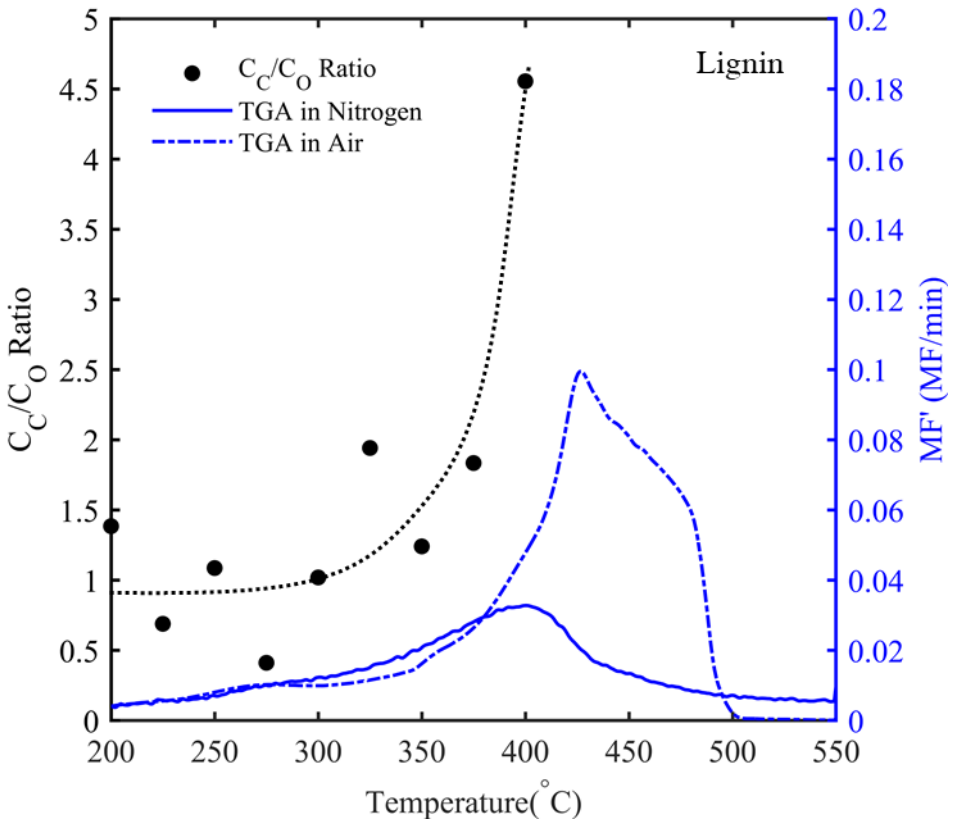

Figure 5.2: XPS and TGA results for lignin. The black dotted line has been added to help guide the eye.

For the Douglas-fir latewood (Figure 5.4), the onset of thermal degradation from the TGA results occurs at temperatures of 218°C and 233°C in nitrogen and air, respectively. A slight decrease in the C_C/C_O ratio between 100°C and 220°C is due to a decrease observed in the C-O peak ratio. This decrease illustrates that, while there is no mass loss recorded during TGA, the chemical bonds are is changing via scission. The bond that are breaking are likely from the less thermally stable sidechains in the hemicellulose or lignin. Above 350°C, the C_C/C_O ratio begins to increase. This increase correlates with the shoulder that occurs before the peak mass loss rate in the differential TGA curve in nitrogen. The correlation to the TGA curve in nitrogen is due to the limited amount of oxygen that diffuses into the wood during a fire. The TGA results correlate well with the changes observed in the chemical bonds through the gradient from pyrolysis in Douglas-fir latewood. However, the changes in chemical bonds observed using XPS at lower temperatures were not noticeable via the mass loss recorded from TGA.

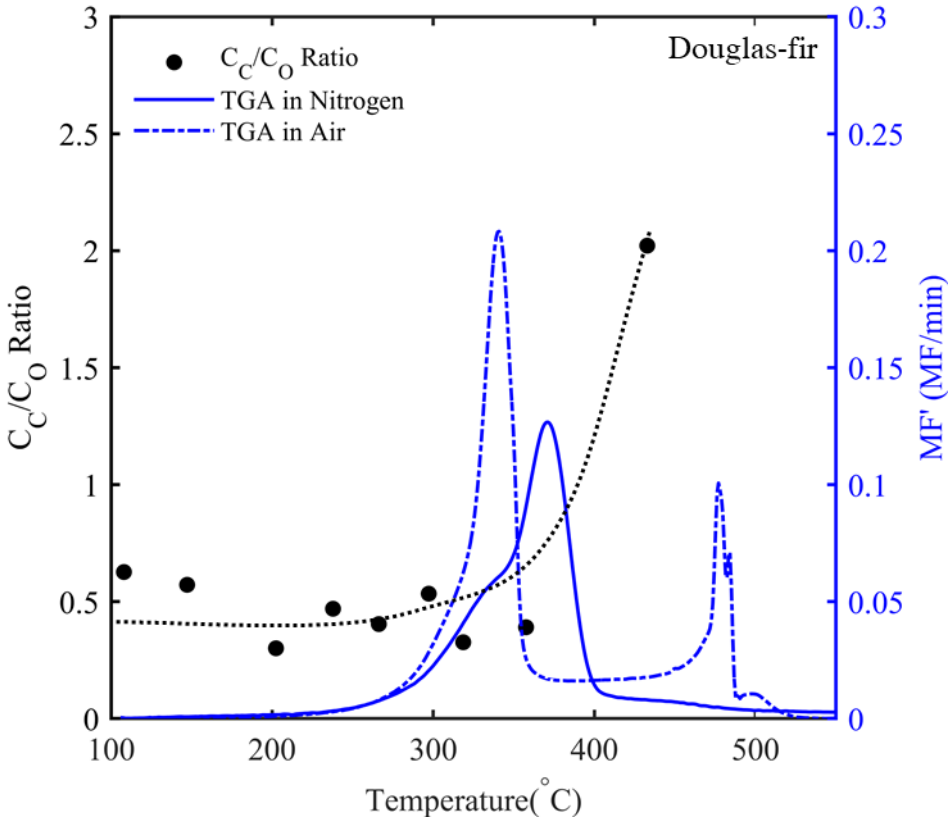

Figure 5.4: XPS and TGA results for charred Douglas-fir latewood. The black dotted line has been added to help guide the eye.

Effect of Elemental Composition on Mechanical Properties

Comparing the chemical changes observed using XPS to the secondary cell wall mechanical properties, the effects of the exact composition and gradual pyrolysis can be observed. Figure 5.5 plots the C_C/C_O ratio versus to modulus and hardness. The C_C/C_O ratio remains relatively constant for temperatures between 100°C and 380°C. In this same temperature range, the transverse and longitudinal E_s^{NI} and H remain unchanged and indicate the wood is still anisotropic. Notable changes in the longitudinal E_s^{NI} and transverse H are not observed until after the C-C peak becomes the predominate C1s component, which is observed in the increase in C_C/C_O ratio. Collectively, these results suggest that, at dry conditions, although matrix biopolymers are being volatized is it

not enough to decrease the mechanical properties until the cellulose completely degrades in the char region.

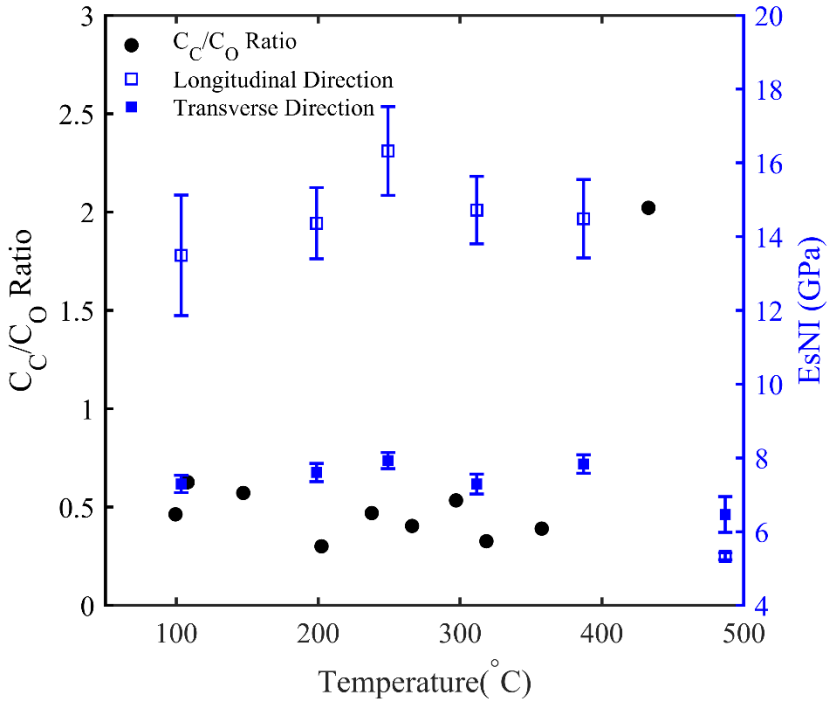

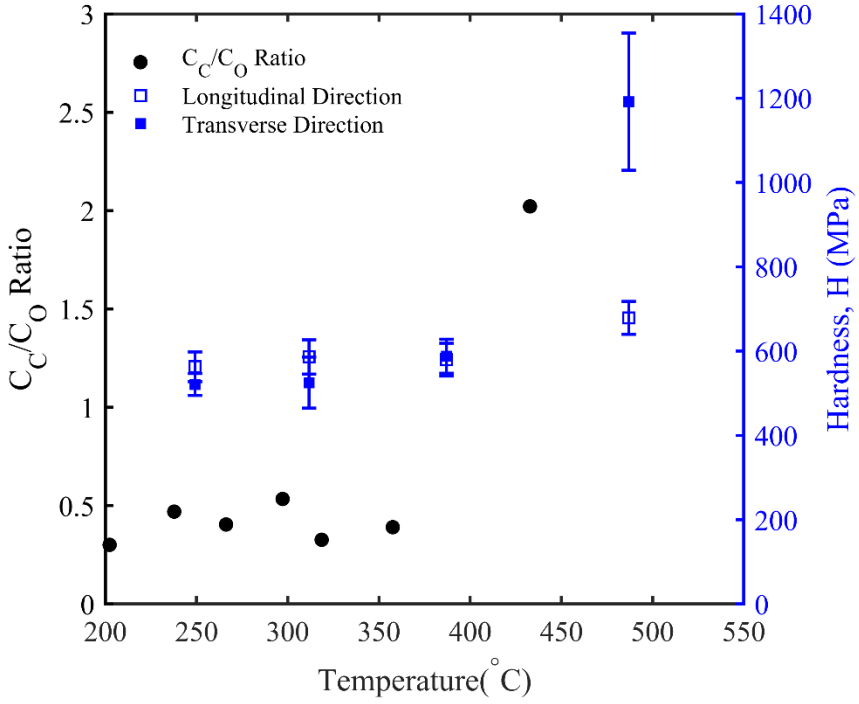

Figure 5.5: C_C/C_O ratio obtained with XPS plotted with E_s^{NI} (top) and H (bottom) for charred Douglas-fir latewood.

Ultimately, the combined results from XPS, TGA, and nanoindentation to construct a more complete picture of pyrolysis in wood. There is a correlation between the TGA and XPS data with XPS providing a deeper understanding into the chemical changes causing mass loss in whole wood. The combined TGA and XPS data also indicate that the atmosphere in which the specimens were pyrolyzed in matters and that the reducing atmosphere better describes the changes caused by pyrolysis in the Douglas-fir latewood. By combining the chemical changes from XPS with the mechanical changes from nanoindentation, the cell wall mechanical response remains constant until the carbon atoms bound to other carbon atoms exceeds the carbon atoms bound to oxygen.

5.3 References

[1] T. Ohlemiller, T. Kashiwagi, and K. Werner, "Wood gasification at fire level heat fluxes," *Combustion and Flame,* vol. 69, pp. 155-170, 1987.

[2] M. Fang, D. Shen, Y. Li, C. Yu, Z. Luo, and K. Cen, "Kinetic study on pyrolysis and combustion of wood under different oxygen concentrations by using TG-FTIR analysis," *Journal of analytical and applied pyrolysis,* vol. 77, pp. 22-27, 2006.

[3] N. Liu, W. Fan, R. Dobashi, and L. Huang, "Kinetic modeling of thermal decomposition of natural cellulosic materials in air atmosphere," *Journal of Analytical and Applied Pyrolysis,* vol. 63, pp. 303-325, 2002.

[4] G. Zickler, T. Schöberl, and O. Paris, "Mechanical properties of pyrolysed wood: a nanoindentation study," *Philosophical Magazine,* vol. 86, pp. 1373-1386, 2006.

[5] B. Brandt, C. Zollfrank, O. Franke, J. Fromm, M. Göken, and K. Durst, "Micromechanics and ultrastructure of pyrolysed softwood cell walls," *Acta biomaterialia,* vol. 6, pp. 4345-4351, 2010.

[6] M. Brebu and C. Vasile, "Thermal degradation of lignin—a review," *Cellulose Chemistry & Technology,* vol. 44, p. 353, 2010.

Chapter 6. Conclusions and Outlook

6.1 Conclusions

Three experimental techniques were used to gain a deeper understanding of the molecular-scale changes in bulk wood as it undergoes pyrolysis.

- A systematic study using thermogravimetric analysis (TGA) in both nitrogen and air showed that the thermal degradation of the Douglas-fir latewood cannot be represented by the weighted average of the individual polymers, as is often assumed [1-3] and, instead, a rate-limiting model is required. This result suggests that the in situ interactions among intermingled wood polymers affect the kinetics of pyrolysis.
- X-ray photoelectron spectroscopy (XPS) revealed, for the first time, the chemical changes caused by pyrolysis in thermally thick wood. XPS showed that thermal degradation via bond scission begins at lower temperatures (100°C to 200°C) than suggested from TGA (>200°C).
- Nanoindentation reveals that the hardness and modulus of the S2 cell wall in dry, charred Douglas-fir at the cellular level remains unchanged until the cellulose completely degrades at temperatures above 400°C. This varies from previous work [4, 5] that showed a decrease in the modulus at lower tempers and signifies that, when dry at ambient temperatures, the mechanical response does not change until the char layer.
- The bond scission that occurs during pyrolysis in bulk wood correlates well with the mass loss changes observed using TGA and the changes observed from the anisotropic wood becoming isotropic char.

6.2 Recommendations for Research Directions

The use of XPS can be expanded in numerous ways to provide a deeper understanding of pyrolysis of the wood polymers in situ caused by exposure to fire. XPS provided the elemental composition through the pyrolyzed region of wood. This technique could be combined with other spectroscopic techniques to compare the pyrolyzates to the remaining material. For instance, Fourier-transform infrared spectroscopy (FTIR) or gas chromatography–mass spectrometry (GC-MS) could analyze the pyrolysis products generated with time as wood is exposed to a heat flux. Then, XPS can be conducted on the pyrolysis region to compare the temporal and spatial results, providing a more complete picture of wood pyrolysis.

Here, one heat flux was used to develop the thermal profile in the Douglas-fir specimen. Conducting XPS on wood that has been exposed to other fire scenarios could provide details related to how deep the thermally affected region is below the char layer. This information is useful for pyrolysis models and engineering design calculations. It is also important information for the manufacturing of, and designing with, engineered wood products that rely on adhesives to remain structurally sound at high temperatures. Because adhesives can penetrate wood cell walls, the elemental compositional changes as the thermally affected region migrates closer to an adhesive bond line could cause adhesive formulations to be reconsidered. XPS could also provide valuable information on how other chemical modifications not discussed in this research, such as the addition of fire-retardant chemicals, alters the thermal degradation of the wood polymers.

While Douglas-fir was used here, the investigations related to the changes caused by pyrolysis in other species should be explored for further validation of the results. It has been shown that different species produce char at different rates [6]. White noted that one reason for this is the different quantities of the polymeric components present since the chemical composition will

influences the kinetics of pyrolysis. For instance, lignin constitutes 23% to 33% of the wood substance in softwoods and 16% to 25% in hardwoods. The pyrolysis region in species that represent the upper and lower bounds of the polymer components can be compared using XPS to evaluate the effect of the chemical composition.

As pointed out by Lautenberger, the ability the model various pyrolysis phenomena for practical solid combustibles is limited by the ability to determine the model input parameters that control the phenomena [3]. The TGA results can be systematically expanded (e.g., more components and vary the fraction of components in different temperature ranges) to develop a model that more closely represent the pyrolysis in wood. Additionally, to obtain the necessary model input parameters, a study to measure material properties, such as the thermal conductivity, is still required. Once the material properties are measured, they can be provided as input parameters to a model and used to simulate pyrolysis in appreciably thick wood. The potential to use XPS to obtain additional material properties should be investigated. In particular, the potential use of the charge compensation from XPS, in conjunction with other methods such as scanning thermal microscopy, to determine the thermal conductivity through the pyrolysis region would be of interest.

The nanoindentation experiments here were conducted at room temperature. The development of a hot stage to allow nanoindentation experiments to be conducted at temperatures above 400°C is recommended to compare to the results here. This will determine if the moisture content or the temperature has a larger effect on the cell wall mechanical properties. This knowledge would provide a deeper understanding related to the heat-affected depth in wood building products.

Using XPS and nanoindentation to evaluate the pyrolyzed region in wood exposed to fire has increased the understanding the chemical and physical changes that occur during pyrolysis and created new avenues for research directions.

6.3 References

[1] C. A. Hill, *Wood modification: chemical, thermal and other processes*. West Sussex, England: John Wiley & Sons, 2006.

[2] F. Richter and G. Rein, "Pyrolysis kinetics and multi-objective inverse modelling of cellulose at the microscale," *Fire Safety Journal,* vol. 91, pp. 191-199, 2017/07// 2017.

[3] C. Lautenberger, "A Generalized Pyrolysis Model for Combustible Solids (PhD. thesis) University of California," ed: Berkeley, 2007.

[4] G. Zickler, T. Schöberl, and O. Paris, "Mechanical properties of pyrolysed wood: a nanoindentation study," *Philosophical Magazine,* vol. 86, pp. 1373-1386, 2006.

[5] B. Brandt, C. Zollfrank, O. Franke, J. Fromm, M. Göken, and K. Durst, "Micromechanics and ultrastructure of pyrolysed softwood cell walls," *Acta biomaterialia,* vol. 6, pp. 4345-4351, 2010.

[6] R. H. White, *Charring rates of different wood species*: University of Wisconsin--Madison, 1988.

Appendix A: Co-Pyrolysis Kinetic Model

Introduction

The weighted average model assumes wood pyrolyzes the same way that a loosely aggregated, physical mixture of the isolated polymers might, i.e., without interactions among them. Indeed, the weighted average model offers a rough approximation to pyrolysis of Douglas-fir. However, a close examination of the curves in Figure 2.4, suggests that a better agreement would be obtained if the cellulose more heavily weighted than hemicellulose and lignin. Since the cellulose, hemicellulose, and lignin are closely intertwined on the nm-level within the wood cell walls; it goes against reason that there will be no interactions. Here, a new "co-pyrolysis" model is proposed in which pyrolysis of portions of the hemicellulose and lignin is rate-controlled by pyrolysis of the cellulose. The basis for the idea is illustrated in Figure A.1. Because of the close intermingling of the polymers, the most prevalent polymer, cellulose, controls the rate of pyrolysis of the other two polymers.

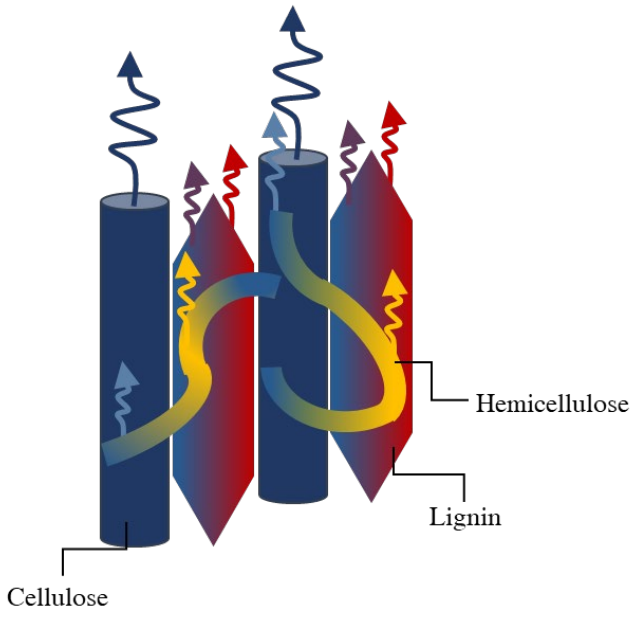

Figure A.1: Co-pyrolysis of intertwined wood polymers

Model for co-pyrolysis of wood polymers

Physical model for evaporation of isolated polymers

We introduce a reasonable physical picture to describe the active and passive phases of pyrolysis without having to incorporate ad-hoc assumptions or an additional physical mechanism. We assume that mass loss during pyrolysis results from a reaction in which a portion of the substance is released into the environment, leaving behind a residue. The residue pyrolyzes at a much higher temperature. It might also incorporate part of the atmosphere, for instance, if the reaction takes place in an oxidizing atmosphere, but we neglect this possibility for now. Here, it is assumed that the substance and its residue are mutually soluble, and that their thermodynamics can be described by regular solution theory [1]. Therefore, as the reaction continues and residue accumulates, the activity of the remaining unreacted mass diminishes (by a path that follows the prediction of the regular solution model), slowing down the reaction and leading to the passive phase of pyrolysis. Adaptation from regular solution theory to Flory-Huggins theory will follow [1].

We begin with the Hertz-Knudsen Equation [2, 3],

$$\frac{dN_s}{dt} = \frac{\alpha p_s}{\sqrt{2\pi m_s k_B T}} \qquad \text{eq. A.5}$$

which describes the rate of s-type molecules (N) sticking to surface (in units of $m^{-2}s^{-1}$) in an atmosphere with vapor pressure p_s. α is the sticking coefficient, p the vapor pressure, m_s is the mass of a particle (in kg), k_B is the Boltzmann constant, and T is temperature (in K). At equilibrium, this equation must also represent the number of *s*-type molecules leaving the surface per unit time, since for equilibrium the rates of evaporation and deposition must be equal. Therefore, if all molecules are removed from the system, this equation represents the number of molecules leaving per unit time: the rate of evaporation. We are interested in the effects of activity and temperature

on evaporation. Since activity is merely $a_s = p_s/p_s^0$ where p_s^0 is vapor pressure of the pure substance, then the rate of atoms leaving the surface can be written as

$$\dot{N}_s = a_s \dot{N}_s^0 A(m_s) \qquad \text{eq. A.6}$$

where $\dot{N}_s^0$ is the rate of molecules leaving the surface per unit time per unit area for the pure substance. A is the surface area of mass m_s

The total rate of loss of molecules is:

$$\dot{N}_s^0 = K_0 a_s \exp\left(-\frac{E}{k_B T}\right) A(m_s) \qquad \text{eq. A.7}$$

where A is the surface area of the substance. Equations (A.6) and (A.7) establish the equilibrium vapor pressure as a function of time. Lastly, the activity of a component in solution (the molecule, e.g., cellulose, dissolved in its residue) is estimated from the regular solution model as:

$$a_s = \exp\left[\frac{\Omega}{RT}(1 - x_s)^2\right] \qquad \text{eq. A.8}$$

where Ω is the regular solution energy parameter describing the enthalpy of mixing, $\Delta H = \Omega x_s(1 - x_s)$, for a solute of concentration x_s and solvent of concentration $(1 - x_s)$. The rate of evaporation, per unit area, can therefore be represented as:

$$\dot{N}_s = a_s K_0{}' \exp\left(-\frac{E}{k_B T}\right) \qquad \text{eq. A.9}$$

where $K_0{}'$ takes into account the area of the evaporating particle which, in principle, depends on the loss of mass depending on how the area of evaporation changes as mass is lost. However, for the moment we assume this effect is small compared to the exponential and activity parameter, which dominate the temperature-dependence of pyrolysis during heating.

Mass balance considerations are:

$$\text{Rate of evaporation} = \frac{dm_s}{dt} \qquad \text{eq. A.10}$$

Rate of accumulation of residue

$$\frac{dm_r}{dt} = -f\frac{dm_s}{dt} \qquad \text{eq. A.11}$$

where f is the fraction of mass left behind (which is typically less than 1 but not constrained by this condition). f can even be greater than 1 if something from the atmosphere is incorporated into the residue). Remaining mass:

$$m_{tot} = m_s + m_r \qquad \text{eq. A.12}$$

Mass fractions

$$x_s = m_s/(m_s + m_r);\ x_r = 1 - x_s \qquad \text{eq. A.13}$$

Rate of change in m_s:

$$\frac{dm_s}{dt} = -a_s K_0'' \exp\left(-\frac{E}{k_B T}\right) \qquad \text{eq. A.14}$$

Or removing the (unnecessary) primes

$$\frac{dm_s}{dt} = -a_s K_0 \exp\left(-\frac{E}{k_B T}\right) \qquad \text{eq. A.15}$$

If, in the experiment $r_0 = \frac{dT}{dt}$ is the rate of change in temperature, then we may write

$$dm_s = -a_s K_0 \exp\left(-\frac{E}{k_B T}\right)\frac{dT}{r_0} \qquad \text{eq. A.16}$$

This equation can be integrated numerically and compared with the mass loss data. It is necessary to take into account the mass balance equations A.10 to A.12 and activity A.8, which can be updated during the integration.

References

[1] D. R. Gaskell and D. E. Laughlin, *Introduction to the Thermodynamics of Materials*: CRC press, 2017.

[2] A. H. Persad and C. A. Ward, "Expressions for the evaporation and condensation coefficients in the Hertz-Knudsen relation," *Chemical reviews,* vol. 116, pp. 7727-7767, 2016.

[3] K. W. Kolasinski, *Surface science: foundations of catalysis and nanoscience*: John Wiley & Sons, 2012.